Doctoral Dissertation

Doctoral Program in Structural Engineering (36th Cycle)

Enhancing Mechanical Performance of Brittle Materials through Fiber Reinforcement:

A Study on FRC and FRI

By Farmehr M Dehkordi

******

Supervisors:

Prof. Barbara Frigo

Prof. Alessandro P. Fantilli, Co-Supervisor

Politecnico di Torino

2024

Declaration

I affirm that the content and structure of this dissertation represent my original work and do not infringe upon the rights of any third parties, including those pertaining to personal data security.

Farmehr M Dehkordi

2024

* This dissertation is presented in partial fulfillment of the requirements for Ph.D. degree in the Graduate School of Politecnico di Torino (ScuDo).

Acknowledgments

I extend my heartfelt gratitude to my parents, whose unwavering guidance and support have been the cornerstone of my journey. Their exemplary role in my life has shaped me into the person I am today, instilling in me values of perseverance, compassion, and dedication. Their sacrifices and encouragement have been a constant source of inspiration, driving me to pursue my dreams relentlessly. Without their love and guidance, I would not have reached this milestone.

Special thanks are due to my brother Farbod, whose infectious joy and carefree spirit have brought immeasurable happiness to our family. His unwavering support and understanding have been a source of strength during challenging times. His presence has filled our home with laughter and warmth, reminding me of the importance of cherishing every moment with loved ones.

I am deeply appreciative of Martina, whose companionship has enriched my life in countless ways. Each shared moment with her is a treasure, and I am excited for the journey ahead as we continue to create lasting memories together. Her unwavering support and belief in me have been a source of motivation, driving me to strive for excellence in all endeavors.

Furthermore, I extend my sincere gratitude to all family members and friends who have stood by my side throughout the ups and downs of my doctoral research and beyond. Their encouragement, words of wisdom, and unwavering belief in my abilities have been instrumental in overcoming challenges and achieving success. Their presence in my life fills me with gratitude and reminds me of the importance of community and support networks.

Lastly, I am profoundly thankful to Professor Barbara Frigo and Professor Alessandro P. Fantilli and Professor Fariborz M. Tehrani for their invaluable mentorship and guidance. From my undergraduate years to my doctoral program, they have provided me with opportunities for growth and learning, pushing me to expand my horizons and pursue excellence in my research. Their continuous support and belief in my potential have been instrumental in shaping my academic journey and preparing me for the future.

Abstract

This doctoral thesis emerges from the crucial need of enhancing the mechanical performance of brittle materials. This study investigates how the addition of reinforcing fibers into brittle materials can substantially improve their ductility, thereby elevating their overall mechanical performance. A key element of this research is the implementation of a two-step casting process. This casting approach, detailed in subsequent sections, ensures the systematic and controlled integration of reinforcements into brittle matrices.

In the initial phase of this study, our focus was directed towards cementitious materials. This thesis presents the results of experimental research conducted on fiber-reinforced cement-based composites, utilizing polymeric aggregate and recycled steel fibers. A total of 18 concrete prisms were cast using a two-stage procedure. The outcomes of this two-stage casting process revealed multiple cracks and a deflection-hardening behavior in the post-cracking regime, as observed during three-point bending tests. Additionally, both flexural and compressive strength exhibited notable improvements with increasing fiber volume fraction.

In the subsequent phase, the study shifts to the reinforcement of ice as a structural material. In regions characterized by cold climates, construction poses significant challenges and expenses, primarily attributed to the logistical complexities of supply transportation. Consequently, relying on conventional materials becomes impractical, particularly in northern areas. Ice presents itself as a practical, locally sourced, bio-based material with various applications. Ice composites, employed in construction for an extended period, have demonstrated versatility.

However, integrating ice into the construction industry presents notable difficulties. Specifically, utilizing ice in structural applications poses two primary concerns: low strength and brittle failure. Therefore, finding a practical solution to address these issues becomes imperative. This thesis presents the outcomes of an experimental campaign on fiber-reinforced ice composites. These composites were crafted using plain water and fortified with organic fibers. A total of 36 ice prisms were meticulously cast, each with varying fiber content, at temperatures of -24°C, -18°C, and -5°C. Subsequent tension and compression tests revealed that both flexural and compressive strength exhibited enhancement with the addition of fibers. Notably, the Fiber-Reinforced Ice (FRI) composites displayed multiple cracks, indicative of ductile behavior, representing a promising solution to the inherent challenges of utilizing ice as a structural material.

This research highlights the significant potential of fiber-reinforced composites to enhance the mechanical performance of brittle materials. By using Fiber-Reinforced Concrete (FRC) as a methodological reference, the study leverages a well-established framework for evaluating mechanical and elastic indices (MI/EI) in composite materials. Drawing parallels between FRC and Fiber-Reinforced Ice (FRI), this approach facilitates the application of proven concepts to FRI, enhancing the understanding and assessment of its properties. The outcomes of this research have the potential to influence the design and development of materials across various industries, paving the way for creating robust and durable structures capable of withstanding challenging mechanical environments.

Notation

B = width of beam cross-section

L = length of the beam span

H = height of the beam cross-section

P = applied load

P_c = maximum load of compression test

P_{cr} = applied load at first cracking in bending

P_u = maximum load of bending test

f_c = compressive strength of ice

$f_{f,u}$ = ultimate flexural strength

$f_{f,cr}$ = flexural strength at cracking

QF = quantity of organic fibers

V_f = steel fiber volume fraction

W = work (or the energy) released during the deflection-hardening

wt = weight of the samples

R^2 = Coefficient of determination

Δ = difference between the deflection measured at P_u and that in correspondence of P_{cr}

η = mid-span deflection

MI = mechanical index

MI_{inf} = minimum required value for MI

S_x = elastic section modulus

Y_G = y-coordinate of the centroid (geometric center)

I_{xG} = inertia about the minor y-axis of section

α, β = parameters in Eq. (5.4)

γ, δ = coefficients of Eq. (2.3) (refer to Table 2.5)

λ = coefficients of Eq. (5.5) (refer to Table 5.12)

A,B,C = coefficients of Eq. (3.4) (refer to Table 3.6)

Contents

1- Introduction & Literature Review…..…..…….…….……..……1

1.1- Recycled Fiber Reinforced Concrete…….…….…….……1

1.1.1- Material Background & Characterizatio.…….……..….1

1.1.2- HPFRCC: High Performance Fiber-Reinforced Cementitious Composites.…….….2

1.1.3- Steel Reinforced Cementitious Composites Elements in Tension….……...……..4

1.1.4- Using Waste Materials in Concrete Mixes……...…..……..6

1.1.5- Eco-Mechanical Analysis……..…….……7

1.1.6- Evaluation Of Ecological & Mechanical Indexes….……..9

1.2- Fiber Reinforced Ice…….……...10

1.2.1- Background & Characterization……...…..…….10

1.2.2- Ice Material Properties…….……..…..……...….12

1.2.3- Ice Reinforcement…….……..……16

1.2.4- Ice Molecular Behavior…….…….……18

2- Recycled Fiber Reinforced Concrete….……..……..…….……...19

2.1- Experimental Procedure…….…….…….19

2.1.1- Introductory Remarks & Work Methodology…….……...……..……..19

2.1.2- Specimen Preparation…….…….……...20

2.1.3- Mixing & Fiber Content…….……...….……24

2.1.4- Testing Procedure…….……..27

2.2- Experimental Data…….……...29

2.2.1- Test results…….…….29

2.2.2- Discussion on the results……..…….…….31

2.2.3- Eco-mechanical analysis ……..…….……...….34

2.3- Cement Based Mortar Case Study ……...……...37

2.3.1- Work Methodology……...…….37

2.3.2- Experimental Procedure & Results ….……..…….38

2.4- Conclusion…….....…….…….....……...43

3- Fiber Reinforced Ice …….…….……...……...……...44

3.1- Experimental Procedure……..……..44

3.1.1- Differences in the work methodology between FRI and FRC …..…….44

3.1.2- Specimen preparation …….……...…….46

3.1.3- Testing Procedure…..…….……..…….50
3.2- Experimental data…….……..……..52
3.2.1- Test results…….……..52
3.2.2- Discussion on the results……...……...…….54
3.3- Conclusion…….…….....……...58
4- Factors Influencing Strength……..……....59
4.1- The Effect of Water-to-Cement Ratio …….……...……..59
4.1.1- Introduction …….…….…….…59
4.2- Ice Temperature sensitivity ……..…….…….……..65
4.2.1- Introduction……...…….…….…….…..65
4.2.2- Experimental data ……...……..……...…….……65
4.2.3- Experimental discusion ……...……...……...…….……72
4.4- Conclusion…….…….....……...81
5- Relationship Between Flexural Strength & Compressive Strength …….....…….....82
5.1- Cement Based Mortar…….……..82
5.1.1- Introduction …….…….…….…82
5.1.2- Experimental Analysis…….... …….…….....…….....……..…..83
5.2- Ice materials..……..…….……..86
5.2.1- Experimental Process.……..…….…….…86
5.2.2- Experimental Analysis...……..…….…….…88
5.3- FRC and FRI.……..……..……..90
5.3.1- Experimental Analysis...……..…….…….…90
5.4- Conclusion….……..…….……...……..94
Conclusion.…….……...……...……..95
References.……...…...……...……...……...97

List of Figures

Chapter 1

1.1 Reinforced cementitious composite structure in tension …..……..……3
1.2 HPFRCC tensile stress-strain diagram ……...……..……4
1.3 Modeled stress-strain curves in design ……...……..……..……5
1.4 The waste hierarchy diagram……...……...……..……6
1.5 Schematic chart for evaluation of Eco-mechanical performances……8
1.6 Compressive and tensile strength versus temperature……13
1.7 A wide range of values for flexural strength of ice…….…….....……14
1.8 (a)Tensile strength of snow/ice plotted against density, (b)Tensile strength plotted against grain….15
1.9 Relative increase in modulus of rupture: 5*10*89 cm3 beams reinforced with various materials; temperature: 12°C to 8°C……17
1.10 Load-deflection for ice cantilever beams with various amounts of reinforcement……17

Chapter 2

2.1. Work Methodology Scheme…….…...……..……..……20
2.2. Specimens preparation mode…….……21
2.3. (a) geometrical properties of the mold, (b) filled mold…….……22
2.4. Specimens after curing……..……..23
2.5. Testing machine…….……24
2.6. Geometrical properties of the recycled steel fibers used in this project…….……25
2.7. Three-point bending tests for cementitious mortars…….……..27
2.8. Scheme of loading machine for compressive test…….…….28
2.9. The load-midspan deflection diagrams measured with the three-point bending tests……..……..29
2.10. The results of the three-point bending tests……30
2.11. Possible $f_{f,u}$ vs. V_f relationships ……...……...……33
2.12. The non-dimensional diagram used for the eco-mechanical analysis…….35
2.13. The eco-mechanical analysis of the HPFRC investigated herein……...36
2.14. Some concrete elements…….…...……...……37
2.15. Three-point bending tests on samples extracted from corrugated slabs…….38
2.16. Three-point bending tests on concrete rings of manhole covers…….38
2.17. The load-midspan deflection diagrams measured with the three point bending tests……39

2.18. Possible $f_{f,u}$ *vs.* V_f relationships……..……..…41
2.19. Comparison between the strength of series 1 and series 2……....……..42

Chapter 3

3.1. Resin mold and the plain ice specimen …...……..…..……...44
3.2. Polystyrene Molds for Ice Specimens…….……45
3.3. Pine needle used as fiber-reinforcment for ice……46
3.4. Geometrical properties of pine needles used in this project……...47
3.5. Pine needle used as fiber……..……48
3.6. Fiber-reinforced ice specimens geometrical measurments……49
3.7. Mechanical performances of Fiber reinforced ice……..50
3.8. Load-midspan deflection diagrams measured with three-point bending tests……52
3.9. Results of three-point bending tests……53
3.10. Average values of strength measured in flexural and compressive tests……55
3.11. Quadratic regression between f_c, $f_{f,cr}$, $f_{f,u}$, W, and the quantity of fibers (QF)……56

Chapter 4

4.1 Relationship between water to cement ratio and compressive strength…….60
4.2 Relationship between water to cement ratio and split tensile strength……...60
4.3 Compressive strength for different FRCA replacement……..…….63
4.4 (a): Detaching the Ice Samples from the Polystyrene Mold. (b): De-molded ice specimens…….66
4.5 Load-midspan deflection diagrams measured with three-point bending tests……68
4.6 Load-midspan deflection diagrams measured with three-point bending tests……69
4.7 Load-midspan deflection diagrams measured with three-point bending tests……70
4.8 average flexural and compressive strength results of plain ice and FRI-1……..74
4.9 Average values of strength measured in flexural and compressive tests (-18°C)……...……75
4.10 Average values of strength measured in flexural and compressive tests (-24°C)……...……76
4.11 Quadratic regression of $f_{f,cr}$, $f_{f,u}$, W, and f_c, with respect to the quantity of fibers QF (-18°C).. …77
4.12 Quadratic regression of $f_{f,cr}$, $f_{f,u}$, W, and f_c, with respect to the quantity of fibers QF (-24°C).. …78
4.13 average flexural and compressive strength results……..80

Chapter 5

5.1 (a): Three-point bending tests for cementitious mortars, (b): Compressive test…..……...……84
5.2 Load deflection diagram for cement-based mortar…….84
5.3 Tests on plane ice specimens……..86

5.4 Load deflection diagram for Ice specimens……87
5.5 The average values of flexural and compressive strength of ice and mortar……..88
5.6 Possible relationships among the strengths: (a) f_c vs. $f_{f,cr}$; (b) f_c vs. $f_{f,u}$..……..……..91
5.7 Linear regression between $f_{f,cr}$, $f_{f,u}$ and f_c..……..……..……..92

List of Tables

Chapter 1

1.1 Carbon footprint and embodied energy of concrete components……...……..……..10
1.2 Some historical events regarding the ice structural application……..……11
1.3 compressive strength values of ice……...……..13

Chapter 2

2.1. Compositions of the UNI-sand according to UNI EN 196-1…..……..……..……26
2.2. Compositions of the series investigated in this research……26
2.3. Mechanical and geometrical properties measured in the experimental analysis……31
2.4. The average values of the strengths measured in the experimental analysis……..32
2.5. The parameters γ and δ to be used in Eq. (2.3)…….…..33
2.6. The evaluation of EI referred to 1 m^3 of HPFRC……...……35
2.7. Mechanical and geometrical properties measured in the experimental analysis ..…….....…..……40
2.8. The parameters γ and δ to be used in Eq (2.3)……40

Chapter 3

3.1. Ice specimen with freezing temperature of -5°C properties…..……...46
3.2. Size and density measurements for samples with freezing temperature of -18 degree Celsius…….49
3.3. Mechanical properties measured in the three-point bending test……53
3.4. strength values measured in flexural and compressive analysis…….54
3.5. values of the parameters A and B and C in Eq. 3.3……..……..57

Chapter 4

4.1. Results of Slump Test on Concrete and Lateritic Concrete Mixes…….61
4.2. Size and density measurements for specimens with freezing temperature of -18°C ……..……67
4.3. Mechanical properties measured in the three-point bending test……71
4.4. strength values measured in flexural and compressive analysis…….73
4.5. values of the parameters A and B and C in Eq. 4.1 for specimens with two freezing temperatures..79

Chapter 5

5.1. Compositions of the UNI-sand according to UNI EN 196-1…….…..……...……83
5.2. Composition of the cement-based mortar……...83

5.3. Properties of the cement-based mortar……...83
5.4. Result of flexural and compressive tests performed on mortar specimens…….85
5.5. Ice specimen properties……...86
5.6. Result of flexural and compressive tests on ice……..87
5.7. Ice compressive strength evaluated by Wu et al (2020) at different temperatures…….……88
5.8. The ratio flexural/compressive strength in mortar and ice…….89
5.9. The ratio flexural/compressive strength in mortar and ice……...90
5.10. The parameters α and β to be used in Eq.(5.4)……...……91
5.11. strength values measured in flexural and compressive analysis……92
5.12. values of the parameters ὼ. and R^2 in Eq. 5.5…….……93

Chapter 1:

Introduction & Literature Review

1.1- Recycled Fiber Reinforced Concrete

1.1.1- Material Background & Characterization

The concrete construction industry stands as a significant contributor to environmental degradation due to substantial annual greenhouse gas emissions. At the forefront of this environmental impact is the carbon footprint associated with portland cement, constituting approximately 6% of the Earth's yearly carbon dioxide production [1]. The extraction of natural resources, notably aggregates, further intensifies the industry's ecological impact. Aligned with global sustainability goals outlined in the 2030 Agenda for Sustainable Development, research is increasingly focusing on substituting traditional concrete components with recycled materials, such as plastic or rubber from end-of-life tires, to address concerns related to resource depletion and waste landfill issues [2].

Using recycled materials in concrete reduces the need for traditional cement, which in turn lowers its carbon footprint. Furthermore, recycling these materials decreases the energy required for processing and helps manage waste, aligning with sustainability objectives. Although this method doesn't directly cut cement's carbon emissions, it supports overall efforts to lessen environmental impact [1]. Recycled plastic, for instance, can be used as a partial replacement for aggregates, improving the flexibility and reducing the density of concrete [3]. Rubber from discarded tires is another promising material that enhances the shock absorption properties of concrete, making it suitable for applications where impact resistance is critical [4]. Additionally, recycled glass can be finely ground to replace a portion of cement, contributing to a reduction in carbon emissions associated with cement production [5]. Industrial by-products like fly ash and slag not only provide an effective way to recycle waste but also enhance the durability and strength of concrete [6]. These innovative approaches not only help in managing waste effectively but also contribute to the development of more sustainable construction practices.

Steel waste originating from discarded tires emerges as a notable environmental challenge, particularly in developing countries where tire management heavily relies on environmental regulations [7]. The improper disposal of approximately 1 billion tires globally each year not only poses environmental risks but also raises concerns about public health [8]. In response, the European Commission has mandated that EU countries develop markets for used tires as secondary raw materials. This initiative aims to mitigate the environmental impact of tire disposal and address concerns related to the energy recovery practices in cement kilns [9].

Recycled fibers from tires, with a particular emphasis on steel fibers from End-of-Life Tires (ELTs), play a crucial role in the development of sustainable concrete [10]. While these fibers offer unique advantages, managing their diverse composition poses challenges that impact the workability of the concrete mixture. Despite these challenges, the well-established technique of

reinforcing concrete matrices with discontinuous steel fibers is known for enhancing the mechanical properties of concrete, particularly influencing post-cracking behavior [11]. However, the use of recycled materials in concrete production presents challenges in terms of reduced strength, especially in compression, compared to traditional concrete [12].

Addressing the disposal of steel waste from discarded tires necessitates a comprehensive approach that takes into account both environmental and health factors. The implementation of sustainable tire disposal practices, such as recycling tire steel in concrete, not only helps mitigate environmental harm but also opens avenues for innovative materials with improved properties. This approach contributes to fostering a more sustainable and eco-friendly construction industry, aligning with the broader goals of global sustainability [13].

1.1.2- HPFRCC: High Performance Fiber-Reinforced Cementitious Composites

Concrete is a widely used building material known for its strong compression strength but falls short in tensile strength, being only about one-tenth of its compressive strength. In areas with significant tensile stress, where steel rebar is typically employed, concrete alone proves inadequate. Innovative concrete forms like High Strength (HSC), High Performance (HPC), and Ultra High Performance concrete (UHPC) have been developed to enhance mechanical properties and durability. However, these innovations introduce challenges such as increased brittleness and autogenous shrinkage due to improved micro-structure [14].

The drawbacks associated with new concrete forms can be effectively addressed by incorporating significant quantities of short steel fiber, resulting in High Performance Fiber-Reinforced Cementitious Composites (HPFRCCs). The mechanical effectiveness of HPFRCCs relies on ensuring an even distribution of fibers throughout the material's bulk, minimizing vulnerability in areas lacking fibers [15]. The distribution is influenced not only by the method of fiber incorporation but also by the shape of the cast material. HPFRCCs, a distinct group of fiber-reinforced cement-based composites, possess the unique ability to flex and self-strengthen before failure, addressing the shortcomings of conventional concrete, such as brittleness and limited long-term durability.

Strain hardening is a critical function of HPFRCCs, enabling the material to strengthen as it undergoes plastic deformation beyond its limit. This is achieved through the development of multiple microscopic cracks, contrasting with the single crack and strain softening behavior of traditional fiber-reinforced concrete. The low density of HPFRCCs presents another positive property, making them potentially more energy-efficient in production and treatment compared to traditional concrete. Compared to lightweight aggregate high-performance concrete (HPC), High-Performance Fiber-Reinforced Cement Composites (HPFRCCs) generally offer enhanced material properties and compositions that result in lower densities. HPFRCCs typically have densities ranging from 1,800 to 2,400 kg/m³, while lightweight HPC usually falls within the range of 1,400 to 2,000 kg/m³. Although lightweight HPC can be lighter at the lower end of the spectrum, HPFRCCs often provide lower densities than traditional concrete (about 2,400 kg/m³) and, in some cases, even lightweight HPC at the upper end of the density range [16]. This characteristic, coupled with their lightweight structure and strain-hardening capabilities, positions HPFRCCs as a promising alternative with enhanced durability and efficiency [17].

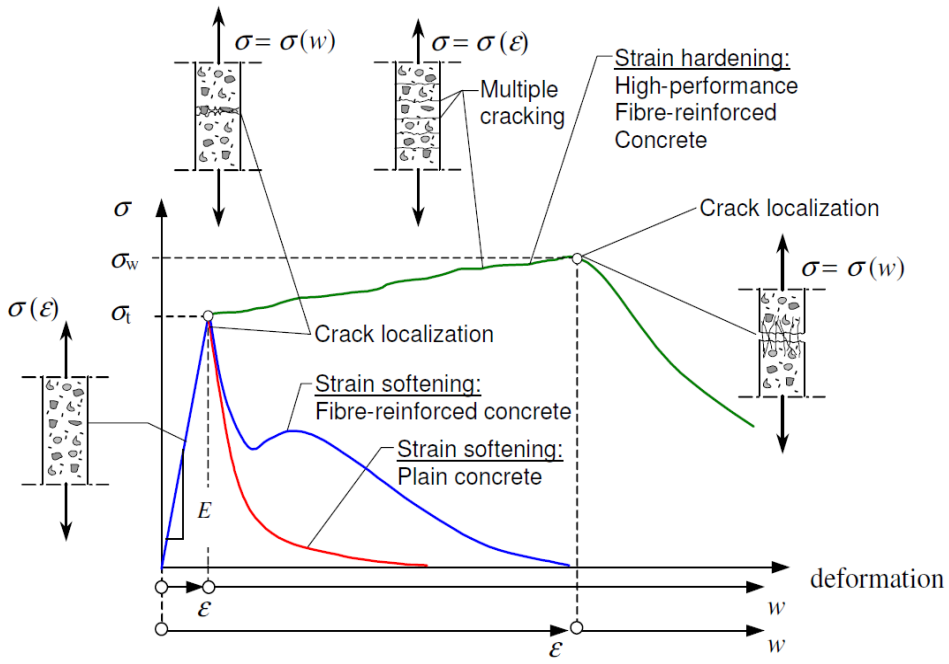

Figure 1.1: Fiber reinforced cementitious composite structure in tension [17]

To reduce steel corrosion in reinforced concrete structures, there is a need to minimize crack width in tensile concrete. Fiber-reinforced concrete (FRC), including High Performance Fiber-Reinforced Cementitious Composites (HPFRCC), proves advantageous in achieving higher ductility and mechanical properties compared to ordinary concrete. However, concrete alone cannot generate tensile stresses comparable to those of steel rebar. In response, HPFRCC have been developed to enhance ductility significantly [18]. Uniaxial tensile tests on concrete prisms reveal a nearly linear stress-strain relationship up to the peak stress, at which point failure occurs due to a single crack, leading to a softening regimen. This behavior can be effectively modeled using a fictitious crack model or a crack band model [19].

Reinforced concrete (RC) structures, especially in areas where they are stretched, often show a complicated pattern of cracks inside. Many tests on stretched RC parts have been done to understand this. The formation of these cracks is mainly due to how steel and concrete grip together, letting the tension (pulling apart) stresses move between two main cracks in the concrete. This complex crack pattern highlights the importance of carefully studying how RC beams behave when stretched [20].

High Performance Fiber-Reinforced Cementitious Composites (HPFRCC) have different recipes, leading to significant differences in how they are structured. Despite these differences, most HPFRCC include small particles, a super-plasticizer, fibers made of plastic or metal, cement, and soil. What makes HPFRCC different from regular concrete is that it doesn't have large particles. Usually, fine particles like silica sand are used in HPFRCCs. However, there are challenges in using a lot of fibers and preventing them from forming clumps, especially with waste steel fibers.

Making sure the fibers are spread out efficiently in the concrete is crucial, which means using more fibers for better distribution and overall effectiveness.

1.1.3- Steel Reinforced Cementitious Composites Elements in Tension

High-performance cementitious composites strengthened by fibers (HPFRCC) are special materials that not only have great strength and resist water penetration but also show flexibility and tiny crack growth when stretched. These qualities come from the super tightly packed structure of the cement mix, along with the use of tiny fibers that can limit the width of cracks. This makes HPFRCC suitable for fixing, renovating, or upgrading reinforced concrete structures [21].

HPFRCC is a kind of cemented material known for becoming significantly harder when pulled and, as a result, being very flexible. These materials are made by combining strong concrete with fibers in a way that is more consistent, using fine sand instead of the usual large particles.

Figure 1.2 shows how HPFRCC material responds when pulled from both ends. Many cracks spread evenly, making the stretching look the same across the material. As the material stretches more, only a few cracks widen, and this is called strain softening. A lot of research has been done to understand and improve the properties of this material, as well as to develop ways to make it, and ideas for how it can be used [22].

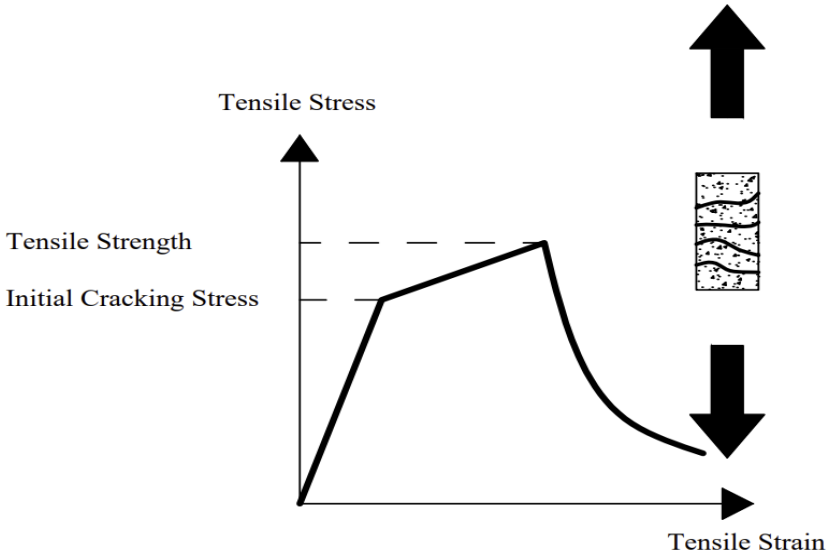

Figure 1.2: HPFRCC tensile stress-strain diagram [22]

In figures 1.1 and 1.2, the unique qualities of High-Performance Fiber-Reinforced Cementitious Composite (HPFRCC), such as strain hardening and multiple cracking, are explained in detail. It is important to use this material properly to take advantage of these innovative features, considering specific performance criteria for structures. One crucial criterion is the crack width limitation, which ensures that cracks remain controlled. For instance, in HPFRCC beams, a crack

width of less than 0.2 mm is often considered acceptable with respect to diffusion [23]. This minimizes the risk of water and chloride ingress, which can lead to reinforcement corrosion and structural deterioration.

As the demand for more durable concrete structures increases, minimizing crack width becomes a key strategy for ensuring robustness. For example, in a bridge deck, ensuring that cracks remain fine and well-distributed under load can greatly enhance the durability and longevity of the structure, reducing maintenance costs and improving safety [23].

To assess the strength of HPFRCC in carrying tensile loads, which is beneficial for structural purposes, a comprehensive evaluation is needed. Although explicit information on deformation is not provided, it is anticipated that structures using HPFRCC with a critical stress comparable to reinforcement yield strain will require more energy for deformation. Various tests with different specimen sizes, shapes, and conditions were proposed and conducted to understand the tensile stress-strain relationship [23]. It is essential for the tensile properties used in design to align with real-world application conditions.

Instead of solely relying on existing conditions, it is crucial to carefully validate the correlation between the test results and current conditions under various circumstances. The bi-linear stress-strain model [24], illustrated in Fig. 1.3, outlines the HPFRCC tensile stress-strain relationship following the Japan Society of Civil Engineers (JSCE) 2005 guidelines [25]. These guidelines recommend initial cracking force and strain at tensile strength as common values for assessing the modeled stress-strain relationships.

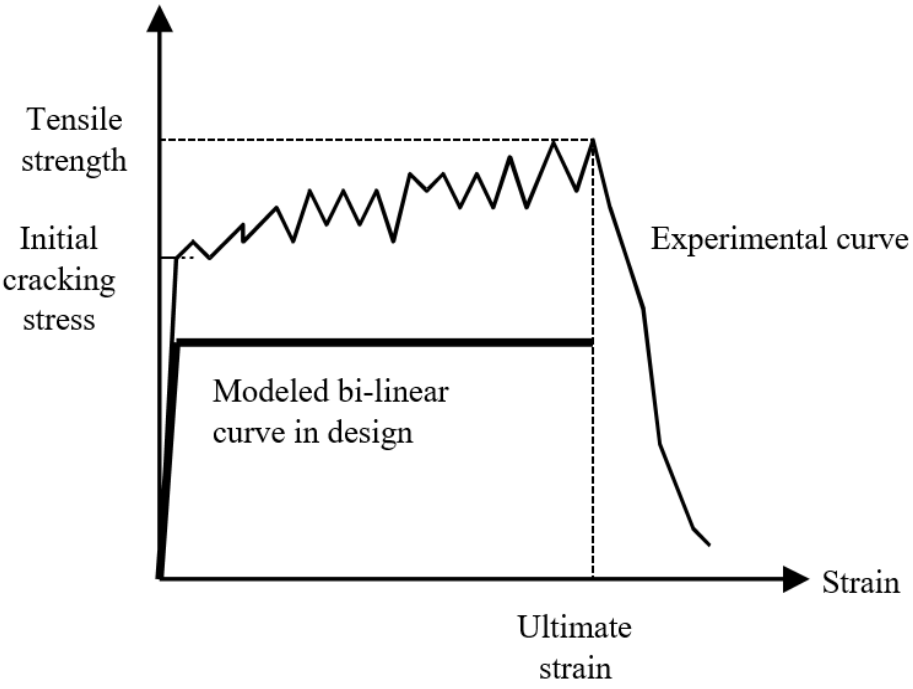

Figure 1.3: Modeled stress-strain curves in design

1.1.4- Using Waste Materials In Concrete Mixes

Due to the increasing global population, the amount and types of waste have also grown. Some of this waste, which does not decompose quickly, can stick around for hundreds or even thousands of years. As mentioned earlier, these non-decomposing wastes create a significant problem by piling up and causing environmental issues. The challenge of waste disposal is a global issue, especially in densely populated areas, where most of these items end up in specific areas like stockpiles around towns, landfills, or even through illegal dumping [26].

Handling such massive amounts of waste is a challenge. However, by finding more sustainable ways to use these waste products, we can lessen the environmental impact. This approach is referred to as "Hierarchy of Wastes". The goal is to prioritize reducing, reusing, or recycling waste, with recycling being the preferred method of waste disposal [27]. Fig. 1.4 illustrates the structure of waste to provide a visual representation. The so called “Hierarchy of Wastes” is a framework that establishes a preferred sequence of actions to manage waste in a manner that minimizes its environmental impact. Typically depicted as a pyramid, it prioritizes the most environmentally friendly options at the pinnacle.

At the top of the pyramid is "prevention," which aims to reduce waste generation by encouraging product design that minimizes waste, promoting reusable products, and fostering behavior changes. Next is "minimization," focusing on optimizing processes to reduce waste during manufacturing and consumption. "Reuse" follows, encouraging the repair, refurbishment, or donation of products to extend their lifespan. "Recycling" involves converting waste materials into new products or materials, followed by "energy recovery," which harnesses energy from waste that cannot be recycled. Lastly, "disposal" is the least preferred option, involving the final disposal of waste through landfilling or incineration without energy recovery [27].

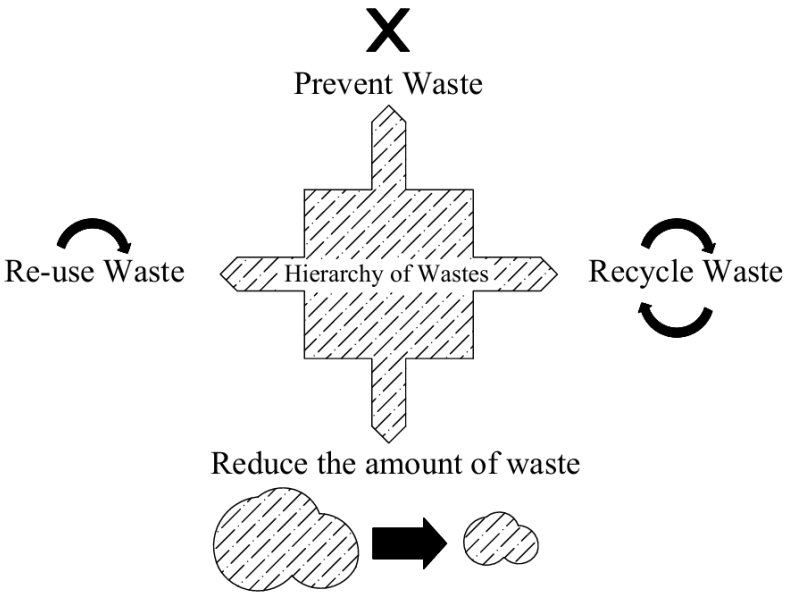

Figure 1.4: The waste hierarchy diagram [27]

Ongoing discussions are gradually exploring innovative uses of waste materials in modern applications. These research initiatives aim to fulfill society's need for environmentally friendly and cost-effective waste disposal. Utilizing recycled aggregates not only conserves natural resources and reduces waste space but also contributes to maintaining a healthy climate [28].

In practice, it is advisable to develop recycling plans before starting any construction project. These plans specify the types of waste expected, outline handling methods, and establish procedures for recycling and disposal. Moreover, designated areas should be marked for the temporary collection or storage of construction waste materials.

1.1.5- Eco-Mechanical Analysis

In the novel construction industry, a fundamental concept revolves around drastically reducing cement usage in new concrete structures, primarily for environmental reasons. However, achieving a balance between mechanical and environmental efficiency is a complex challenge. To develop eco-friendly and high-performance cement-based composites, a thorough comparison of various concrete mixes is necessary. It is noteworthy that 90% of the total life-energy for concrete structures is consumed in material production, mainly clinker, with only 10% associated with manufacturing, transport, and utilization. Eco-design approaches should prioritize components with low embodied energy, a low carbon footprint, and reduced concrete mass [29].

To meet these eco-design goals, several techniques can be applied. The product efficiency approach focuses on clinker reduction by minimizing the total amount of concrete and, consequently, the volume of structures. Mechanical efficiency, such as compressive strength, must be improved under the same loading conditions compared to traditional concrete. Another technique involves material replacement, substituting clinker with cemented and/or pozzolanic mineral admixtures like fly ashes. Additionally, utilizing Life Cycle Assessment (LCA) aids in selecting concrete materials with the lowest carbon footprint [29].

While these techniques contribute to environmental sustainability, they may introduce drawbacks in concrete's mechanical performance. For instance, concrete with high strength can exhibit brittle behavior, especially under compression. Even when cement is partially replaced by mineral additives, compressive strength may not significantly alter, but the post-peak response can become more brittle than ordinary concrete. Despite potential drawbacks in mechanical efficiency, using recycled aggregates with a favorable carbon footprint, instead of virgin aggregates, can lead to a drastic reduction in compressive strength, exceeding 50% [29].

In evaluating concrete mixtures, various attributes such as strength and ductility must be weighed against environmental impacts. Nowadays, however, the ideal concrete mixture is also determined by considering its ecological characteristics along with its mechanical properties. Striking a balance between these factors is crucial for advancing sustainable construction practices in the modern era. In the context of evaluating concrete's environmental impact, researchers like Fantilli and Chiaia [30] proposed the Eco-Mechanical Index (EMI) defined as:

$$EMI = \frac{\mathrm{MI}}{\mathrm{EI}} \tag{1.1}$$

where MI is the Mechanical Index and EI the Ecological Index. On the other hand, in the context of evaluating concrete's environmental impact, researchers such as Damineli et al. have proposed additional ecological factors. [31]. They consider factors such as the total carbon dioxide emitted and the quantity of binder needed to produce 1 MPa of compressive force to define the environmental impact (EI). However, this approach, shared by Flower and Sanjayan [32], tends to focus only on compressive strength, neglecting post-peak energy absorption (ductility) and underestimating the beneficial effects of fibers. For instance, if the fiber volume fraction is less than 1%, the strength (and MI) may not differ significantly from non-fiber-reinforced concrete, but the environmental impact (and EI) increases. Consequently, Fiber-Reinforced Concrete (FRC) might exhibit poorer eco-mechanical efficiency than regular concrete.

A more sophisticated concept of EMI suggests pairing product properties with structural efficiency at serviceability and ultimate limit stages. This entails not solely relying on concrete strength but also considering other mechanical properties, particularly when full-scale concrete members are involved. Fantilli and Chiaia [30] propose a novel eco-design method that evaluates MI based on not only concrete strength but also other mechanical properties, such as elasticity, toughness, and ductility. They emphasize that serviceability and durability, associated with the fracture mechanism in tension, can be evaluated using the work of fracture, especially for Reinforced Concrete (RC) beams with narrow crack widths, as allowed by code rules (UNI EN 196-1).

Fantilli and Chiaia's research employs a chart (Fig. 1.5) where the mechanical response (MI divided by MI_{inf}) is recorded on the horizontal axis, representing the mechanical characteristics' lowest bound value. Simultaneously, the ecological performance (EI divided by EI_{sup}) is recorded on the vertical axis, reflecting the upper limit value of ecological impact expressed by EI_{sup}. This innovative approach aims to provide a more comprehensive understanding of the eco-mechanical efficiency of concrete, considering both its mechanical properties and environmental impact.

The chart distinguishes four different zones: Zone I with low mechanical and ecological performances, Zone II with high mechanical but low ecological performances, Zone III with high mechanical and ecological performances, and Zone IV with low mechanical but high ecological performances.

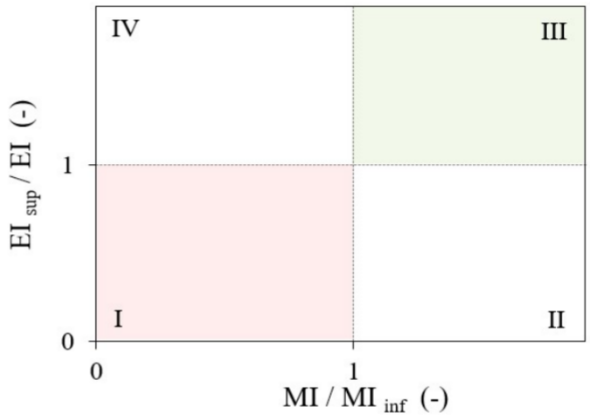

Figure 1.5: Schematic chart for evaluation of Eco-Mechanical performances

In summary, when mineral additives and fiber reinforcement are combined effectively, it opens the door to a new category of cement-based composites. These composites not only match the mechanical strength of traditional concrete but also bring about a positive impact on the environment and enhanced durability. By skillfully blending these components, we have the potential to create materials that offer a balanced solution, maintaining the robustness expected from conventional concrete while lessening the environmental footprint. This conclusion suggests a promising direction for sustainable construction practices, where we can achieve both structural strength and improved ecological responsibility through the thoughtful integration of mineral additives and fiber reinforcement.

1.1.6- Evaluation of Ecological & Mechanical Indexes

The key ecological factors we consider are the carbon footprint, embodied energy, and water usage per cubic meter of concrete, as outlined in the fib-Guidelines for Green Concrete Structures [30]. Additionally, waste management is a crucial factor for assessing the ecological impact of concrete as highlighted in earlier sections. To calculate the Ecological Index (EI), we use the following equation:

$$EI = (\alpha \cdot wc_{\alpha}) \cdot (\beta \cdot wc_{\beta}) \cdot (\gamma \cdot wc_{\gamma}) \quad (1.2)$$

α = quantity of carbon dioxide (CO_2)

β = quantity of embodied energy

γ = volume of water

The ecological performance of concrete is influenced by local conditions, such as water availability, transportation, and raw material extraction. To account for these factors, three weighting coefficients (wc_{α}, wc_{β}, wc_{γ}) are introduced in Eq. (1.2), allowing adjustments based on considerations like water scarcity or the distance between the concrete plant and the construction site. For example, a longer transportation distance may increase the value of wcɣ due to the environmental impact of transportation [33-34].

Additionally, Eq. (1.2) can be expanded to include other parameters like biodiversity, toxic substances, and resource depletion. However, for the evaluation of ecological performance in this context, we focus specifically on the carbon footprint and embodied energy of cement and steel fibers. These values, obtained from sources like fib and the Eco Invent database [59-60], are summarized in Table 1.1. It is important to note that this procedure is designed for comparing similar types of concrete cast in the same location with identical aggregates, rather than for detailed calculations.

When considering recycled steel fibers, the process of shredding tires and separating rubber and steel incurs some expenses. Despite this, for the purpose of this assessment, it is assumed that recycled steel fibers have zero carbon and energy impacts. However, it is crucial to acknowledge the environmental impacts related to the end-of-life treatment of the product. By assuming no environmental impact for recycled steel fibers, the net CO_2 savings when the product is reused or recycled are recognized and credited [33-34].

Table 1.1. Carbon footprint and embodied energy of concrete components

	Carbon footprint ($kgCO_2/kg$)	Embodied energy (MJ/kg)
Normal Portland Cement	0.90	4.73
Industrial Steel fibers	1.50	20.60
Recycled fibers	0.00	0.00

In accordance with fib [34], both the material and the structural performances must be incorporated into the mechanical index. Thus, MI can be estimated by means of the following equations:

$$MI = mp_m * mp_s \tag{1.3}$$

Where mp_m is the mechanical parameter of concrete material and mp_s the mechanical parameter of concrete structure, respectively. In considering durability, the material property mps is inversely related to the crack width measured under a predetermined external load. In Reinforced Concrete (RC) structures, permeability is primarily influenced by cracks in the tensile zones rather than concrete porosity. These cracks result from the interaction known as "tension stiffening" between concrete and steel. Both numerical simulations and experimental findings indicate that a higher fracture energy of concrete leads to a narrower crack width due to tension-stiffening. Essentially, the work of fracture in tension becomes a crucial factor in assessing the durability performance of Reinforced Concrete (RC) structures, and mpm can be equated to the work of fracture.

1.2- Fiber Reinforced Ice

1.2.1- Background & Characterization

Many materials used in engineering today are created artificially, providing engineers with better control over their properties and a more consistent composition. Examples of these man-made materials include steel, various metals and alloys, ceramics, concrete, asphalt, plastics, and other synthetic organic compounds [35]. These materials have controllable properties, allowing for the prediction and reliance on their mechanical behavior. Although ice is a naturally occurring solid, it is also considered an engineering material due to its numerous applications.

In the realm of scientific research, there is a growing emphasis on creating new materials and technologies, particularly in Cold Regions. Ice has gained increased attention as both a subject for scientific study and a material that could address significant issues in Civil Engineering [36], such as constructing temporary buildings and long-term hydraulic systems in polar climates. Construction in these areas is challenging and expensive due to logistical difficulties in transporting supplies, and ice offers a potential solution to reduce resource needs.

The use of ice in Engineering has a historical context, dating back to the 19th century when ice blocks were traded globally in the frozen water industry for the storage and preservation of food and other commercial purposes. Ice composites, notably the igloo, have been used to construct structures since ancient times [37].

Table 1.2. Some historical events regarding the ice structural application [35-36]

Period	Material or Method	Structure
Ancient	Lichen	Igloo
Second world war	logs, branches and twigs Wood pulp (pykrete)	Ice roads and ferries Aircraft carrier
Cold war	Fiberglass Sawdust (pykrete) Wooden covering	Ice airstrip Ice roads crossing swamps Ice working space
Nowadays	Geo-nets from fiberglass Cytotropic gel formation Pykrete	Ice roads Watertight elements Ice dome

In recent years, one of the most notable engineering applications of ice has been in the creation of ice hotels and other temporary structures. These constructions, known for their strength, showcase intricate designs and stunning beauty [38]. Ice blocks are meticulously carved, stacked, and fused together to form walls, floors, and even furniture, highlighting the durability and hardness of this frozen element. Table 1.2 provides an overview of the evolution of ice structure formation. Ice constructions can be implemented in countries with a Polar Environment.

Ice is a readily available natural material with various applications, including structural uses [39]. Recently, there has been an increased interest in utilizing ice and snow architecture for festivals and exhibitions. Moreover, exploring new applications for constructing ice-based infrastructure in Polar Regions with consistently low temperatures is gaining attention. These constructions, often simple and low-tech, have proven to be energy-efficient and environmentally sustainable [40].

In regions with year-round low temperatures, such as over half of the Russian Federation, natural cooling ice and ice ground installations can be constructed and operated. Countries like Canada, Norway, Sweden, Finland, Switzerland, Austria, and Japan have successfully built ice structures, particularly bridges, using a straightforward technique. By spraying water over specially designed molds, ice bridges are formed, gradually freezing into robust, load-bearing structures. However, the use of freshwater for constructing these ice structures necessitates careful environmental consideration [41]. These ice bridges offer an affordable and environmentally friendly option for temporary crossings in remote areas or during winter celebrations.

Ice buildings can serve as a practical alternative to traditional construction materials, especially in challenging environments where conventional structures may face difficulties. Ongoing research is investigating the feasibility of constructing durable ice buildings in Arctic regions. This involves innovative insulation methods and unique designs to withstand extreme weather conditions. Despite extensive research on ice composites, the actual implementation of ice constructions remains limited. This limitation is mainly attributed to a gap between the development of reinforcement techniques and the practical application of construction methods in the field of Ice Engineering [42].

1.2.2- Ice Material Properties

The strength of ice plays a crucial role in Ice Engineering, influencing various problem-solving methods. An example of this is to understand the local and global pressure that ice exerts on a structure, which is essential for design purposes. Ice strength, defined as the highest load a material can support, is a key consideration. However, ice structures face challenges due to weak strength and brittle failure. In the past, field and laboratory testing were conducted to determine the required ice strengths for engineering calculations [40]. Enhancing the understanding of ice behavior under different loads and conditions allows engineers to improve the reliability and durability of ice structures.

High temperatures significantly affect the behavior and safety of ice structures. Exposure to elevated temperatures alters the properties of ice, making it difficult to ensure structural stability and safety. In warmer climates, ice constructions are unsuitable for commercial use due to their tendency to melt and lose strength. Moreover, higher temperatures accelerate the melting of ice, which shortens the lifespan of the structure. The mechanical properties of ice are temperature-dependent, even in the coldest regions, necessitating measures for melting protection to maintain desired qualities and stability [43]. Climate change and global warming exacerbate these challenges by increasing global temperatures and causing more frequent heat waves, leading to accelerated melting and reduced reliability of ice structures [44]. As a result, innovative engineering solutions and materials are required to adapt to these changing conditions and mitigate the effects of rising temperatures on ice structures.

Various tactics are employed to ensure the safety and endurance of ice formations and mitigate the negative impacts of high temperatures. Insulation techniques, such as using insulating materials or creating air gaps, reduce heat transfer and maintain lower internal temperatures. Active cooling technologies, such as refrigeration or fluid circulation, may also be utilized to counter the effects of external heat sources.

Ice exhibits significantly lower strength in tension compared to compression, resembling un-reinforced concrete in this aspect. The tensile strength of ice is approximately one-tenth of its compressive strength. For temperatures below -5°C, freshwater ice typically shows an average compressive strength of 1.73 MPa. Additionally, Table 1.3 provides the compressive strength values of ice measured by Wu et al, where strength increases with decreasing freezing point [45].

Table 1.3. compressive strength values of ice

Temperature (°C)	compressive strength f_c (MPa)
-5 °C	1.78
-10 °C	2.59
-15 °C	3.08
-20 °C	3.40

At temperatures between -10°C and -20°C, ice has a compressive strength of 5-25 MPa. As illustrated in the graph below, the strength of ice increases as temperature decreases in both tension and compression. However, the impact of temperature on strength is more pronounced in compression than in tension [46]. It is important to note that ice's strength is not a singular property. The compressive strength values obtained from tests are index values with limited practical applications because ice is a natural material with inherent variations. Various factors, including strain rate, temperature, grain size, grain structure, and porosity, all influence ice strength.

In addition to its compressive strength, ice often exhibits lower shear strength. For example, depending on factors like grain size and density, the shear strength of freshwater ice at temperatures below -5°C can vary from 0.2 to 0.7 MPa [46].

A three-point or four-point bending test assesses the flexural strength of ice. For temperatures below -5°C, freshwater ice typically shows a range of 0.5 to 3 MPa in flexural strength, with an average of 1.73 MPa. Although there is little dependence on temperature or strain rate, there is considerable variability in measured flexural strength, with smaller samples yielding higher values and larger samples yielding lower values.

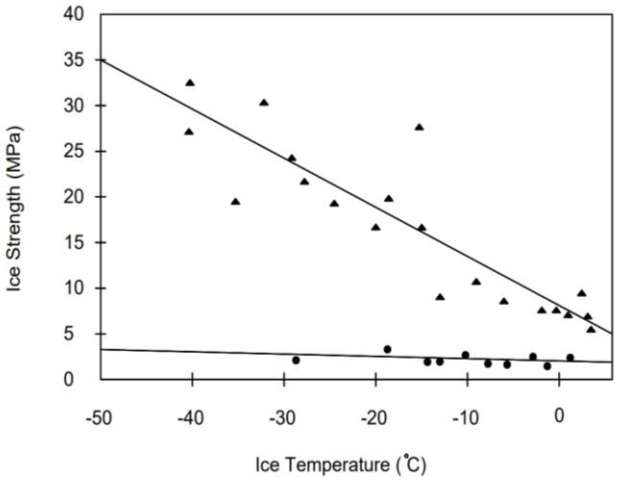

Figure 1.6: Compressive and tensile strength versus temperature [45]

While there is little dependence on temperature or strain rate, there is a considerable range in measured flexural strength. Smaller samples tend to yield higher values, while larger samples show lower values [47]. The following graph highlights the significant difference in behavior between the compressive and tensile strengths of ice as the temperature varies. Compressive strength decreases sharply with increasing temperature, while tensile strength remains low and relatively unchanged.

On the contrary, based on earlier research, there is a method to estimate flexural strength using compressive strength, and it aligns with the conventional approach proposed by Eurocode 2 (UNI EN 1992-1-1, 2004) for concrete. This methodology can be readily extended to apply to ice as well, as suggested by Famtilli and Frigo Dehkordi in 2022. The details of this extension will be discussed in Chapter 3 [48].

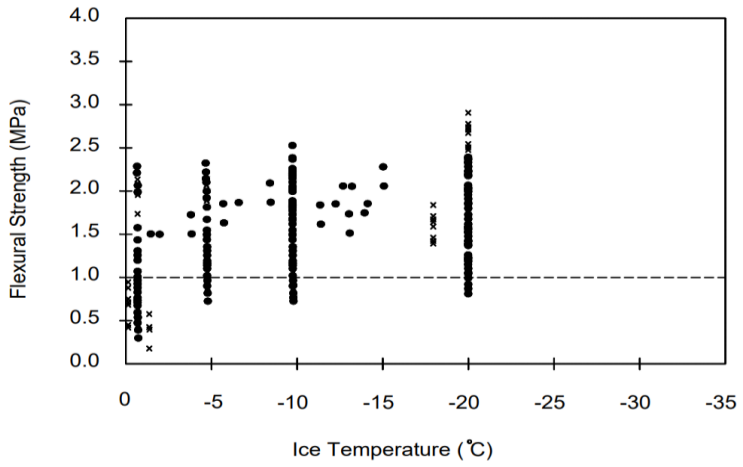

Figure 1.7: A wide range of values for flexural strength of ice [46]

In recent studies, the flexural strength and the mechanical behavior of ice under different loading conditions have been extensively analyzed by researchers at Dartmouth's Ice Research Laboratory (IRL), led by Professor Erland M. Schulson. Their work has significantly contributed to our understanding of the flexural properties of ice, particularly in the context of bonded ice. For instance, Murdza et al. (2021) investigated the flexural strength of bonded ice and provided valuable insights into the factors that limit this strength under various environmental conditions [49]. Additionally, Renshaw and Schulson (2017) explored strength-limiting mechanisms in ice, specifically focusing on high-confinement brittle-like failure, which has profound implications for the design and engineering of ice structures under stress. Their findings suggest that adiabatic transformational faulting plays a crucial role in limiting the strength of ice, providing a deeper understanding of its mechanical behavior under extreme conditions [50].

As per existing research, the typical tensile strength of ice within the temperature range of 10 to 20°C is recorded at 1.43 MPa. It is worth noting that the tensile strength of ice tends to decrease as the grain size increases, as highlighted by J.J. Petrovic [46].

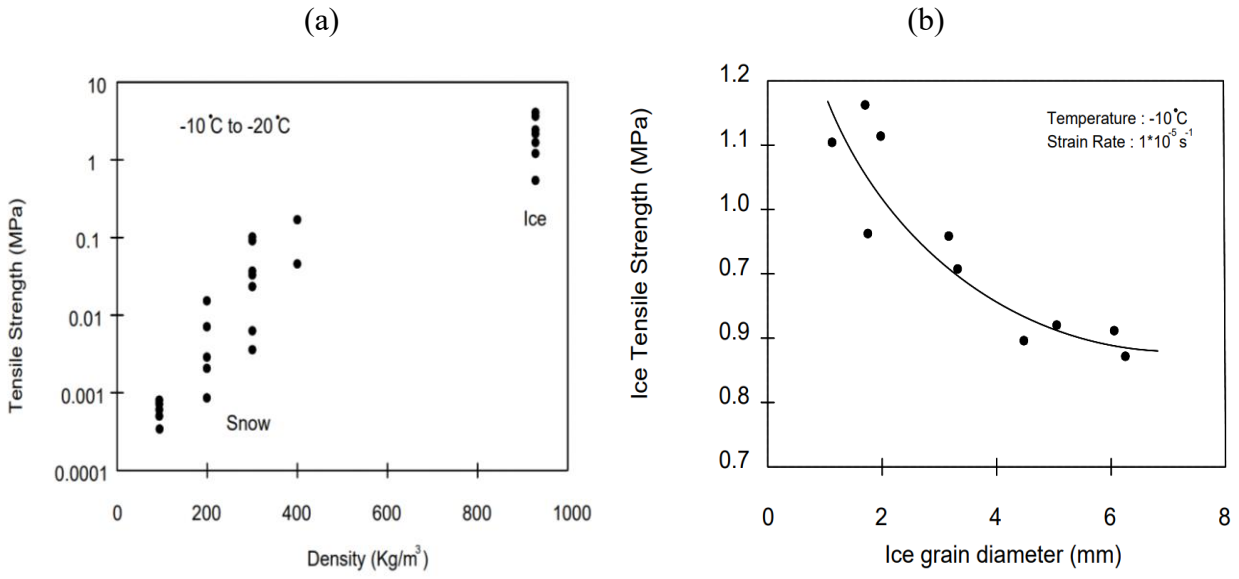

Figure 1.8: (a) Tensile strength of snow/ice plotted against density, (b) Tensile strength plotted against grain size [45]

Young's modulus, which indicates a material's stiffness or elasticity, also changes with temperature for ice. The Young's modulus of freshwater ice is approximately 7 GPa at around -10°C and increases to about 10 GPa at around -50°C.

Poisson's ratio, a fundamental mechanical property, describes how a material contracts laterally under tension or compression. For ice, the typical Poisson's ratio falls within the range of 0.3. This indicates that when subjected to tensile stress, ice not only elongates in the direction of the applied force but also experiences lateral contraction perpendicular to that force. In simpler terms, as ice stretches, it tends to become slightly thinner in the transverse direction. A Poisson's ratio of around 0.3 suggests that ice shows a moderate level of lateral contraction in response to applied tensile stress [46].

The fracture toughness of ice varies due to factors like its composition, crystal structure, and environmental conditions. Typically, ice fracture toughness ranges between 0.2 and 1 MPa/m. This indicates that ice offers a moderate resistance to the propagation of cracks. Understanding this property is essential when evaluating the structural integrity of ice formations or applications involving ice.

Thermal conductivity of ice is influenced by factors such as temperature and density. For example, normal freshwater ice at -10 °C has a thermal conductivity of about 2 W/(mK). This value suggests that ice has a respectable ability to transfer heat. It is important to note that as the temperature drops, ice thermal conductivity tends to decrease. Lower temperatures lead to the formation of crystalline structures, reducing molecular vibrations and limiting heat transfer through the material [51].

The thermal conductivity of ice significantly impacts various natural and engineering phenomena. In Arctic regions, for instance, the thermal conductivity of sea ice affects the rate at which heat is

transferred from water to the atmosphere. Understanding the thermal conductivity of ice is crucial for optimizing energy efficiency in cryogenic applications, such as designing insulated storage systems. Control over thermal conductivity is also vital in the realm of ice-based technology, including ice rinks or storage systems, to maintain optimal temperature conditions and minimize undesired heat transmission.

1.2.3- Ice Reinforcement

The structural application of ice presents challenges, including weak strength and brittle failure, limiting its use in various scenarios. Depending on the rate of loading, ice can exhibit either brittle or ductile behavior. Despite its appearance of flowing effortlessly as a glacier, ice can break like glass when dropped as individual cubes. This dual nature of ice, being both extremely ductile and extremely brittle, adds complexity to its structural considerations [52].

Research indicates that incorporating fibers into ice can significantly enhance its compressive strength, with improvements of up to 100%. Compressive strength measurements for Fiber-Reinforced Ice (FRI) typically range from 4 to 10 MPa, surpassing the average range of 2 to 3 MPa for plain ice. The reinforcing action of fibers plays a key role in distributing stresses more effectively and inhibiting the growth of fractures, contributing to the overall strength of the material [53].

Reinforced ice exhibits greater strength and resilience to cyclic loading, opening up possibilities for constructing long-lasting structures in challenging environments. Numerous scientific studies have delved into the concept of reinforced ice, exploring various materials and methods to enhance its mechanical properties. For instance, historical research by Coble and Kingery, Dykins, Dunaev, Kagan, Nixon, Kuehn, and others has explored the use of materials like wood, fiberglass, and even asbestos to reinforce ice, evaluating their effectiveness in improving structural integrity [52].

Two primary methods of reinforcement for ice are identified: macroscopic and microscopic. Macroscopic reinforcement involves embedding materials in areas experiencing tension, while microscopic reinforcement uniformly blends substances with ice to enhance tensile strength. An example of the latter is Fiber-Reinforced Ice (FRI), where fibers are unevenly distributed within the ice matrix. This creates a material resembling reinforced concrete, where fibers act as reinforcements and ice serves as the stressed matrix.

In cold regions, the use of locally sourced, natural materials like wood pulp, sawdust, and vegetal plants for reinforcement is explored. Eco-friendly options are emphasized, considering the need for sustainable practices in regions remote from industrial centers. Historical studies during World War II demonstrate that reinforcement positively influences ice structures, leading to increased loading capacity in reinforced ice beams [54].

Recent advancements have also highlighted the potential of cyclic loading to strengthen ice, which has important implications for reinforced ice structures. Schulson and his team have explored the effects of cyclic loading on the mechanical properties of ice, demonstrating that this process can significantly enhance the material's strength. Specifically, Iliescu et al. (2017) showed that cyclic loading leads to a substantial increase in the strength of ice, making it more resilient to repeated stress [55]. This finding opens up new possibilities for using ice in engineering applications where

durability under cyclic loads is critical, such as in polar construction and other cold-region infrastructure projects.

Field tests further confirm the benefits of reinforcement, showing that ice reinforced with materials such as geogrid or wooden bars exhibits higher bearing capacity and increased protection against thermal shock. Understanding the positive effects of reinforcement on ice structures contributes valuable insights into potential applications, emphasizing durability, and eco-friendly choices for construction in cold regions [56].

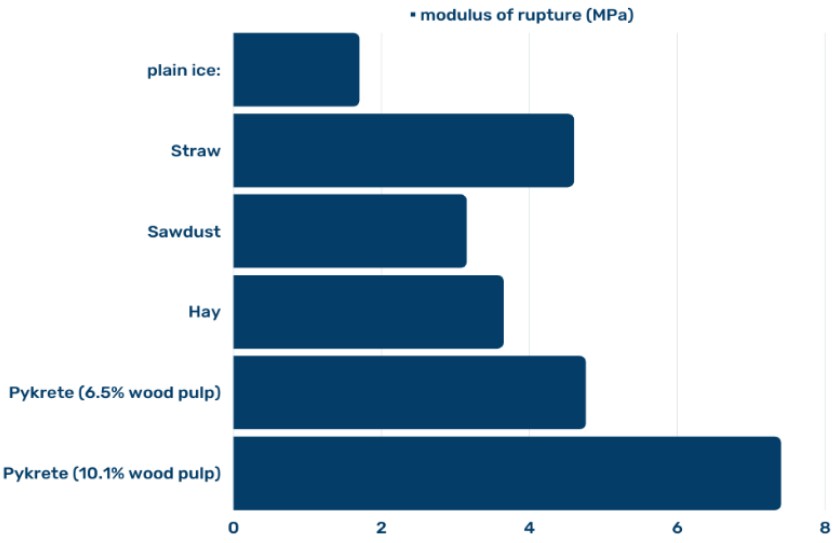

Figure 1.9: Relative increase in modulus of rupture: 5*10*89 cm3 beams reinforced with various materials; temperature: 12°C to 8°C [56]

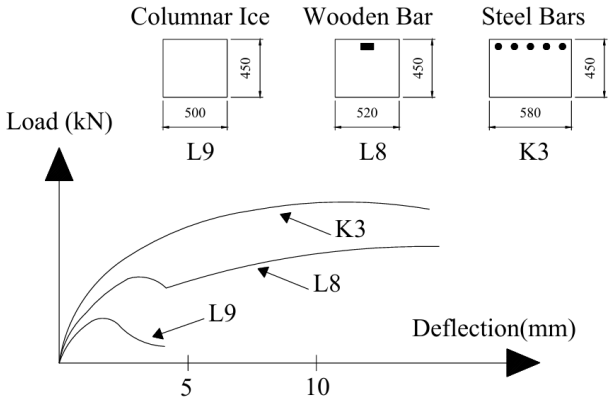

Figure 1.10: Load-deflection for ice cantilever beams with various amounts of reinforcement [57]

1.2.4- Ice Molecular Behavior

Ice has an extremely intricate structure that surely involves many molecules working together. The substantial hydrogen bonding between the molecules in liquid water produces larger values for qualities like viscosity, surface tension, and boiling point than would be anticipated for a typical liquid containing tiny molecules. Ice structures may deteriorate by fracture, creep, and melting. Because these ice composite structures are still in the experimental stage, many new possibilities with this material and technology may be discovered and explored. However, restrictions like the albedo effect, sublimation, creep behavior, and the significant relationship between temperature and structural behavior must be considered.

Ice is also known for its ability to stick to surfaces. This good adherence frequently causes considerable problems; hence, strategies to lessen the strength of the adhesive link between the ice and the substrate to which it is stuck are sought. The strong adhesive characteristics of ice are regarded as a big disadvantage in a variety of situations. Aircraft freezing, ice on roadways and runways, and ice adhesion on power lines and other slender structures are among these categories. Reduced adhesive binding strength is clearly desirable in these settings but achieving that aim has proven challenging not just due to the basic chemistry of the surface, but also because no effective means of evaluating bond strength has been devised [58].

Research indicates that interfacial fracture mechanics is a promising strategy in this field. This approach's effectiveness is supported by the work of Weber and Nixon [58-59-60]. A vital step in conducting interfacial fracture experiments, however, is the creation of a clean sharp starting crack that may then be propagated along the interface. Research aimed at measuring the fracture toughness of ice and has shown that such starter cracks can be introduced into an ice specimen in a reliable and repeatable manner [58-59-60].

The crack was completely contained within the ice in that example. This is a more problematic condition since the beginning fracture must run along the plane separating the ice from the sub-strate. To solve this issue, a mechanical method was suggested by Weber and Nixon[58-59]. The basis of this method is to mechanically create a crack. This was attempted in three ways: Using a saw directly on the ice; using a saw on a styrofoam wafer; and using a plastic sheet, which was removed before testing.

Chapter 2:

Recycled Fiber Reinforced Concrete**

2.1- Experimental Procedure

2.1.1- Introductory Remarks & Work Methodology

This chapter delves into the experimental investigation of Waste Steel Fiber Reinforced Concrete (WSFRC) using reused steel fibers from end-of-life tires. Various dosages and blends were explored, using cubes to evaluate the performance of an innovative concrete mix.

Before delving into the test procedures and experimental details, it is essential to provide a brief overview of the laboratory where these tests were conducted. The experimental work took place at the MASTRLAB Laboratory of Department of Structural, Geotechnical and Building Engineering of Politecnico di Torino, Italy. This state-of-the-art facility is dedicated to civil engineering research projects and education. Operated by trained specialists, the laboratory is well equipped with mechanical and physical measurement instruments, supporting a wide range of studies from building and structural component research to investigations into the chemical-physical and mechanical properties of construction materials.

To meet the fundamental objectives of each project efficiently and effectively, a working methodology has been essential. This methodology outlines the key phases of the research process, providing a structured approach to achieving the research goals.

The primary objective of this experimental program was to investigate whether incorporating waste steel from end-of-life tires could enhance the ecological aspects of a concrete mixture while preserving its mechanical properties.

To examine this objective in detail, several samples were prepared and subjected to a series of tests. The preparation process involved selecting appropriate materials, accurately measuring and mixing these materials to create uniform samples, and then curing the samples under controlled conditions to ensure consistency. This process is visually represented in Fig. 2.1.

Following the curing phase, the samples underwent a testing regimen designed to evaluate their properties and performance. The results of these tests will be discussed in detail in the subsequent sections. The analysis will focus on interpreting the data, identifying patterns and trends, and drawing conclusions that address the initial objective.

** This chapter's article has been published in the ACI journal and can be accessed via the following DOI: http://dx.doi.org/10.14359/51734300

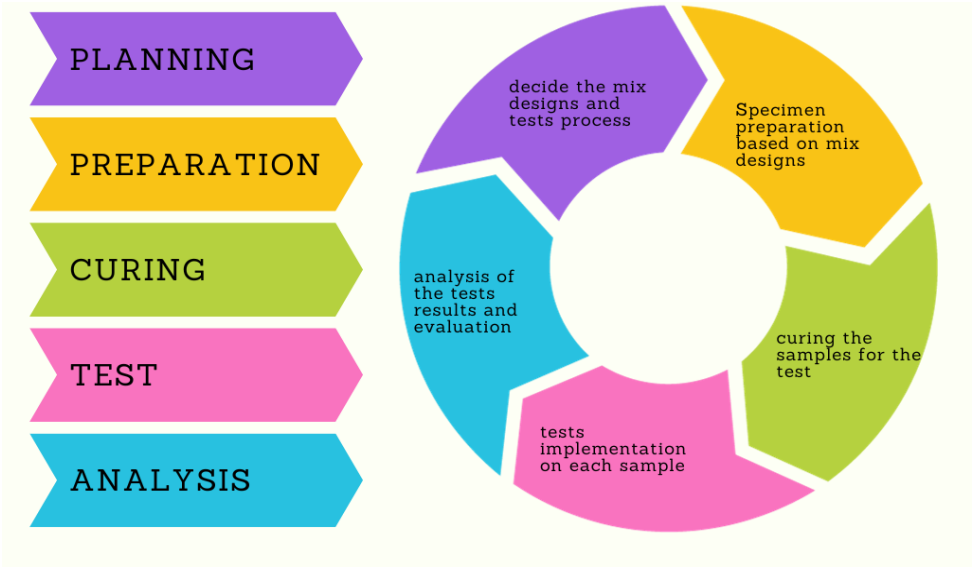

Figure 2.1: Work Methodology Scheme

2.1.2- Specimen Preparation

The experimental process involves two main phases: specimen preparation and the execution of tensile and compressive tests. (i) specimen preparation and (ii) the execution of tensile and compressive tests. In the first phase, specimens are prepared based on the mix design, involving the careful blending of various particles. The detailed casting routine is outlined below and can be visualized in the next figures (Fig. 2.2).

In the upcoming section, a series of images will illustrate the process in detail. Initially, the necessary materials for each mixture were meticulously prepared. The steel extracted from tires underwent manual separation to remove any rubber components. Subsequently, the molds were filled with this prepared steel, followed by the careful addition of mortar. The mortar was applied methodically to ensure thorough filling of each mold, optimizing the distribution and integrity of the concrete mixture. This approach was crucial to maintain consistency and accurately assess the impact of incorporating waste steel on both ecological parameters and mechanical properties.

The preparation of fibers involved a screening process to eliminate any remaining rubber and to filter out short fibers below 15 mm. Additionally, dust removal was performed to enhance the bonding of fibers with the concrete [61].

For each of the various mixes, three prisms were cast, adhering to the UNI EN196-1 standards [62]. The method involved creating prismatic test specimens sized at 40mm * 40mm * 160mm. These specimens were subjected to flexural and compressive strength testing at the specified age. The laboratory maintained a temperature around 20°C with a relative humidity not less than 50%.

(a) (b)

(c) (d)

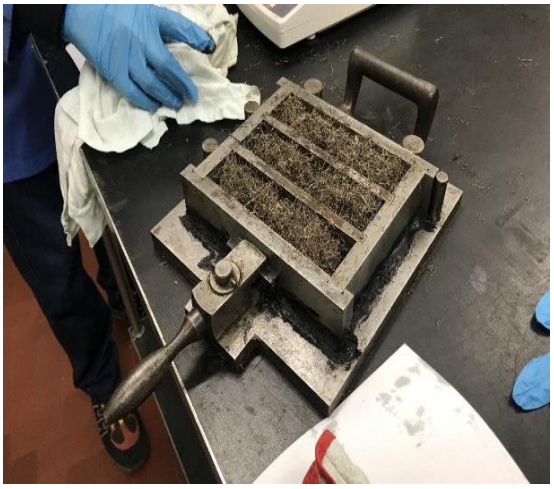

(e) (f)

Figure 2.2: Specimens preparation mode: (a): provide the mix materials, (b): separating fibers from tire particles, (c): filling the mold with fibers, (d): mix and produce concrete, (e): pouring mortar, (f): filled mold.

In accordance with Standard Sand CEN EN 196-1, certified by the National Standardization Organization, was utilized. Due to challenges in fully and unambiguously specifying CEN Standard Sand, certification and quality control testing involved standardizing the sand against the CEN Reference Sand, as outlined in EN 196-1.

To create these specimens for our study, a two-stage process commonly used for making concrete with high fiber concentrations was followed. This method has been successful in previous research [63]. The construction process involves the following steps:

1. Placement of Inert Materials

- Instead of using coarse aggregate, the mold was filled with recycled steel fibers.
- The mold has three horizontal compartments, each measuring 40 x 40 x 160 mm, adhering to the dimensions specified in UNI EN 196-1 for mortar samples. (Fig. 2.3.a)
- This design allows us to cast three specimens simultaneously, as illustrated in Figures 2.3.b.

2. Grout Injection

- The next step involves injecting grout into each compartment.
- The grout can be poured like molten metal, as demonstrated in Fig. 2.2.e.

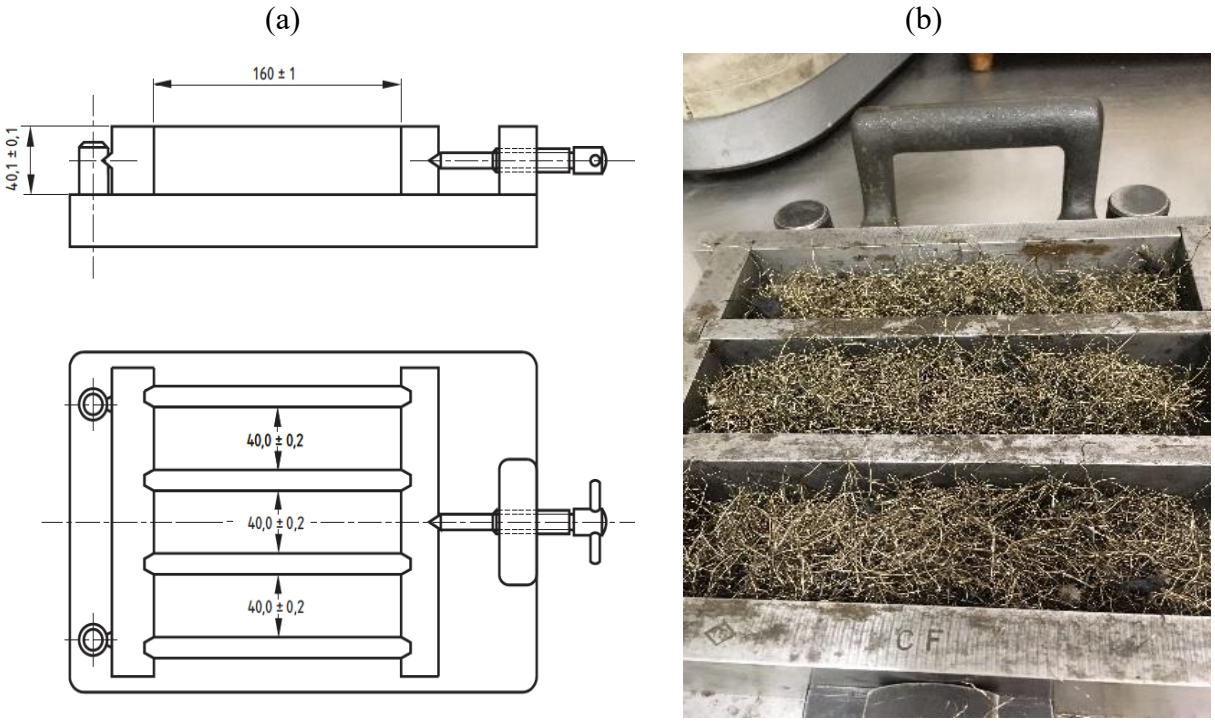

Figure 2.3: (a) geometrical properties of the mold, (b) filled mold.

Afterwards, Specimens stored for more than 24 hours between sampling and testing was kept in airtight containers made from non-reactive material. Fig. 2.4 displays three specimens of a specific mixture after the curing process.

To facilitate mold filling, a closely fitting metal hopper with vertical walls (20mm to 40mm in height) was employed. When viewed from above, the hopper walls slightly overlapped the internal mold walls by no more than 1 mm. The outer walls of the hopper were designed for proper positioning over the mold, ensuring accuracy during the filling process.

Mixing of fiber reinforced concrete needs careful conditions to avoid balling of fibers, segregation and in general the difficulty of mixing the materials uniformly. Challenges become more pronounced with higher aspect ratios, increased volume percentages, and larger quantities of coarse aggregate. Difficulties and the tendency to form clumps are intensified with steel fiber content exceeding 2% by volume and an aspect ratio surpassing 100.

To prepare the molds for casting, a releasing agent, known as the de-molding oil, was applied 15 to 30 minutes before pouring the concrete. Subsequently, the molds were positioned on a laboratory vibrating table, ready to be filled with concrete. The concrete was poured in layers, and vibration was applied after each layer. The duration of vibration varied from 10 to 20 seconds, depending on the consistency of the concrete. It is important to note that fluid concrete does not require vibration.

The entire casting process was completed within a day, and the specimens were left to cure in the molds for 48 hours. After the curing period, the specimens were de-molded, grouped on pallets, and stored inside the laboratory. Following 28 days of curing in a controlled indoor environment, any hessian and plastic sheets were removed, and the specimens were left to dry.

Figure 2.4: Specimens after curing.

This process is aimed to assess the flexural and compressive properties of High-Performance Fiber-Reinforced Cementitious Composites (HPFRCC). The goal was to conduct a thorough parametric study, examining how slight variations in fiber dosages impact the concrete's flexural properties. So, the second phase is performed using a loading machine (having a capacity of 50 kN) which can be seen in Fig. 2.5. During the test, the loading rate had been specified according to the UNI EN 196-1 code rules.

Figure 2.5: Testing Machine. (a) The general configuration of the machine consists of the testing component and the computer. (b) Politecnico di Torino machine.

2.1.3- Mixing & Fiber Content

To ensure the adequacy of the fiber mix, a series of tests following the specified regulations were conducted. For each mix, we created three different specimens in a single day. After allowing 28 days for curing, the specimens were subjected to both flexural and compressive tests in accordance with UNI EN 196-1 regulations.

Before proceeding with the tests, a preliminary check was carried out to assess whether the samples met basic requirements. For instance, in cases where larger aggregates were used, we verified if the specimen could effectively accommodate these materials. Additionally, the specimens were inspected upon demolding to ensure they were free of significant cracks or holes. This step is crucial for confirming the suitability of the mix and the integrity of the specimens for subsequent testing.

Using the previously described process (Fig. 2.2), we created two distinct series of cement-based mortars employing Recycled Steel Fibers (RSF) supplied by Etra IT scarl. The dimensions of approximately 600 fibers, with an accuracy of 0.01 mm, were measured and their statistical

distributions are presented in Figure 2.6.a (diameter) and Figure 2.6.b (length), with average values of 0.262 mm and 15.8 mm, respectively. Figure 2.6.c illustrates the statistical distribution of the aspect ratio (length/diameter ratio), with average values of 0.262 mm, 15.8 mm, and 62.8, respectively.

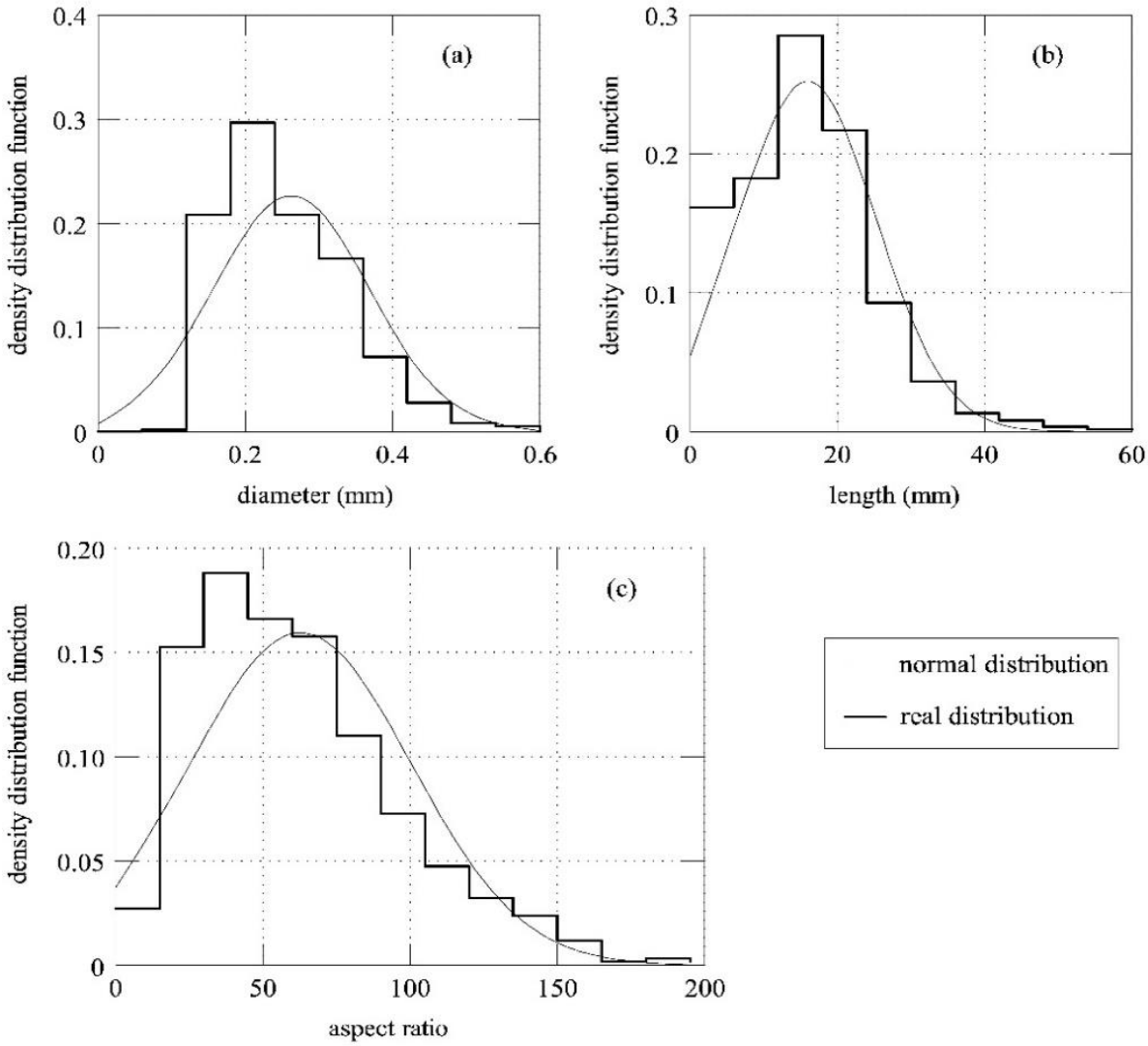

Figure 2.6: Geometrical properties of the Recycled Steel Fibers used in this project: (a) statistical distribution of diameter; (b) statistical distribution of the length; (c) statistical distribution of the aspect ratio.

An analogous aspect ratio (64) was achieved with DE 35/0.55 fibers (diameter of 0.55 mm and length of 35 mm), manufactured steel fibers (MSF) by Krampe Harex. These MSF were utilized in the reference series, named Ref, cast in a single stage using CEM I 52.5 R, tap water, and UNI EN 196-1 recommended siliceous sand (S-sand), with rounded particles adhering to size distribution limits in Table 2.1.

Table 2.1. Compositions of the UNI-sand according to UNI EN 196-1

square mesh size (mm)	2.00	1.60	1.00	0.50	0.16	0.08
Cumulative sieve residue (%)	0	7±5	33±5	67±5	87±5	99±5

Table 2.2. Compositions of the series investigated in this research.

Series	Ref	1			2	
		Specimens			Specimens	
		1-A	1-B	1-C	2-A	2-B
Water (kg)	290	430			430	
Cement (kg)	580	645			580	
S-sand (kg)	1350	0			0	
M-sand (kg)	0	510			680	
PW (kg)	0	45			0	
MSF (%vol)	2.1	0			0	
RSF (%vol)	0	2.1	3	4.2	3	6
Silica fume (kg)	0	215			280	
Super-plasticizer (kg)		6			5	
Day of casting	21_11	06_11	18_02	10_12	28_05	28_05

In contrast, the two-stage composites, Series 1 and Series 2, utilized Modified sand (M-sand). Only fractions with a particle size below 0.2 mm from Table 1 composition were included in M-sand. Table 2.2 describes the mixture proportions for each series. Series 1 includes plastic waste (PW) particles, made from a mixture of polyamide, glass fiber, and polypropylene, with a size below 0.2 mm. Silica fume and an acrylic super-plasticizer were added as additives.

In the Ref series, the cement-based matrix is a traditional mortar with a paste/aggregate volumetric ratio of 1. On the other hand, Series 1 and Series 2 matrices are grouts, resulting in a cement paste volume three times that of the aggregate.

2.1.4- Testing Procedure

As per the specified code regulations, it is necessary to position the prism in the testing machine, as depicted in Fig. 2.7. Place one side face of the prism on the supporting rollers, ensuring that its longitudinal axis is perpendicular to the supports. A distance of 100 mm ± 0.5 mm between the supports is maintained. The load should be applied vertically using the loading roller, directed towards the opposite side face of the prism. Gradually increase the load at a controlled rate of 50 ± 10 N/s until the prism fractures.

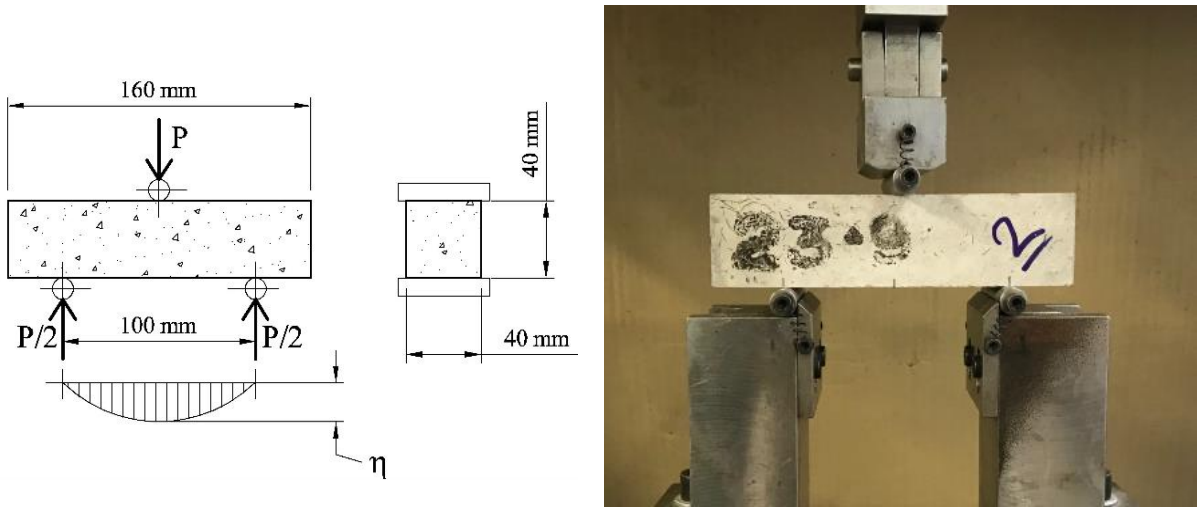

Figure 2.7: Three-point bending tests for cementitious mortars.

The tensile behavior of steel fiber concrete measured by examining the remaining flexural tensile strength, determined from the curve depicting the relationship between applied load and either crack mouth opening displacement or deflection. This evaluation is conducted through a center-point load applied to a simply supported prism.

The three-point bending flexural test yields valuable information, including the modulus of elasticity of the material in bending, flexural stress, flexural strain, and its stress–strain response. This testing method is advantageous due to its straightforward specimen preparation and testing procedure. However, it comes with certain drawbacks. The results are sensitive to both the characteristics of the specimen, the geometry of loading, as well as the rate at which strain is applied

After testing the flexural strength, the prisms split into halves. These halves are then subjected to a compression test. To ensure accurate compression testing, the prism halves are laterally centered on hard steel auxiliary platens, which precisely define the compressive area due to the irregular shape of the prism halves.

Following EN 196-1 guidelines, the platens should measure 40 mm x 40 mm and have a thickness of at least 10 mm. Throughout the loading process, the upper and lower platens must maintain a

fixed relative position. The forces applied should result in a smooth increase in load at a rate of 2400 ± 200 N/s until the specimen fractures.

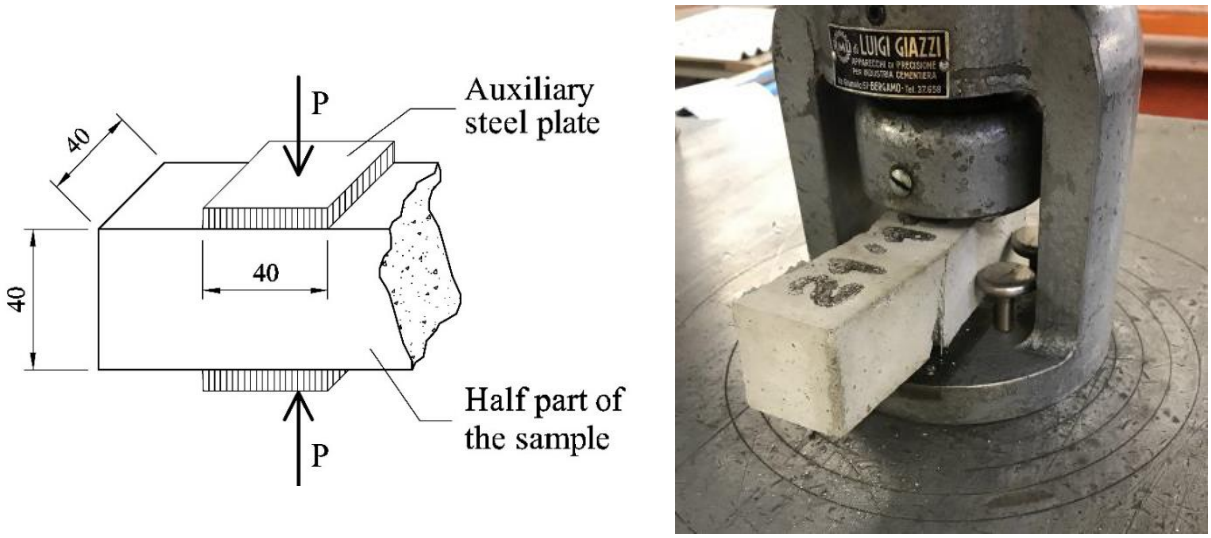

Figure 2.8: Scheme of loading machine for compressive test

2.2- Experimental Data

2.2.1- Test results

After a 28-day period, before conducting tests on our specimens, the diameter and size of our samples were measured. The outcomes obtained from various mixes are highlighted, before checking the test results. Through the three-point bending tests described earlier, the applied load (P) and mid-span deflection (η) as shown in the next Figure 2.9.

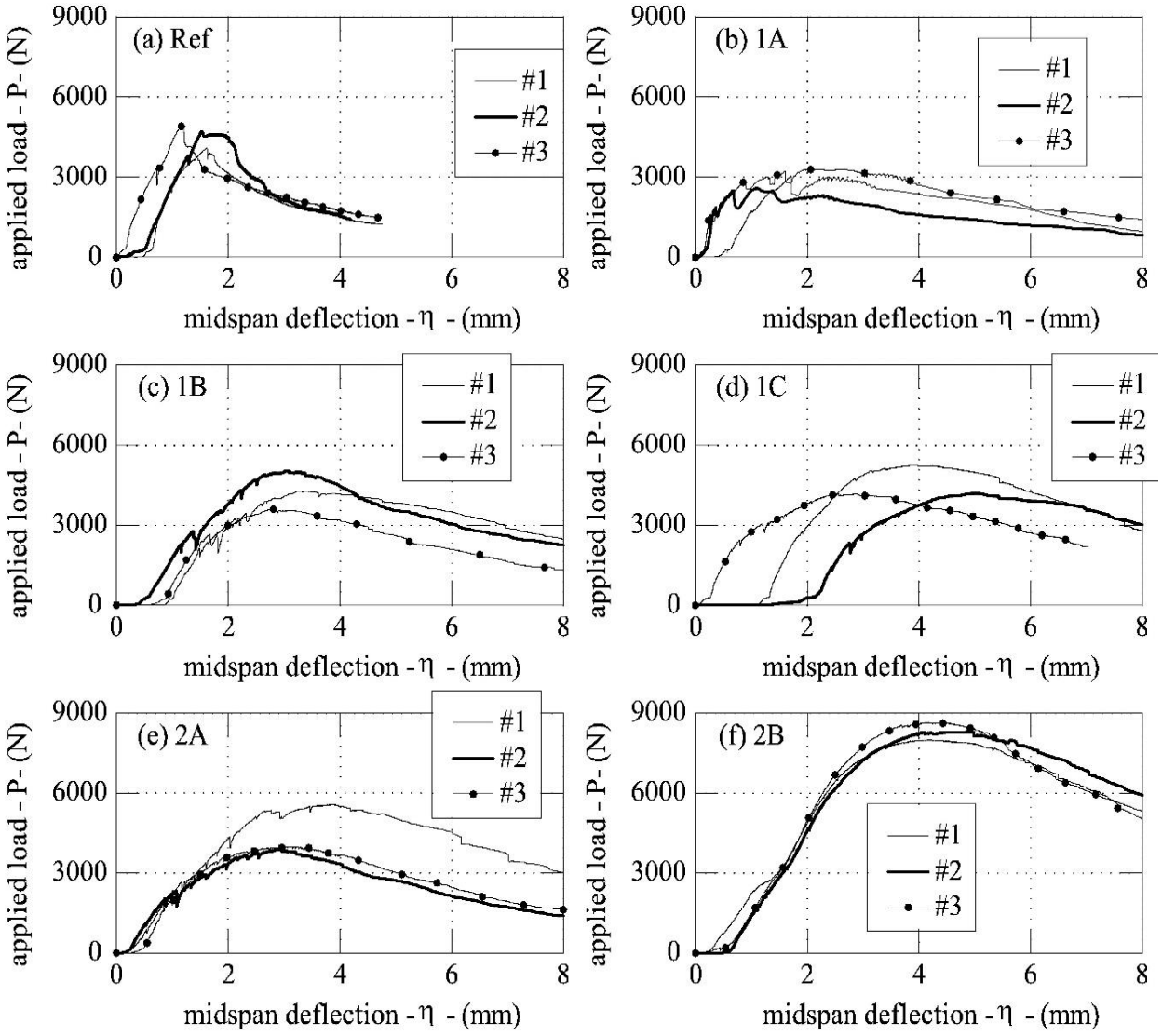

Figure 2.9: The load-midspan deflection diagrams measured with the three-point bending tests performed in this research project.

Figure 2.10.a illustrates that these diagrams from Fig. 2.9 can be simplified, dividing the entire P-η diagram into two sections. In the first ascending branch, two key points were identfied: (i) the load at first cracking (P_{cr}) and (ii) the ultimate load (P_u). As the load increases from P_{cr} to P_u, multiple cracks form (Figure 2.10.b), resulting in a deflection hardening branch, like the behavior observed in High-Performance Fiber-Reinforced Concrete (HPFRC).

In the second part of the P-η diagram, starting from P_u, a softening effect is noticeable, with loads decreasing as deflections increase [62]. This softening is attributed to the localization of curvatures in one of the previously formed cracks. When the fiber content is low, the specimens break into two separate parts during bending tests. Conversely, when the fiber content exceeds 2%, the halves remain connected because the fibers bridge the crack where curvatures localize.

(a) (b)

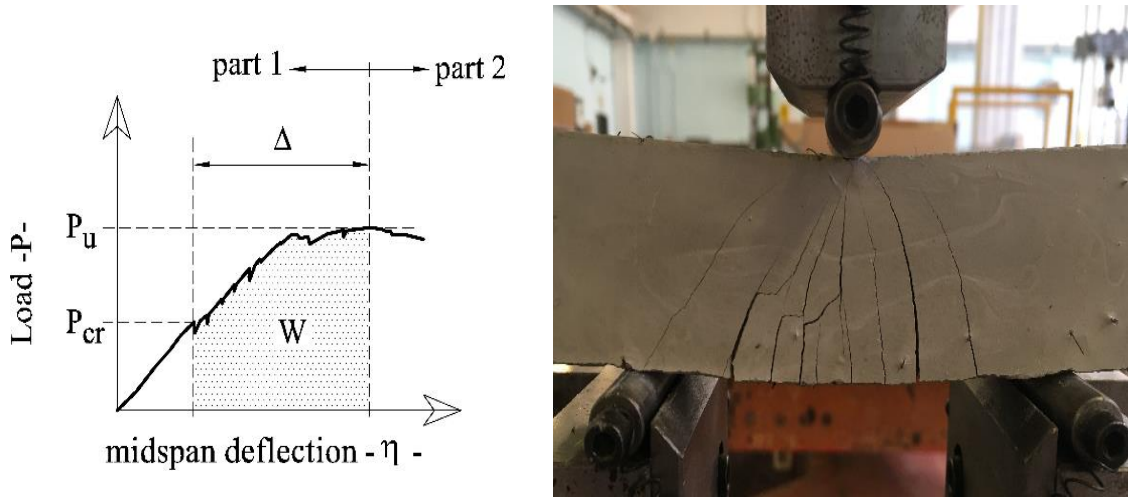

Figure 2.10: The results of the three-point bending tests: (a) the ideal P- η diagram; (b) multiple cracking in a specimen.

Beyond the values of P_{cr} and P_u, the most intriguing aspect of the P-η diagram is the hatched area depicted in Figure 2.10.a. This shaded region represents the work (or energy) denoted as W, associated with multiple cracking and deflection hardening in HPFRC. The computation of this work, essentially a measure of the flexural toughness of HPFRC, is as follows:

$$W = \Delta \cdot \frac{P_{cr}+P_u}{2} \tag{2.1}$$

The symbol Δ indicates the variance between the deflection measured at the load P_u and that corresponding to P_{cr}, as illustrated in the previous Figure 2.10.

In the next table, you can locate the values for different mechanical and geometrical properties measured in the tests. Also, in the last two columns of this table, the maximum compressive loads P_c, measured on the halves of each specimen, are listed.

Table 2.3. Mechanical and geometrical properties measured in the experimental analysis.

									P_c	
series	specimens		B	H	L	P_u	P_{cr}	Δ	Right half	Left half
			(mm)	(mm)	(mm)	N	N	(mm)	(KN)	(KN)
Ref		#1	42.63	39.75	160.2	4096	2625	0.6339	82.70	80.90
		#2	42.28	39.85	159.9	4709	3752	0.2389	87.85	79.39
		#3	41.48	39.97	159.9	4909	3278	0.4445	58.64	89.53
1	1A	#1	42.33	40.63	159.9	3058	1675	0.7371	55.24	60.62
		#2	42.37	40.18	159.7	2588	1840	0.7328	58.95	56.70
		#3	41.8	40.58	159.7	3306	1577	1.7535	59.31	63.90
	1B	#1	41.53	39.79	159.7	4277	2121	1.7849	62.91	70.58
		#2	42.68	40.05	159.6	5036	2229	1.9197	66.08	74.13
		#3	41.19	39.79	159.6	3596	2313	1.3238	70.97	62.94
	1C	#1	43.23	39.77	159.9	5230	2721	2.0362	65.39	65.47
		#2	43.19	39.9	159.8	4176	1408	2.5798	60.29	70.42
		#3	42.72	39.96	160.8	4155	1538	2.3970	53.01	68.53
2	2A	#1	41.94	39.81	159.6	5553	877	3.3256	63.65	67.19
		#2	41.85	40.03	160.0	3874	1032	2.3749	66.59	62.26
		#3	42.02	39.84	159.7	3985	1200	2.4093	60.38	56.74
	2B	#1	43.99	39.97	160.4	8000	1574	3.3802	79.17	80.20
		#2	43.51	39.87	159.8	8298	1673	3.7665	68.58	70.60
		#3	44.45	39.9	159.8	8628	1972	3.0384	67.93	76.61

In cases where polymeric aggregates are used (found in specimens of series 1), there is a tendency for compressive strength to decrease compared to concrete systems made solely with stone aggregates. On the contrary, in both series 1 and series 2, both flexural and compressive strengths show an increase with the inclusion of RSF.

2.2.2- Discussion of the results

According to UNI EN 196-1, assuming materials behave linearly elastic, and the cross-section remains uncracked, the flexural strength (f) can be determined using the formula:

$$f = P \cdot \frac{3 \cdot L}{2 \cdot B \cdot H^2} \tag{2.2}$$

Here, L represents the beam span (100 mm), and B and H are the width and height of the beam cross-section (40 mm). Specifically, this formula proposes the measurement of $f_{f,u}$ representing the flexural strength (by substituting $P = P_u$ into Eq. (2.1)), and $f_{f,cr}$ indicating the flexural strength at cracking (calculated using Eq. (2.2) when $P = P_{cr}$).

In particular, $f_{f,u}$ as the ultimate flexural strength is measured by substituting ($P = P_u$) into the equation mentioned above. Similarly, $f_{f,cr}$ represents the flexural strength at cracking, computed using the same equation (Eq. 2.2) with ($P = P_{cr}$). Moreover, as mentioned previously, according to the P-η diagram it is possible to calculate the work (or energy) W associated with the multiple cracking during the deflection-hardening stage of the P-η diagrams.

When polymeric aggregates are used (i.e., in the specimens of series 1), compressive strength tends to reduce with respect to that measured in concrete systems made with only stone aggregates. But on the other hand, both in Series 1 and Series 2, the flexural and compressive strengths increase with the content of RSF.

The average values of both ultimate flexural strength ($f_{f,u}$) and flexural strength at first cracking ($f_{f,cr}$) are presented in Table 2.4, along with the compressive strength (f_c). Compressive strength is calculated by dividing P_c (as indicated in Table 2.3) by the loading surface area (i.e., 40 × 40 mm, as shown in Fig. 2.8). Additionally, the average values of the work (W) are included in the last column of Table 2.4.

Table 2.4. The average values of the strengths measured in the experimental analysis.

series	specimens	V_f	$f_{f,cr}$	$f_{f,u}$	f_c	W
		(%)	(MPa)	(MPa)	(MPa)	(N.mm)
Ref		2.1	7.19	10.22	49.9	1653
1	1-A	2.1	3.69	6.48	36.95	5250
	1-B	3	5.01	9.69	42.46	5531
	1-C	4.2	4.14	9.91	39.91	7374
2	2-A	3	2.33	10.05	39.25	7588
	2-B	6	3.72	17.79	46.16	17021

In Series 1, the flexural strength at first cracking is higher compared to Series 2, while greater ultimate flexural strength is observed in Series 1 specimens. In simple terms, when polymeric particles are present, there is a reduction in ultimate flexural strength, but at the same time, the flexural strength at first cracking increases, for a given compressive strength.

Moreover, ultimate flexural strength ($f_{f,u}$) shows an increase with the fiber volume fraction (V_f) in both series 1 (Fig. 2.11.a) and series 2 (Fig. 2.11.b).

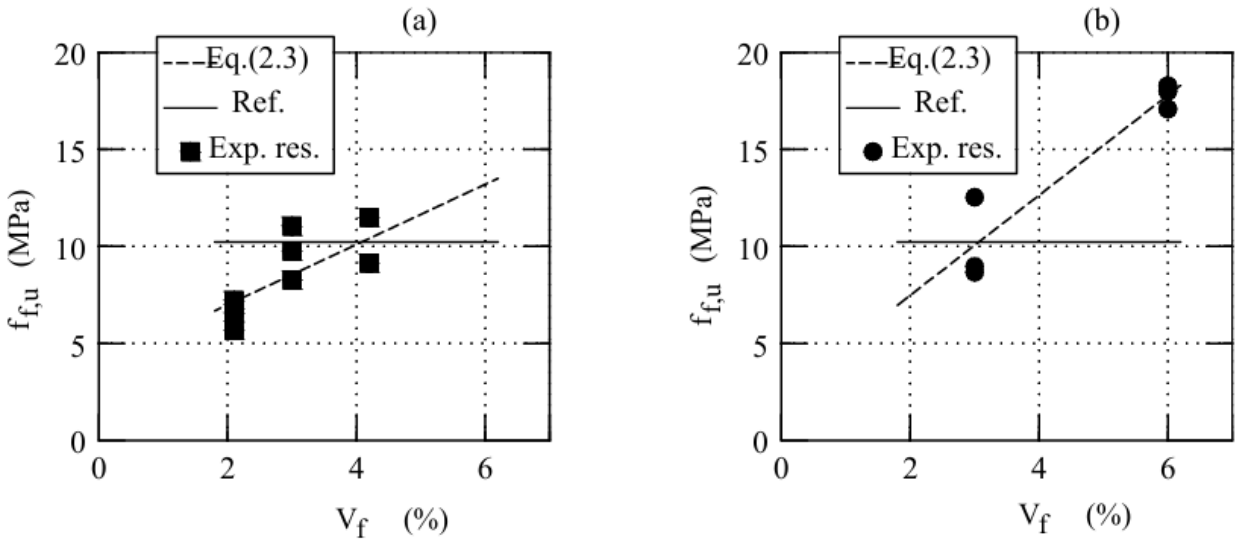

Figure 2.11: Possible $f_{f,u}$ vs. V_f relationships: (a) tests on series 1; (b) tests on series 2.

Considering that flexural strength increases more or less linearly with the content of fibers [63], the following equation can be used to relate ultimate flexural strength ($f_{f,u}$) and fiber volume fraction (V_f):

$$f_{f,u} = \gamma + \delta \cdot V_f \tag{2.3}$$

Where the coefficient γ and δ are reported in Table 2.5.

Table 2.5. The parameters γ and δ to be used in Eq. (2.3).

series		γ	δ
1	$f_{f,u}$	3.88	1.55
2	$f_{f,u}$	2.32	2.58

Fig. 2.11 illustrates the potential relationships between flexural strength and the fiber volume fraction for series 1 (Fig. 2.11.a) and series 2 (Fig. 2.11.b). In the same diagrams, the strength of the reference (Ref), corresponding to (V_f = 2.1%), is also indicated. At this common fiber volume fraction (V_f = 2.1%), the average value of ultimate flexural strength ($f_{f,u}$) measured in both series 1 and series 2 is lower than that exhibited by the reference (Ref), which is equal to 10.22 MPa.

The flexural strength of the Ref series can also be represented by a single point. However, it is depicted with a line to determine the volume of fibers needed to achieve the same strength as

compositions in series one and series two. Using Eq. (2.3), the fiber volume fraction that compensates for this loss of strength can be calculated. Specifically, ($f_{f,u}$ = 10.22 MPa) in series 1 is achieved when (V_f = 4.1%) (Figure 2.11.a), and for a lower fiber content (i.e., (V_f = 3.1%)) in series 2 (Figure 2.11.b).

2.2.3- Eco-mechanical analysis

Concrete is a widely utilized material, with an annual global production exceeding 10 billion m³, making it a cornerstone in various industries. In European countries, the building and development sector alone contributes to approximately 40% of total energy consumption, while the construction industry accounts for about 70% of the overall material flow. Additionally, the concrete industry globally generates a significant amount of anthropogenic CO_2 emissions. Recognizing these facts underscores the crucial role the building sector plays in promoting sustainability. Consequently, sustainability has gained increased attention in recent years, emerging as a key focus in the construction materials industry alongside initiatives to produce new building materials.

To address the substantial environmental impact of concrete, especially in High Performance Fiber-Reinforced Cementitious Composites (HPFRC) with high cement content, exploring alternatives to replace cement has become imperative. The excessive volume of cement used in HPFRC is a primary contributor to its significant environmental effects. Evaluating ecological efficiency involves assessing the amount of CO_2 released during the various activities associated with HPFRC production. This research aims to contribute to the ongoing efforts in the construction materials industry by exploring sustainable alternatives and promoting environmentally conscious practices in concrete production.

To evaluate the possibility of substituting the current cement-based composites with new High-Performance Fiber-Reinforced Concrete (HPFRC) made with recycled materials, an investigation into the environmental impact of this substitution is necessary. Eco-mechanical analyses [64], as described in reference, involve a comparative study among different construction materials. This analysis is conducted using the non-dimensional chart depicted in Figure 2.12.

In this chart, two key parameters, MI (Mechanical Index) and EI (Ecological Index), are analyzed for all the composites. MIinf represents the minimum required mechanical performance, while EIsup denotes the maximum acceptable ecological impact. Consequently, four distinct zones emerge in the diagram (see Figure 2.12): Zone 1 indicates low mechanical performance and low ecological impact, Zone 2 shows high mechanical performance and low ecological impact, Zone 3 depicts high mechanical performance and high ecological impact, and Zone 4 illustrates low mechanical performance and high ecological impact.

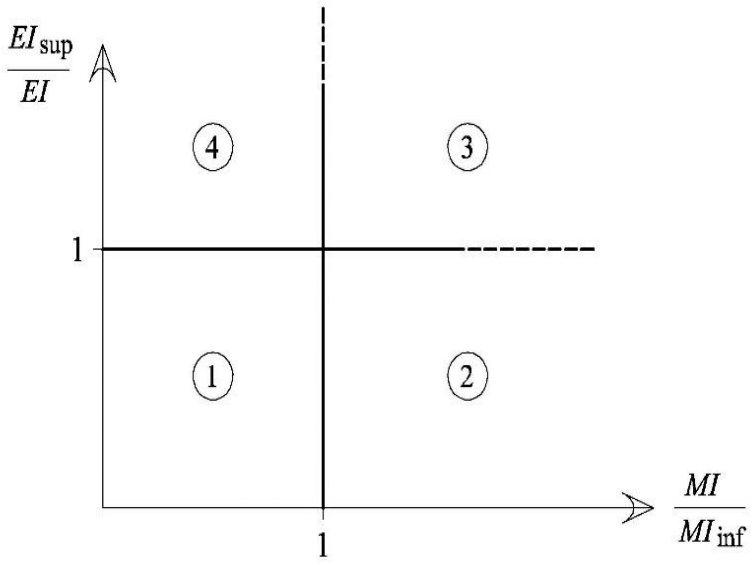

Figure 2.12: The non-dimensional diagram used for the eco-mechanical analysis.

In the analyses, the Ecological Index (EI) corresponds to the carbon footprint generated by the production of the mixtures listed in Table 2.2. It is calculated by considering the equivalent CO_2 released by the unit mass of the concrete components, as detailed in Table 2.6. The environmental impact is largely attributed to manufactured materials, such as fibers, cement, and superplasticizer. However, the superplasticizer's contribution to EI is deemed negligible, as its mass is less than 1% compared to that of cement (refer to Table 2.2). Additionally, it is assumed that the carbon footprint of Recycled Steel Fibers (RSF) is zero, based on research from the Anagennisi project [66].

Table 2.6. The evaluation of EI referred to 1 m^3 of HPFRC.

	Carbon footprint ($kgCO_2/t$)	Database	series	specimens	EI(Kg)
Portland Cement	902	Eco invent [65]	Ref		907
Industrial Steel fibers	2190	Eco invent	1	1-A	597
Recycled fibers	0	Anagennisi [66]		1-B	597
silica fume	3.1	Eco invent		1-C	597
Silica sand	12	Eco invent	2	2-A	539
Water	0.7	Eco invent		2-B	539
Super-plasticizer	1330	Eco invent			

The EI values, reported in the last column of Table 2.6 for 1 m^3 of the investigated mixtures, are computed by summing the products of mass and unit values of the carbon footprint for each component. Due to high quantities of cement and MSF, Ref exhibits the highest impact (i.e., maximum EI). Conversely, series 2 specimens have the minimum EI, as RSF replaces MSF while maintaining the same cement content. However, in series 1, the environmental benefit from substituting stone aggregate with plastic waste does not offset the impact from the higher cement content compared to Ref and series 2.

The Mechanical Index (MI) serves as the functional unit for the comparative analysis. For structural HPFRC, the mechanical properties from Table 2.4 are considered. Figure 2.13 presents eco-mechanical analyses for three cases (i.e., when MI = $f_{f,u}$, f_c, and W), where MI_{inf} and EI_{sup} are reference values from Ref. Notably, the substitution of Ref with HPFRC from series 1 and series 2 is always advantageous when considering the energy dissipated during the multiple cracking and deflection hardening stage (see Fig. 2.13.c). Moreover, if MI = $f_{f,u}$ (Fig. 2.13.b) only for certain HPFRC, such as those of series 1 with $V_f > 4.1\%$ and series 2 with $V_f > 3.1\%$, the eco-mechanical performance falls within sector 3. Consequently, in some structures subjected to bending actions, like the rings of manhole covers and corrugated slabs, the use of HPFRC made with RSF can be environmentally advantageous.

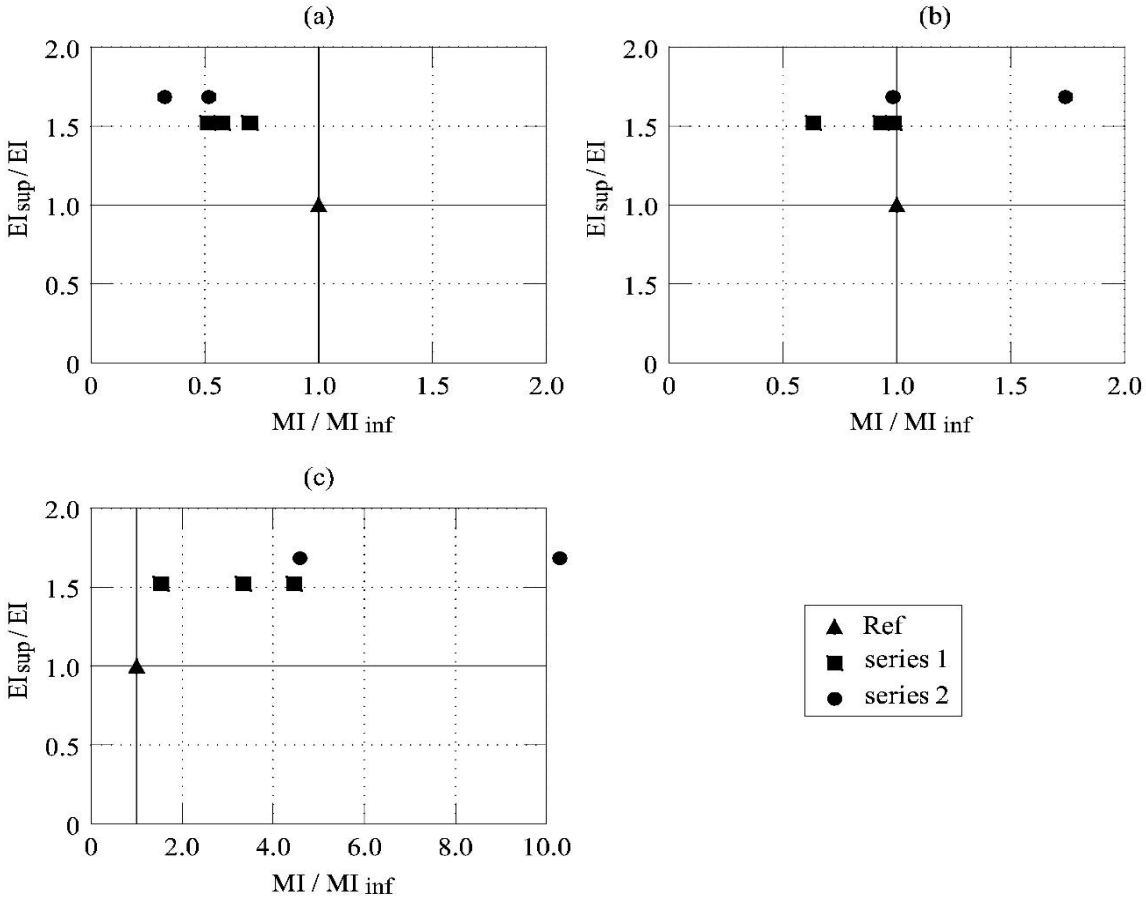

Figure 2.13: The eco-mechanical analysis of the HPFRC investigated herein: (a) MI= f_c ; (b) MI= $f_{f,u}$; and (c) MI = W.

2.3- Cement Based Mortar Case Study**

2.3.1- Work Methodology

Practical uses of High-Performance Fiber-Reinforced Concrete (HPFRC), which exhibits strain hardening leading to multiple cracking due to recycled steel fibers, are quite limited. This limitation arises from the tendency of steel fibers to clump together, affecting the workability. Specifically, a new type of HPFRC is created using a two-stage procedure and a high amount of recycled steel fibers from End-of-Life Tires (ELTs) [73]. Casting specimens with a significant fiber dosage aims to address issues related to uneven fiber distribution in concrete elements.

This part marks the first attempt to assess the impact of recycled steel fibers from ELTs on elements traditionally cast using only new materials. In simpler terms, we explore whether these HPFRCs can effectively be used to manufacture construction industry products, such as corrugated slabs (Fig. 2.14.a) and manhole covers (Fig. 2.14.b).

(a) (b)

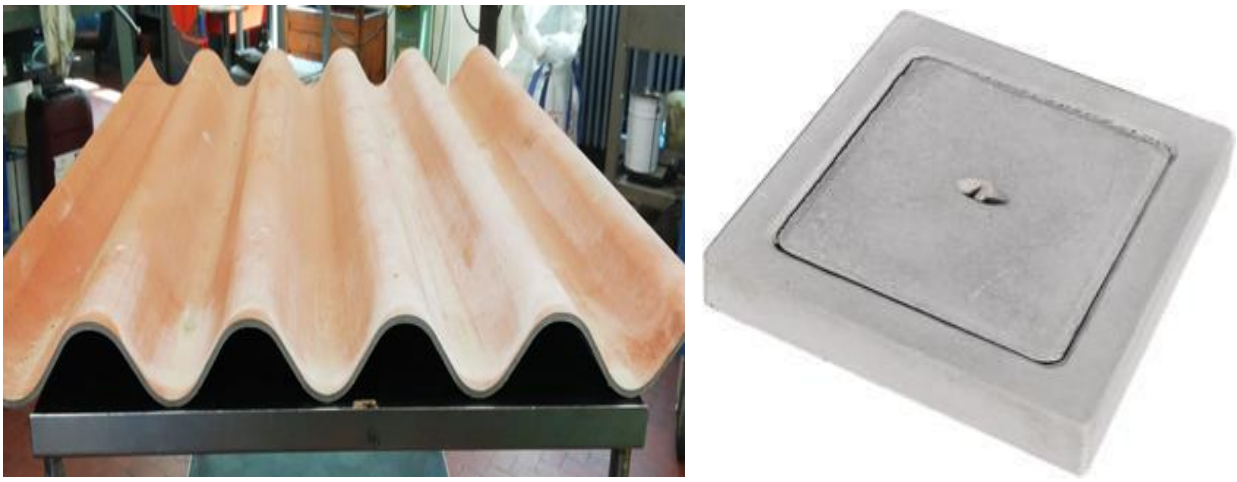

Figure 2.14: Some concrete elements: (a) corrugated slab; (b) manhole cover.

In recent years, various approaches have been employed to mitigate the carbon dioxide emissions associated with reinforced concrete (RC) structures. Many studies have focused solely on assessing the environmental aspects of concrete materials and developing more environmentally friendly cement-based composites. However, only a limited number of studies have delved into a comprehensive comparison of both the structural and environmental performance.

Therefore, this part of study aims to address the following questions:

- Do the fiber-reinforced concrete components utilized in the production of corrugated slabs and manhole covers exhibit similar mechanical behavior when the volume fraction of recycled steel fibers (RSF) is appropriately chosen?
- Can the previously established relationships between mechanical properties and fiber volume be applied to determine the required amount of fiber?

The goal is to bridge the gap between the environmental and structural considerations in the pursuit of more sustainable and effective solutions for concrete structures.

**The content of this section has been presented at the 3rd International Conference on Fiber-Reinforced Concrete (3rd FIB) and is available in their handbook, spanning from page 387 to 393.

2.3.2- Experimental Procedure & Results

Four specimens from the corrugated slab and two specimens of manhole rings were prepared for our study. These specimens underwent three-point bending tests. Figure 2.15 illustrates the geometry of the samples and the test setup for those extracted from the corrugated slab, while Figure 2.16 shows the test setup for concrete rings of manhole covers. Following the tests, the load-midspan deflection diagrams were obtained from the three-point bending. The results of the P-η curves are presented in Figure 2.17.a (for corrugated slabs) and Figure 2.17.b (for manhole covers).

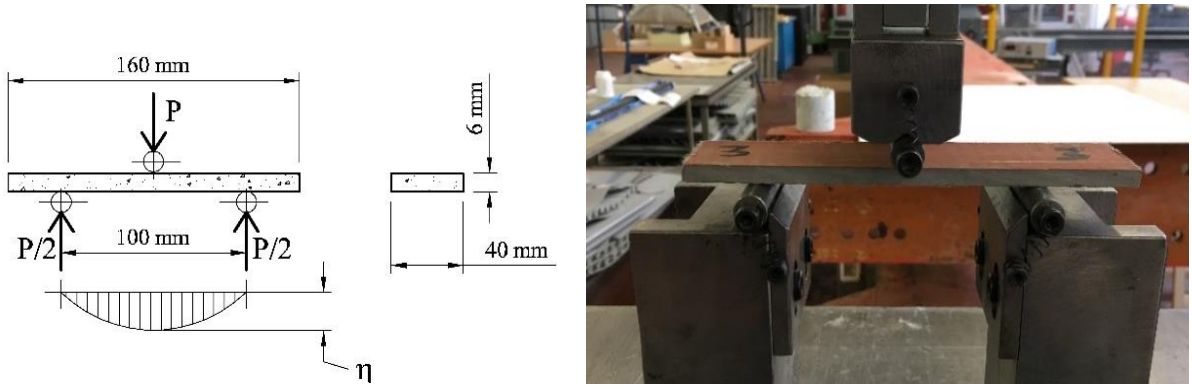

Figure 2.15: Three-point bending tests on samples extracted from corrugated slabs.

Figure 2.16: Three-point bending tests on concrete rings of manhole covers.

By conducting the three-point bending test on each sample, both the maximum applied load and the applied load at the cracking point were estimated. In this study, the focus was solely on the ultimate values. Following the guidelines of UNI EN 196-1, assuming linear elastic behavior and an uncracked cross-section of materials, the flexural strength (f) can be calculated using the formula:

$$f = \mathrm{P} \cdot \frac{3 \cdot L}{2 \cdot B \cdot H^2} \tag{2.2}$$

Where L = spam of the beam (i.e., 100 mm in Fig. 2.15); B and H = width and height of the beam cross-section (i.e., 40 mm and 6 mm in Fig. 2.15), respectively. By introducing P equal to P_u the flexural strength, $f_{f,u}$ was evaluated.

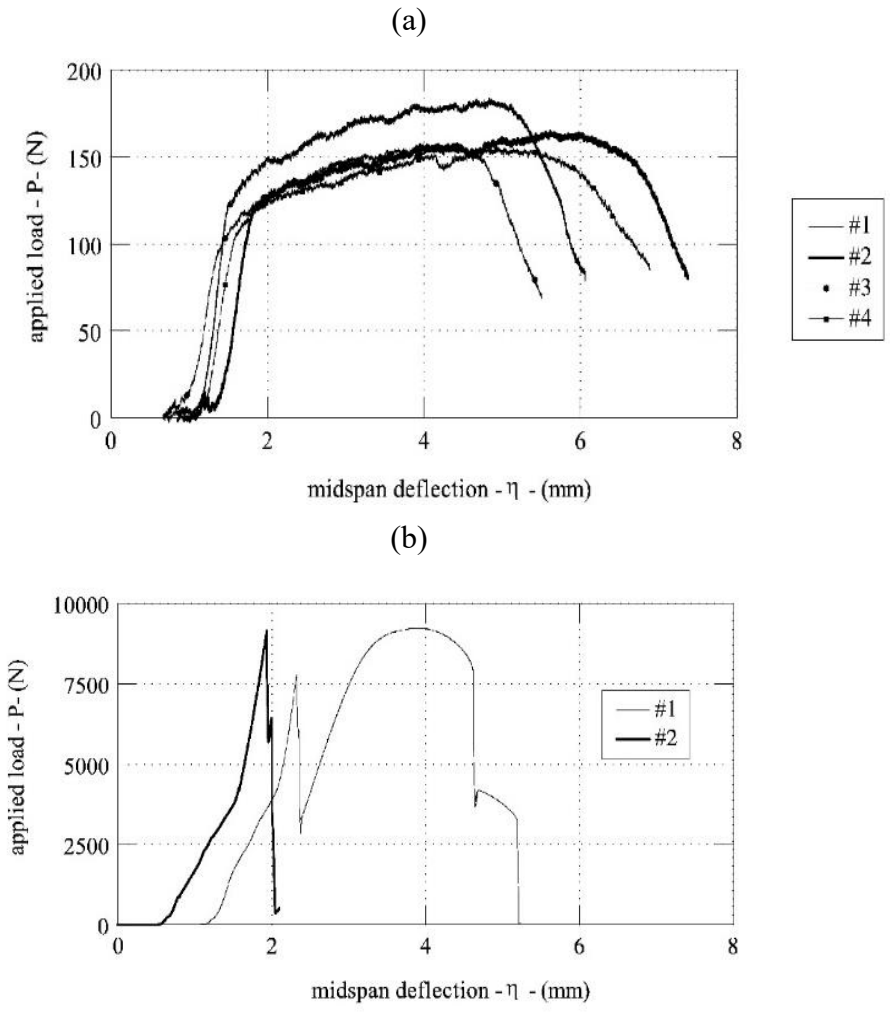

Figure 2.17: The load-midspan deflection diagrams measured with the three point bending tests performed on samples extracted from (a) corrugated slabs, (b) manhole cover.

Table 2.7.a reports the geometrical properties of the samples extracted from corrugated slab, the values of P_u, and the flexural strength $f_{f,u}$ computed with Eq.(2.2) while in the Table 2.7.b we reported the manhole cover results.

Table 2.7 Mechanical and geometrical properties measured in the experimental analysis on samples extracted from (a) corrugated slabs (b) manhole cover.

Table 2.7. Mechanical and geometrical properties measured in the experimental analysis on samples extracted from (a) corrugated slabs (b) manhole cover.

Table a	B	H	L	P_u	$f_{f,u}$
	(m)	(m)	(m)	(N)	(MPa)
#1	37.76	6.32	100.0	184	18.3
#2	37.71	6.2	100.0	165	17.1
#3	37.58	6.15	100.0	157	16.5
#4	36.68	6.19	100.0	156	16.6
Average					17.12

Table b	Area	S_x	Y_G	Ix_G	P_u	$f_{f,u}$
	(m^2)	(m^3)	(m)	(m^4)	(N)	(MPa)
#1	5476	136545	24.9	933266	9233	10.5
#2					9163	10.4
Average						10.44

As it was discussed earlier, flexural strength increases more or less linearly with the content of fibers, and the Eq. 2.3 can be used to relate $f_{f,u}$ and V_f. From the earlier set of tests, the values of γ and δ were assessed, which are detailed in Table 2.9 and visually represented in Fig. 2.18. There the potential relationships can be observed between flexural strength and the fiber volume fraction for both series 1 and series 2.

Table 2.8. The parameters γ and δ to be used in Eq (2.3).

Series		γ	δ
#1	$f_{f,u}$	3.88	1.55
#2	$f_{f,u}$	2.32	2.58

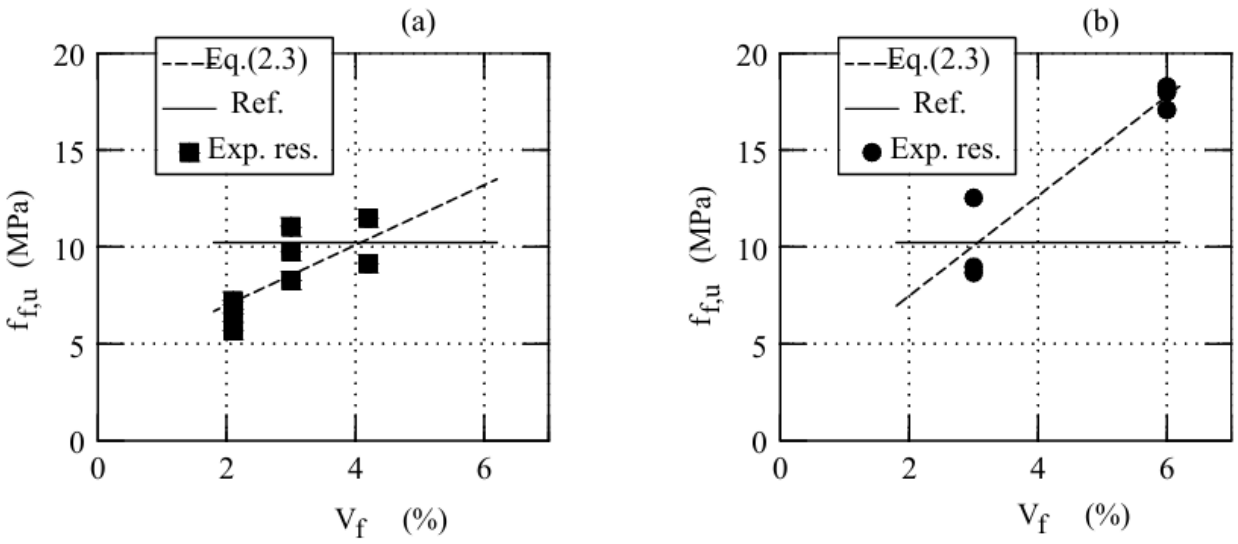

Figure 2.18: Possible $f_{f,u}$ *vs.* V_f relationships: (a) tests on series 1; (b) tests on series 2.

From a practical standpoint, predicting the fiber volume fraction (V_f) that compensates for the loss of strength is crucial for tailoring High-Performance Fiber-Reinforced Concrete (HPFRC) made with Recycled Steel Fibers (RSF) and other recycled materials. This tailored HPFRC has the potential to replace current cement-based composites. Specifically, it can be utilized in the construction industry to manufacture components like corrugated slabs and manhole covers, typically produced using only virgin materials.

To cast these industrial components from HPFRC, we need to determine the appropriate fiber volume fraction (V_f). In this context, the previously established correlation was applied to evaluate the volume of fibers.

As mentioned earlier, flexural tests on corrugated slabs and manhole cover rings resulted in flexural strengths ($f_{f,u}$) of 17.1 MPa and 10.4 MPa, respectively. Following the formulation provided by Eq. 2.3 for both Series 1 and Series 2, the fiber volume was determined. In Fig. 2.19, we compare these values for each tested series. The findings suggest that corrugated slabs can be successfully cast using mixtures from Series 2 when V_f is greater than or equal to 5.7%, exemplified by composite 2B. Similarly, the rings of manhole covers can be effectively replaced by mixtures from Series 1 when V_f is greater than or equal to 4.2%, as seen in the case of composite 1C.

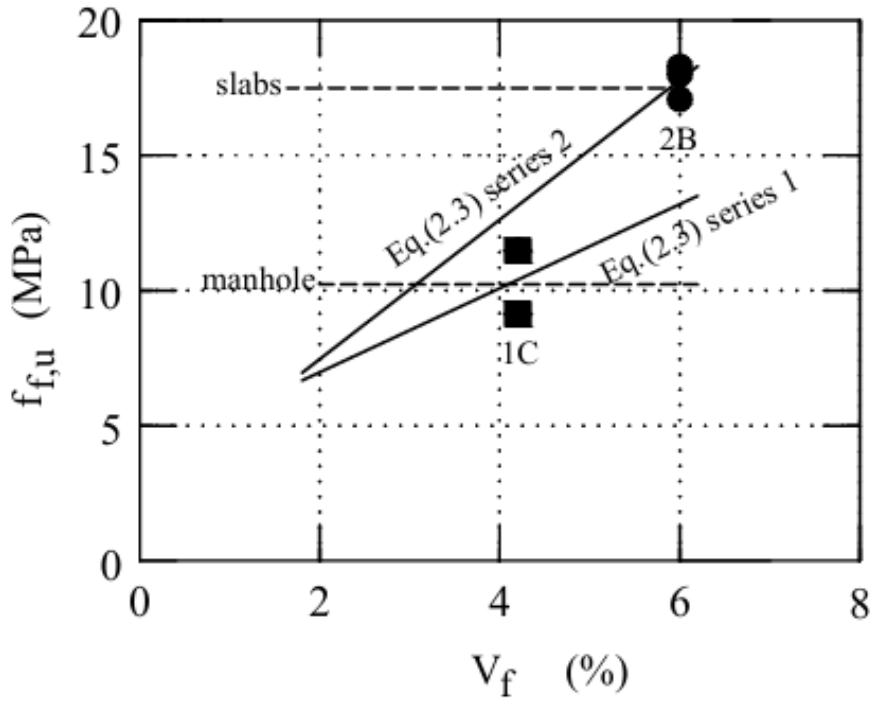

Figure 2.19: Comparison between the strength of Series 1 and Series 2 with those of some precast manufactures.

2.4- Conclusion

Based on the combined findings from the experimental investigations, several key conclusions emerge:

1. Cement-based composites, enriched with a significant volume of recycled steel fibers, can be finely tuned using a two-stage procedure, displaying promising adaptability in material design.

2. Optimal selection of the volume fraction of recycled steel fibers leads to notable enhancements in the mechanical properties of these composites, often surpassing those of traditional concrete compositions composed solely of virgin components.

3. The potential loss of flexural strength resulting from substituting virgin aggregate with recycled materials can be effectively mitigated by increasing the content of recycled steel fibers, suggesting a viable strategy for maintaining structural integrity.

4. Eco-mechanical analyses demonstrate that incorporating substantial volumes of recycled steel fibers can yield improvements in mechanical performance without a concurrent increase in environmental impact, highlighting the sustainability of this approach.

5. Improved performance can contribute to more sustainable materials for several reasons, including reduced material usage and increased resource efficiency. However, the focus of this paragraph is the Ecological Impact (EI).

6. Applying the previously developed correlation between $f_{f,u}$ and V_f can be an option for evaluating the suitable amount of fibers. In this case, by knowing the mechanical properties of the final industrial components and applying these correlations we can evaluate the volume of fiber.

Additionally, future research efforts will focus on the development of pilot projects aimed at fabricating full-scale structural elements using the two-stage composite methodology previously described. Moreover, the application of established correlations between fiber volume fraction and mechanical properties offers a valuable framework for evaluating and optimizing the fiber content in industrial components, paving the way for more efficient and sustainable construction practices.

Chapter 3:

Fiber-Reinforced Ice

3.1- Experimental Procedure

3.1.1- Differences in the work methodology between FRI and FRC

In the ongoing effort to explore new possibilities and enhance the strength of ice structures, the second phase of this project aimed to apply the successful process and methodology used in Reinforced-Concrete (RC) to ice materials.

Notable distinctions were identified in the work methodologies employed for Fiber-Reinforced Ice (FRI) compared to Fiber-Reinforced Concrete (FRC). While both materials share a common framework in terms of fiber reinforcement, subtle variations arise due to the unique properties of ice. In the preparation of ice samples for Fiber-Reinforced Ice (FRI), specific challenges occurred associated with freezing and molding processes.

One primary challenge arose in preparing ice samples, and to address this, a new mold was developed using resilient resin. This mold's flexibility ensured that the ice specimens could be easily removed without any distortion, as shown in Fig 3.1.

Figure 3.1: Resin mold and the plain ice specimen.

During the demolding and testing stages of Fiber-Reinforced Ice (FRI), it is crucial to highlight that all these procedures took place in the room temperature of the MASTRLAB Laboratory of Department of Structural, Geotechnical and Building Engineering of Politecnico di Torino, Italy. Working within this environment presented time-sensitive challenges, prompting us to adopt a fast-paced approach to maintain the integrity of the ice specimens. Therefore, a procedure of promptly placing the specimens in the freezer was addopted as we awaited tests on other samples. This not only ensured efficiency but also displayed our adaptability to the specific conditions of the laboratory, reflecting our commitment to precision and effective execution within the given constraints.

After testing the resin mold, it wasn't as efficient as expected. So, switching to polystyrene molds was necessary, which are shown in the figure. These molds have the same dimensions needed. In the new method, after creating each ice sample in the polystyrene mold, the mold was gently crashed to easily release the specimens. This approach has proven more effective in maintaining the integrity of the ice specimens. The process is illustrated in the Fig. 3.2.

Figure 3.2: Polystyrene Molds for Ice Specimens.

Like the project with mortar specimens, a standardized approach was maintained in creating ice prisms sized 40 × 40 × 160 mm³. These prisms underwent thorough testing for tension and compression, following UNI EN 196-1 (2005) guidelines.

3.1.2- Specimen preparation

In the initial phase, three plain ice specimens were examined, and their characteristics are detailed in Table 3.1. The mold was filled with tap water and frozen at a temperature of -5 °C. Subsequently, after demolding, the specimens were tested at room temperature (i.e., 20 °C).

Table 3.1. Ice specimen with freezing temperature of -5°C properties

Specimen	Length	Depth	Width	Weight	
				before test	after test
	(mm)	(mm)	(mm)	(g)	(g)
Ice-1	158.83	40.41	40.43	233	232
Ice-2	158.39	39.51	40.41	243	241
Ice-3	160.03	40.12	39.43	235	232

Afterwards, we utilized pine needles as reinforcement material (see Fig. 3.3). These natural fibers are commonly found on evergreen trees [67], with over 110 species falling under the "Pinus genus" worldwide. They are distributed across all continents, with a notable presence in Europe, Asia, Mediterranean Africa, North America, and various island nations [67].

Figure 3.3: Pine needle used as fiber-reinforcment for ice.

To gather the requisite data, measurements of the fibers length and diameter were conducted. A precision caliper with an accuracy of 0.01mm was used to ensure meticulous accuracy in the analysis. This methodology mirrored that employed for Fiber-Reinforced Concrete (FRC), underlining the importance of a comprehensive understanding of the reinforcement material in both scenarios.

Approximately 300 measurements were meticulously taken to provide a robust dataset. These measurements unveiled average values of 1.26 mm for diameter, 91.4 mm for length, and an aspect ratio of 73.37. The significance of these findings lies not only in their numerical values but also in their portrayal of the statistical distributions, as depicted in Fig. (3.4).

This comprehensive analysis not only furnishes crucial data but also enhances comprehension of the testing processes involved. By delving into the intricate details of the material properties, a better grasp of the behavior and performance of the composite materials under scrutiny is achieved.

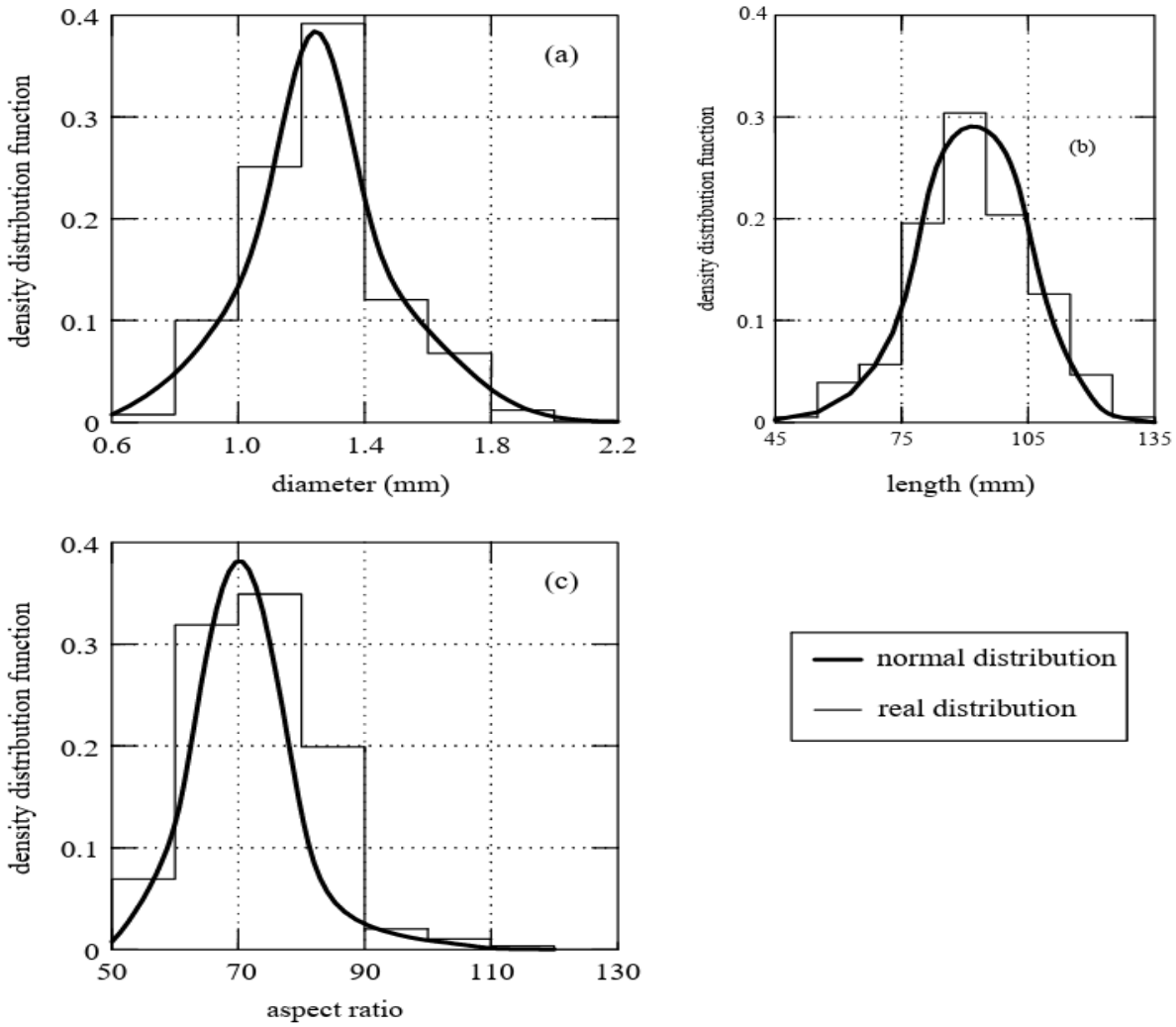

Figure 3.4: Geometrical properties of pine needles used in this project: (a) statistical distribution of fiber diameter; (b) statistical distribution of fiber length; and (c) statistical distribution of fiber aspect ratio.

To cast FRI specimens, a two-step casting procedure was employed. Initially, pine needles were positioned in polystyrene molds, as depicted in Fig (3.5.a). Each mold accommodated three specimens with dimensions of 40×40×160 mm^3, following a similar approach used for the preparation of cement-based mortars [68].

Next, the molds were filled with tap water, allowing both the fibers and water to remain at ambient conditions for one day. Subsequently, the molds were refilled with water (accounting for evaporation and fiber absorption), and then placed in the freezer at varying temperatures for 48 hours, as previously described. Following demolding, the samples were stored in the freezer to prevent melting at room temperature.

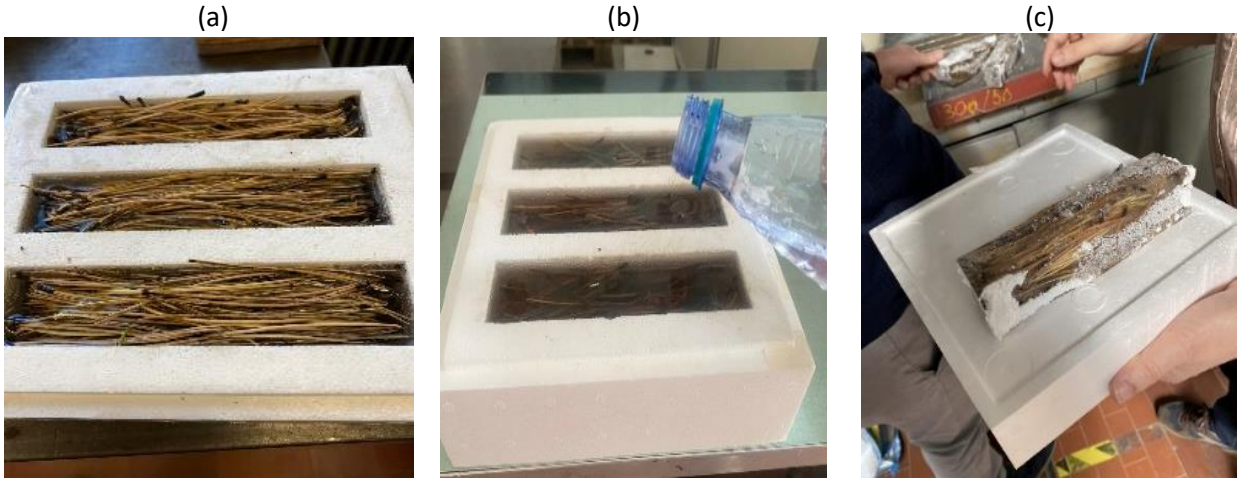

Figure 3.5: Pine needle used as fiber: (a) placing fibers in the molds; (b) pouring the water in the molds; (c) After freezing.

We made four sets of three specimens each using a particular casting method. The amount of fibers varied in each set: no fibers in plain ice (PI), 39 grams per liter in FRI-1, 56 grams per liter in FRI-2, and 78 grams per liter in FRI-3. We prepared a total of 12 specimens for each freezing temperature. The testing followed a standard procedure (UNI EN 196-1) for cement-based mortars and was carried out at three different freezing temperatures: -24, -21, and -18 degrees Celsius.

Before conducting the tests, the weight (wt) was measured with a precision of 1g, and the width (B), height (H), and length (L) of the samples were measured with a caliper accurate to 0.01mm (Fig. 3.6). The findings from these measurements for samples with a freezing temperature of -18°C are detailed in Table 3.2. Using this information, the density for all the series studied in this research project was calculated. The results, presented in the last column of Table 3.2, indicate that the density remains relatively consistent even with the addition of fibers. Specifically, the average value of 870 kg/m^3 aligns with measurements from previous experimental studies [69]. Since the tests were carried out at room temperature, the weight and density were measured both before and after the test. As indicated in Table 3.2, there was not a substantial loss of weight (resulting from ice melting) during the test.

Figure 3.6: Fiber-reinforced ice specimens geometrical measurments.

Table 3.2. Size and density measurements for samples with freezing temperature of -18 degree Celsius

	Fiber	Sample	B	H	L	Wt (before)	Density (before)	wt (after)	Density (after)
	(g/dm^3)		(mm)	(mm)	(mm)	(N)	(kg/m^3)	(N)	(kg/m^3)
PI	0	1	41.02	39.97	159.53	2.28	870	2.28	870
		2	42.53	39.75	159.17	2.35	870	2.34	870
		3	43.18	40.17	159.12	2.45	890	2.44	890
FRI-1	39	1	38.17	40.25	159.57	2.16	880	2.16	880
		2	38.57	40.65	159.67	2.25	900	2.25	900
		3	39.75	41.3	159.76	2.16	820	2.16	820
FRI-2	56	1	39.11	41.43	160.14	2.33	900	2.33	900
		2	41.45	40.53	160.11	2.34	870	2.34	870
		3	43.05	40.81	160.19	2.34	830	2.34	830
FRI-3	78	1	43.02	41.4	160.4	2.37	830	2.37	830
		2	43.01	40.78	160.34	2.4	850	2.38	850
		3	41.85	40.85	159.43	2.34	860	2.34	860

3.1.3- Testing Procedure

In the initial phase of reviewing the test results, the primary emphasis is on the outcomes derived from samples exposed to freezing temperatures of -18°C. Subsequently, a comparative analysis was conducted with the results obtained from samples subjected to freezing temperatures of -24°C and -21°C. This comparative examination helps discern any temperature-specific trends or variations.

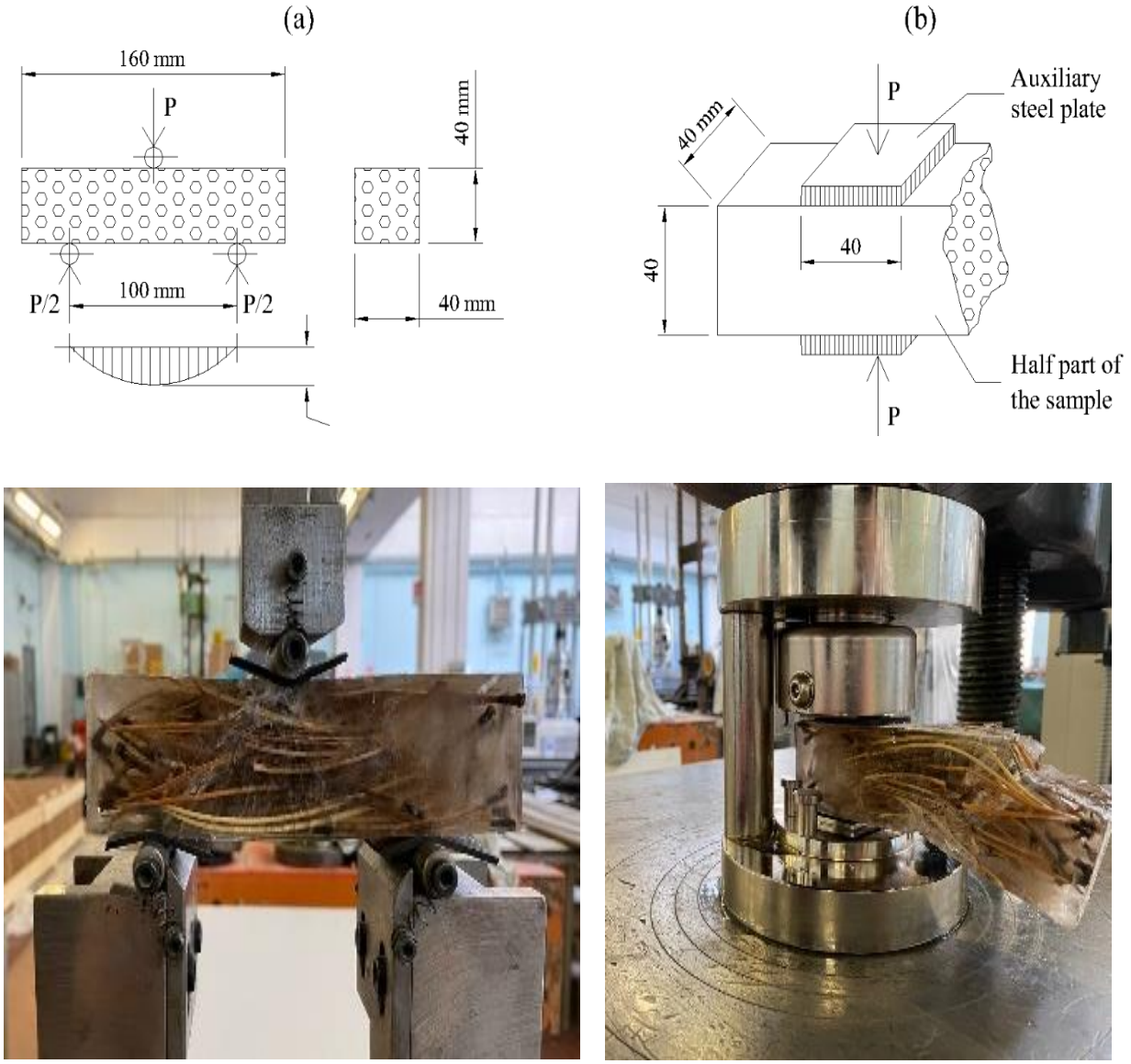

Figure 3.7: Mechanical performances of Fiber reinforced ice: (a) three-point bending tests; and (b) compressive test.

Moving on to the next chapter, the focus shifts to another aspect of this study, which involves establishing a correlation between the flexural strength and compressive strength of ice materials. A similar approach to the one previously employed for mortar specimens is adopted. This segment of the study involves the analysis of samples exposed to a freezing temperature of -5°C. By exploring the relationship between flexural and compressive strength, insights into the mechanical properties of ice under specific temperature conditions are sought.

As anticipated, the mechanical properties of the samples are measured to determine if adding fibers positively affects their strength. This leads to the evaluation of both flexural and compressive strength for all the prepared samples.

Following UNI EN 196-1 standards, both flexural and compressive strength can be measured using the same specimen. As mentioned, this method was previously used for mortars with and without fibers. For the tests, all the prisms were subjected to three-point bending (see Fig. 3.7.a). The load (P) was applied in the middle of the ice prisms using a loading machine with a capacity of 50 kN.

During the tests, both the applied load (P) and the mid-span deflection (η) of the beam were measured until the specimen failed. Usually, this resulted in the specimen breaking into two halves, which were then tested in compression (Fig. 3.7.b).

In the compression test, the load (P) was applied to a 40 × 40 mm² loading area using a device with platens that were 10 mm thick. The compressive force (P) gradually increased at a rate of 200 N/s until failure. To prevent ice melting around the supports, rubber pieces were placed at the points where the specimens and loading machine came into contact in both tests. In both tests, to avoid the problem of specimen melting, a set of rubber pieces was located at the contact points between the machine and the ice specimens.

3.2- Experimental Data

3.2.1- Test results

First, through three-point bending tests, the load (P) versus midspan deflection (η) diagrams were obtained for all specimens, grouped based on fiber content and presented in Figure 3.8. The results were presented for each type of sample, with varying fiber content as follows: 0 g/liter in plain ice (PI), 39 g/liter in FRI-1, 56 g/liter in FRI-2, and 78 g/liter in FRI-3.

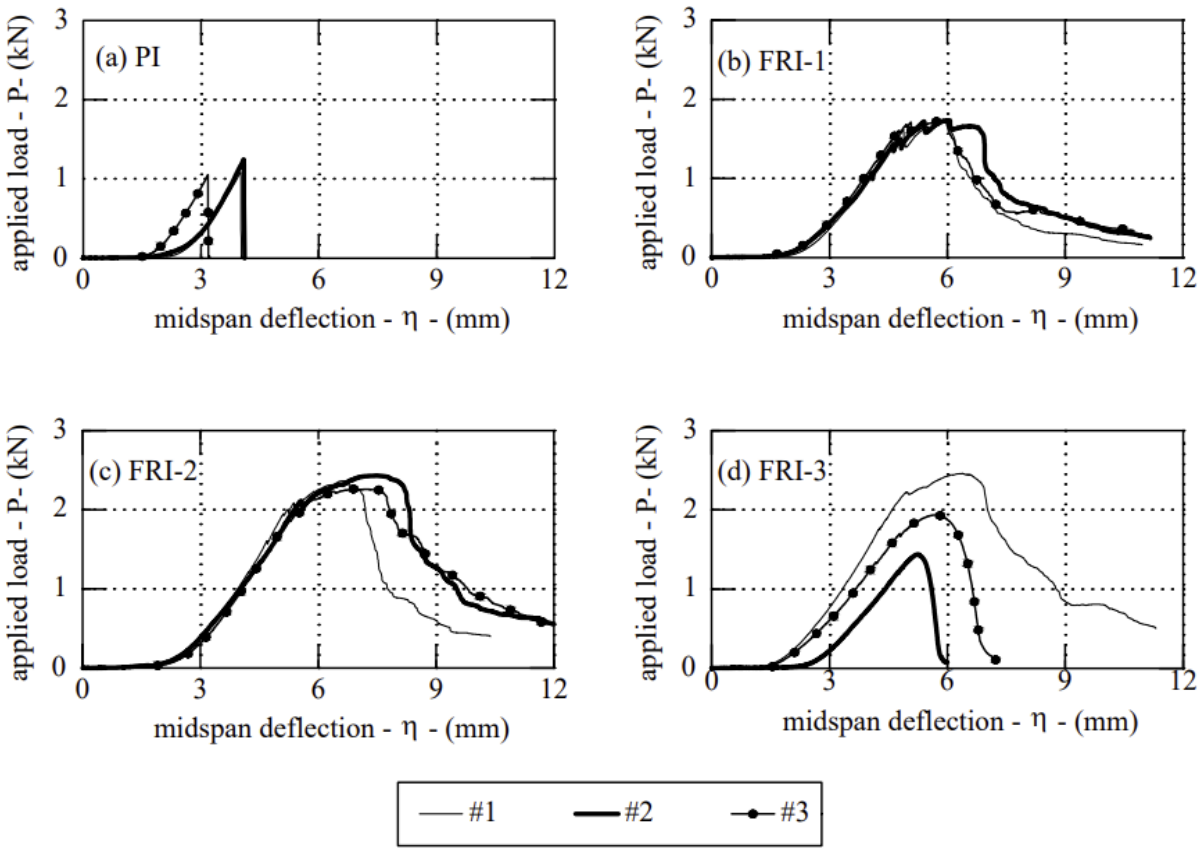

Figure 3.8: Load-midspan deflection diagrams measured with three-point bending tests.

The overall ascending branch of the P-η diagrams is collectively depicted in the idealized graph of Figure 3.9.a. In this segment of the load-deflection curve, multiple cracks develop, leading to the appearance of a deflection hardening branch. Subsequently, a softening tail is observable, with loads decreasing as deflection increases. The figure highlights two crucial loads: P_{cr}, marking the initiation of the first crack (Point A in Fig. 3.9.a), and P_u, representing the maximum load (Point B in Fig. 3.9.a). The values of these loads, along with the distance Δ between P_u and P_{cr} (see Fig.

3.9.a) in terms of the difference between displacements η, are reported in Table 3.3. Additionally, Table 3.3 includes the maximum load (P_c) measured during compression tests (Fig. 3.7.b).

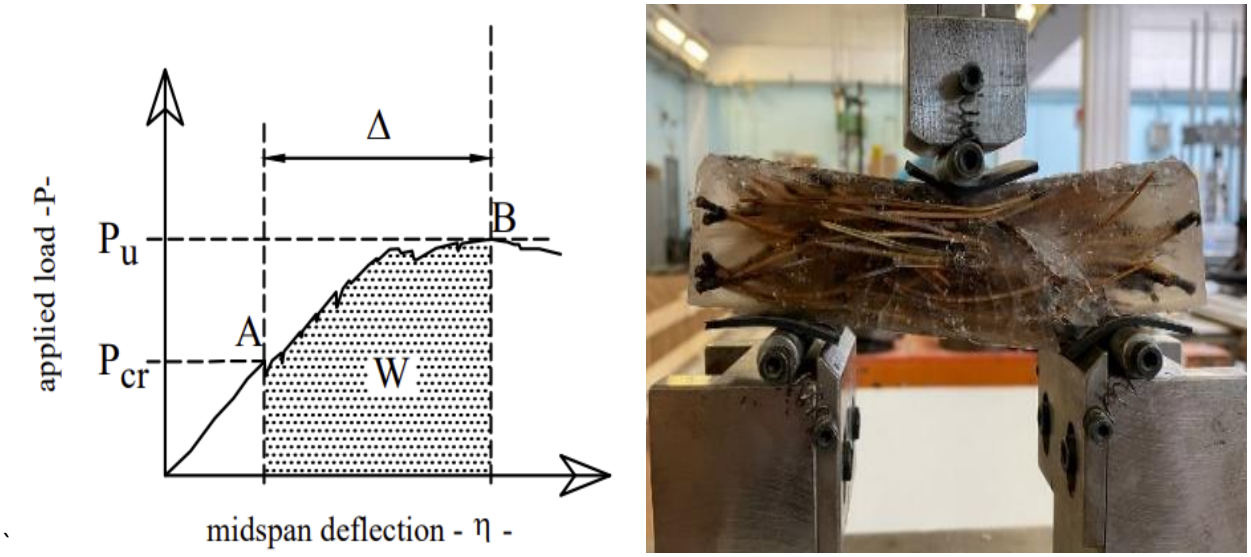

Figure 3.9: Results of three-point bending tests: (a) ideal P-η curve in the rising branch. (b) multiple cracking in the specimen.

Table 3.3. Mechanical properties measured in the three-point bending test.

	Fiber	Sample	^{P}u	^{P}cr	Δ	^{P}c	W
	(g/dm³)		(N)	(N)	(mm)	(N)	(N*mm)
PI	0	1	1089	1089	0	3654.14	0.0
		2	1236	1236	0	2595.43	0.0
		3	1044	1044	0	3017.55	0.0
FRI-1	39	1	1719	1617	1.025	5305.73	1709.0
		2	1725	1488	1.242	5042.40	1996.7
		3	1724	1600	1.060	3972.87	1761.8
FRI-2	56	1	2365	2006	1.429	4681.68	3124.3
		2	2423	2101	1.907	4295.47	4313.0
		3	2251	1950	1.487	4880.62	3123.9

3.2.2- Discussion on the results

In the context of three-point bending tests, assuming linear elastic material behavior and uncracked cross-sections, the flexural stress (f) can be computed using the Eq 2.2. This equation utilizes the values of P (specifically, P_{cr} and P_u) to determine the cracking strength ($f_{f,cr}$) and ultimate strength ($f_{f,u}$). The results of these strengths are detailed in Table 3.4, and the average values of $f_{f,cr}$ and $f_{f,u}$ for each type of Fiber-Reinforced Ice (FRI) are presented in the histograms of Fig. 3.10.a and Fig. 3.10.b, respectively.

Additionally, based on the ascending branch of the P-η diagram depicted in Fig. 3.9.a, the work (or energy), denoted as W, associated with multiple cracking during the deflection-hardening stage can be calculated using Eq. 2.1. The values of W are provided in the last column of Table 3.3, and the average energy values are illustrated in Fig. 3.10.c. Lastly, the compressive strength is determined by dividing the load (P_c) in Table 3 by the loading area (40 × 40 mm²). The results are reported in Table 3.4, and Fig. 3.10.d displays the average compressive strength values for each type of FRI.

Table 3.4. strength values measured in flexural and compressive analysis.

	Fiber	Sample	$f_{f,cr}$	$f_{f,u}$	fc
	(g/dm³)		(MPa)	(MPa)	(MPa)
PI	0	1	2.49	2.49	2.28
		2	2.76	2.76	1.62
		3	2.25	2.25	1.89
FRI-1	39	1	3.84	4.09	3.32
		2	3.29	3.82	3.15
		3	3.57	3.85	2.48
FRI-2	56	1	4.48	5.28	2.93
		2	4.63	5.33	2.68
		3	4.08	4.71	3.05
FRI-3	78	1	4.51	4.99	2.75
		2	2.52	2.85	2.34
		3	3.63	4.13	2.25

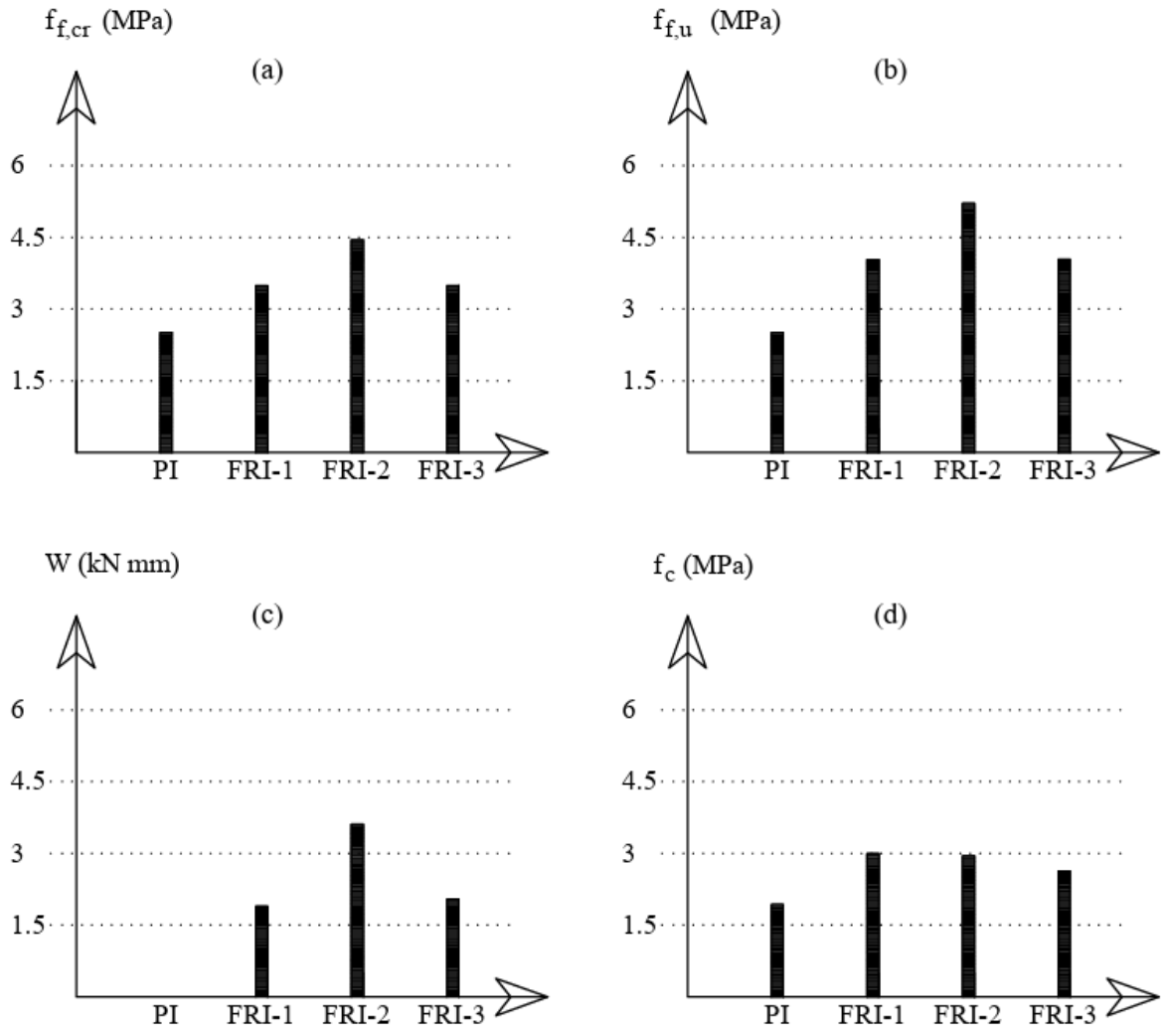

Figure 3.10: Average values of strength measured in flexural and compressive tests: (a) flexural strength at cracking (when P = P_{cr} in Eq. 2.2). (b) flexural strength at peak (when P = P_u in Eq. 2.2). (c) work (or the energy) released during the deflection-hardening (d) compressive strength of ice.

Although the test results can be reported as a function of the quantity of fibers (QF), as depicted in Fig. 3.10, the increment of QF does not necessarily result in an increase in mechanical performance. In fact, the values of strength and energy do not follow monotonic functions of QF, as illustrated in Fig. 3.10. Hence, it becomes of practical interest to evaluate the optimal content of fibers, in which the mechanical performance is maximum.

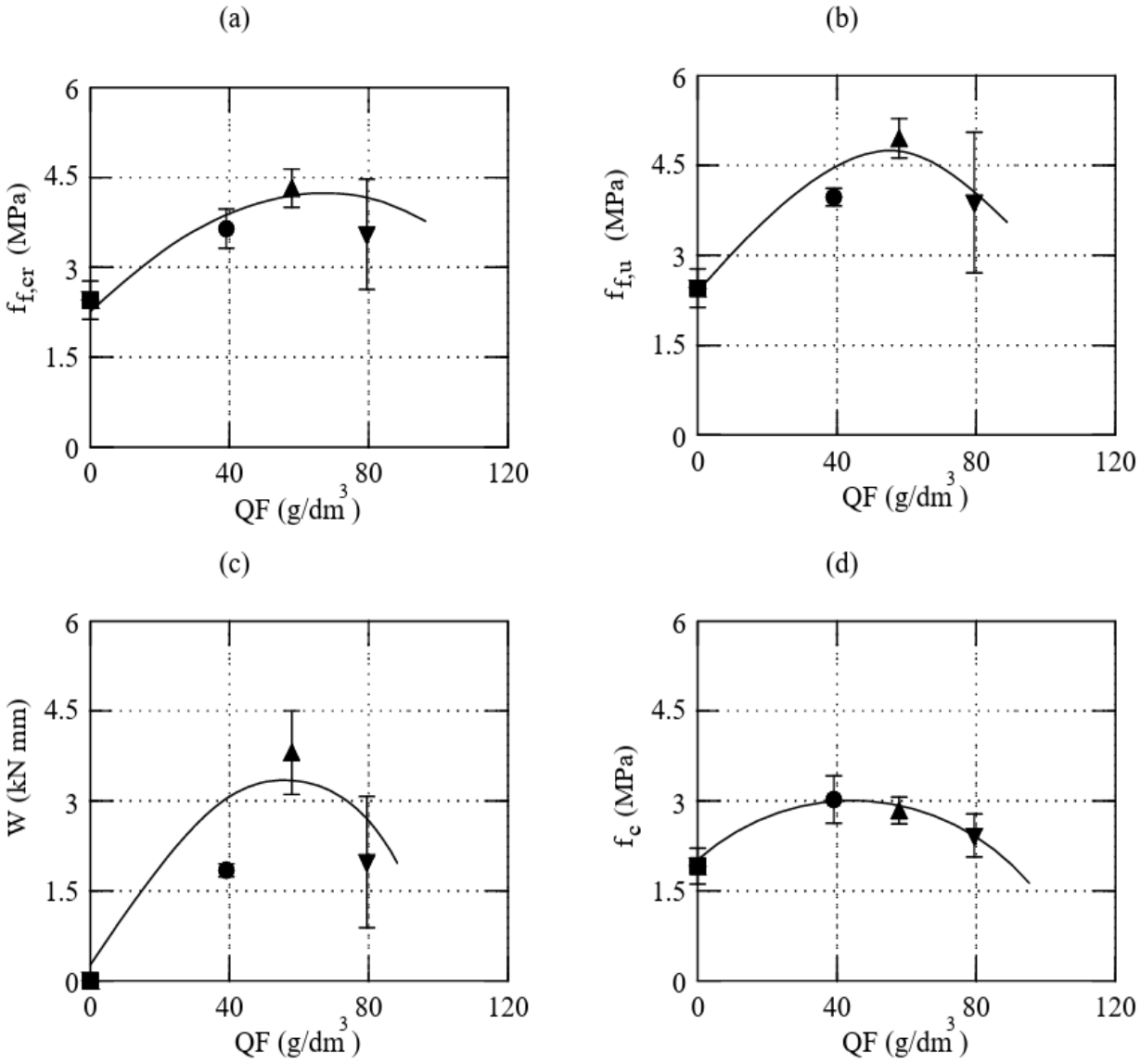

Figure 3.11: Quadratic regression between f_c, $f_{f,cr}$, $f_{f,u}$, W, and the quantity of fibers (QF)

As shown in the diagrams of Fig. 3.11, where values of $f_{f,cr}$, $f_{f,u}$, W, and f_c are reported as a function of QF, a regression analysis, based on the least square approximation of the experimental data, leads to the derivation of the following quadric function:

$$Mechanical\ performance = (\mathrm{A}\,.\,QF^2) + (\mathrm{B}\,.\,\mathrm{QF}) + \mathrm{C} \qquad (3.1)$$

Here, the values of A, B, and C are reported in Table 3.5, based on the type of mechanical performance. The experimental results and correlation Eq. (3.1) indicate an optimal fiber content. Indeed, the peak of the mechanical performance is achieved in FRI-2, where the fiber content is

56 g/liter. Further increments in fiber content, as observed in FRI-3, result in a decrement of all mechanical performances.

Table 3.5. values of the parameters A and B and C in Eq. 3.1.

	A	B	C
$f_{f,cr}$	-0.0005 MPa / $(g/dm^3)^2$	0.058 MPa / (g/dm^3)	2.4525 MPa
$f_{f,u}$	-0.0007 MPa / $(g/dm^3)^2$	0.0774 MPa / (g/dm^3)	2.4319 MPa
W	-0.0009 kN mm / $(g/dm^3)^2$	0.1012 kN mm / (g/dm^3)	- 0.098 kN mm
f_c	-0.0005 MPa/ $(g/dm^3)^2$	0.0467 MPa / (g/dm^3)	1.917 MPa

Based on our experimental findings and the application of Eq.3.1, it is evident that there exists an optimal value for fiber content in achieving peak mechanical performance. Specifically, this optimal performance is observed in FRI-2, where the fiber content is at 56 grams per liter.

Interestingly, when we further increased the fiber content, as seen in FRI-3, we noticed a decline in all mechanical performances. One possible explanation for this behavior lies in the interaction between the matrix, which in this case is water, and the reinforcing elements, i.e., the fibers. Beyond a certain threshold of fiber content, the frozen water area decreases, leading to a reduction in the bonding between fibers and ice. This phenomenon results in a failure mechanism under applied loads, and consequently, there is a premature failure of the samples.

These findings align with those observed by multiple researchers studying fiber-reinforced concrete (FRC), where each level of fiber content exhibits a maximum threshold. Typically, researchers employ a quadratic function, such as Eq. (3.1), to predict the mechanical properties of FRC based on fiber content [71].

In essence, an excessive amount of fiber appears to negatively impact the structural integrity of the ice specimens. This insight into the relationship between fiber content and mechanical performance is crucial for understanding the optimal conditions for reinforcing ice structures and avoiding premature failure [71].

3.3- Conclusion

In this chapter, the mechanical properties of Fiber-Reinforced Ice (FRI) were investigated through three-point bending and uniaxial compression tests. From the test results and experimental data analysis, several key conclusions emerge:

1. In bending, plain ice experiences a significant drop in bearing capacity after reaching peak stress, leading to brittle failure with a single crack. In contrast, FRI displays the formation of multiple cracks as the bending moment increases, accompanied by an increase in bearing capacity. This behavior is attributed to deflection hardening, rendering FRI more ductile than plain ice.
2. Overall, the mechanical properties of FRI are enhanced by the presence of fibers, surpassing those of unreinforced ice. Test results reveal that the ultimate flexural strength of FRI can be double that of plain ice, with flexural strength being directly proportional to compressive strength.
3. However, the mechanical properties of FRI exhibit sensitivity to fiber content, with performance not increasing uniformly with fiber quantity. Optimal performance is achieved at a specific fiber content, exemplified by FRI-2 containing 56 g/dm³ of pine needles.

Looking ahead, the study will explore the influence of temperature on the strength and toughness of FRI in subsequent phases. Since ice structures generally have lower carbon dioxide emissions, this study focused more on the parameters that ensure their safety rather than their Ecological Impact.

Chapter 4:

Factors Influencing Strength of Cement-based Materials and Ice Structures

4.1- The Effect of Water-to-Cement Ratio**

4.1.1- Introduction

The influence of the water-to-cement (w/c) ratio on the mechanical properties of cement-based mortar materials has been extensively discussed in academic literature [74]. Through numerous studies, the effects of this ratio can be categorized into five key domains: strength, durability, workability, shrinkage, and creep. Each of these factors plays a critical role in determining the overall performance and longevity of concrete structures.

Strength is one of the most significant aspects affected by the w/c ratio. It is well-established that the compressive strength of concrete is inversely related to the w/c ratio. Higher ratios tend to yield lower compressive strength due to excess water [74], which weakens the concrete matrix by creating more voids and hindering the binding of aggregates. Conversely, lower w/c ratios lead to denser packing of cement paste, resulting in higher compressive strength. This relationship is attributed to the hydration process, where excess water leads to incomplete cement hydration and weaker interfacial bonding between cement particles [74]. Fig. 4.1 illustrates the correlation between water-to-cement ratio and compressive strength of cement-based mortar materials.

In the existing literature, a considerable body of academic research has focused extensively on the relationship between compressive strength and the water-to-cement ratio in concrete. Additionally, there exists a significant number of studies investigating the correlation between the water-to-cement ratio and tensile strength, although to a lesser extent compared to compressive strength analyses.

These studies have revealed that variations in the water-to-cement ratio indeed impact the tensile strength of concrete, albeit with less pronounced effects compared to compressive strength. Higher water-to-cement ratios have been consistently associated with reduced tensile strength, attributed primarily to increased void content within the concrete matrix and diminished bond strength between aggregates and the cement paste. For example, empirical evidence indicates that a water-to-cement ratio of 0.4 is associated with a tensile strength approximately 20 percent higher than that observed with a water-to-cement ratio of 0.5. [74-79]. It is noteworthy, however, that the measurement of tensile strength often relies on indirect methods such as the split tensile test, which may introduce additional variability into the results [79].

**Due to the abundance of discussion surrounding this relationship and its widespread acknowledgment, there hasn't been a lack of additional testing. The provided content offers a summary of previous research on this topic.

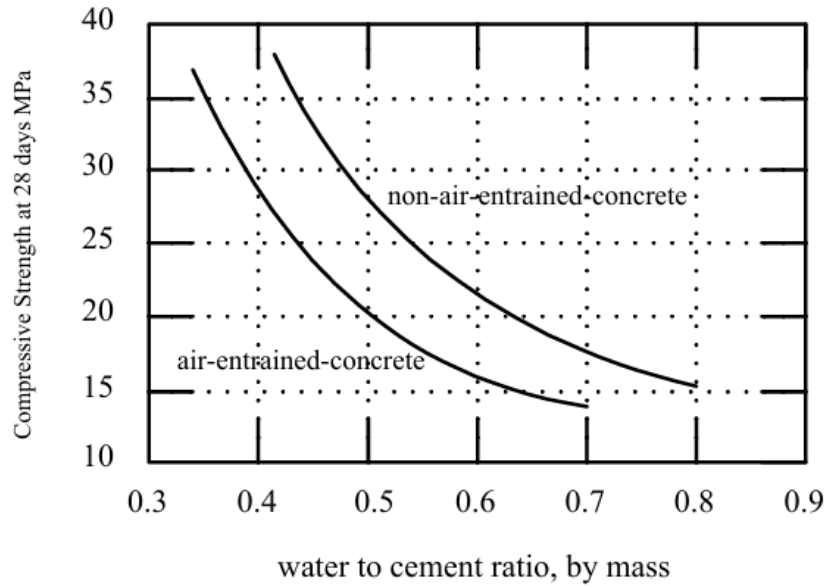

Figure 4.1: – Relationship between water to cement ratio and compressive strength of cement-based mortar materials

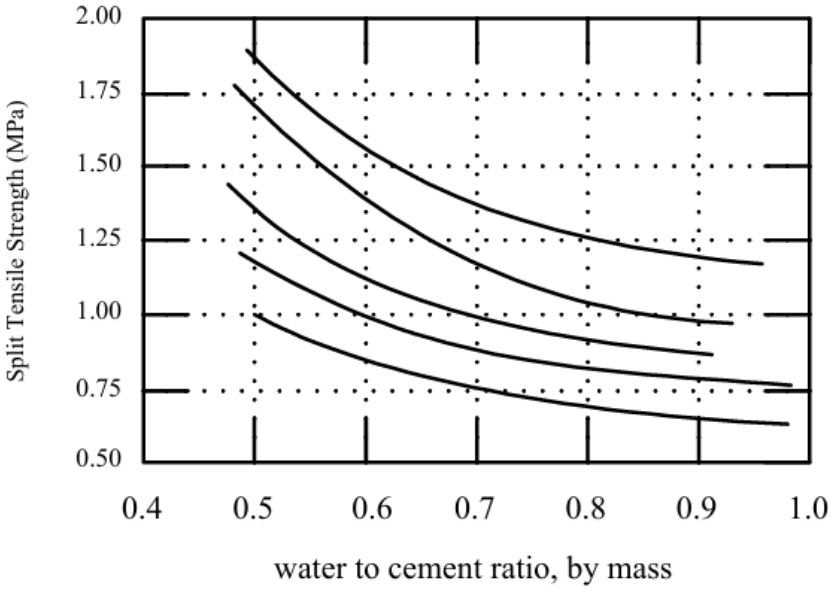

Figure 4.2: – Relationship between water to cement ratio and split tensile strength [76].

Durability is another crucial consideration influenced by the w/c ratio. Lower ratios generally enhance concrete durability by reducing permeability [77]. Excessive water in high w/c mixes increases permeability, allowing harmful substances like chlorides and sulfates to penetrate more easily. This heightened permeability can lead to corrosion of reinforcement and gradual degradation of the concrete over time [78].

Workability, referring to the ease of mixing, placing, and compacting concrete, is significantly impacted by the w/c ratio. Higher ratios typically yield more fluid mixes, enhancing workability. However, excessively high ratios can result in issues such as segregation and bleeding, compromising the quality and uniformity of the concrete [78].

The slump test is a widely accepted technique utilized to gauge the consistency and workability of newly mixed concrete. Through this test, the slump number offers insights into the concrete's workability. A higher slump value signifies enhanced workability, indicating that the concrete is more fluid and can readily undergo deformation. Conversely, a lower slump value indicates less workable concrete, implying a stiffer and less fluid consistency. Following this explanation, a table representation will be provided illustrating the correlation between slump number and the water-to-cement ratio [74-77].

Table 4.1. Results of Slump Test on Concrete and Lateritic Concrete Mixes [77].

Water-Cement Ratio	Concrete Mixes		Lateritic Concrete Mixes	
	Slump (cm)	Type of Slump	Slump (cm)	Type of Slump
0.55	0.9	TRUE	0	TRUE
0.6	1.5	TRUE	0.1	TRUE
0.65	2	TRUE	0.1	TRUE
0.7	2.5	TRUE	0.1	TRUE
0.8	18	Collapse	0.2	TRUE

Shrinkage and cracking are common concerns associated with higher w/c ratios. Excess water evaporates during the curing process, leaving behind more voids in the concrete. This can lead to increased drying shrinkage and a higher propensity for cracking as the concrete undergoes volume changes. Managing the w/c ratio is crucial in mitigating these issues and ensuring structural integrity.

Additionally, creep, the gradual deformation of concrete under sustained load over time [74], is influenced by the w/c ratio. Higher ratios typically result in higher creep deformation due to increased porosity and lower strength of the concrete mix. Understanding and controlling the w/c ratio is therefore essential in optimizing the mechanical properties and long-term performance of concrete structures [77].

The mechanical behavior of concrete undergoes variations during the drying process, leading to local and structural modifications. Desiccation shrinkage [74] is a primary consequence of drying, attributed to increased capillary suction, variations in disjoining pressure, and changes in surface energy at a microscopic level [75]. Non-uniform drying creates saturation gradients within the structure due to the low permeability of concrete and its geometry. Consequently, faster drying

kinetics near the surface compared to deeper within the material induce non-homogeneous strains, resulting in tensile stresses and microcracking. Additionally, microcracking may occur at the interface between cement paste and aggregates, particularly for larger aggregates, impacting the overall integrity of the material even before mechanical loading [78].

To mitigate such damage, specific laboratory conditions are necessary, such as desaturation with minimal relative humidity increments or utilizing thin samples. The induced microcracking not only weakens the material but also increases its permeability, thereby influencing the durability of concrete structures significantly [78].

While uniaxial compressive tests have been commonly used to assess drying-induced variations, limited data from conventional triaxial tests regarding the role of interstitial water are available. Existing literature reports conflicting findings regarding strength variations during drying [79]. Some studies suggest an increase in strength with decreasing relative humidity, while others observe initial increases followed by decreases or vice versa. These variations stem from competitive effects such as increased capillary pressure and induced microcracking, both influenced by factors like aggregate size and water-to-cement ratio (w/c) [80]. Similarly, Young's modulus exhibits complex variations during drying, influenced by concrete composition and curing conditions. Understanding these phenomena is crucial for predicting concrete behavior accurately [81].

The water-to-cement (w/c) ratio stands as a fundamental determinant in shaping the mechanical properties and overall performance of cement-based mortar materials. Through exhaustive exploration in academic literature, it is evident that the w/c ratio exerts a profound influence across various domains crucial for concrete structure integrity. From strength to durability, workability, shrinkage, and creep, each factor underscores the intricate relationship between water content and cement paste, emphasizing the need for precise control and management in concrete mix design [82].

Furthermore, the comprehensive understanding and careful manipulation of the w/c ratio hold paramount importance in ensuring the longevity and resilience of concrete structures. As we navigate the complexities of construction materials, continued research efforts aimed at elucidating the nuanced interactions between the w/c ratio and mechanical properties will undoubtedly pave the way for innovative advancements in concrete technology. By leveraging this knowledge, engineers and designers can optimize concrete formulations, mitigate potential risks, and ultimately contribute to the creation of safer, more sustainable built environments for generations to come.

As outlined in this section of the thesis, the water-to-cement ratio impacts various mechanical characteristics of cement-based materials, both in the early stages and after 28 days from casting. This understanding prompts us to consider a factor that similarly affects ice structures. In the following section, we will examine the effect of freezing temperature on ice structures.

Another study, focusing on the Effect of Water to Cement Ratio and Replacement Percentage of Recycled Concrete Aggregate on Concrete Strength [84], also supports the notion that the water-to-cement ratio significantly influences mechanical performance, particularly compressive strength. It concludes that the replacement of Fine-Recycled-Concrete-Aggregate (FRCA) up to 30% does not compromise concrete strength. Optimal replacement occurs at 20%, where the most significant interaction of FRCA within the concrete enhances compressive strength by neutralizing the porosity properties of FRCA through an optimum filler effect generated during mixing.

However, deviations from this optimal replacement percentage, particularly at 40% and 60% replacement levels, result in a drastic drop in compressive strength. Additionally, at a water-to-cement ratio of 0.45, concrete workability is notably low, while the most suitable condition for consistent strength, indicating effective cement hydration, is observed at a ratio of 0.5. These findings suggest a high potential for utilizing FRCA in concrete mix designs, emphasizing the importance of considering FRCA properties in such formulations.

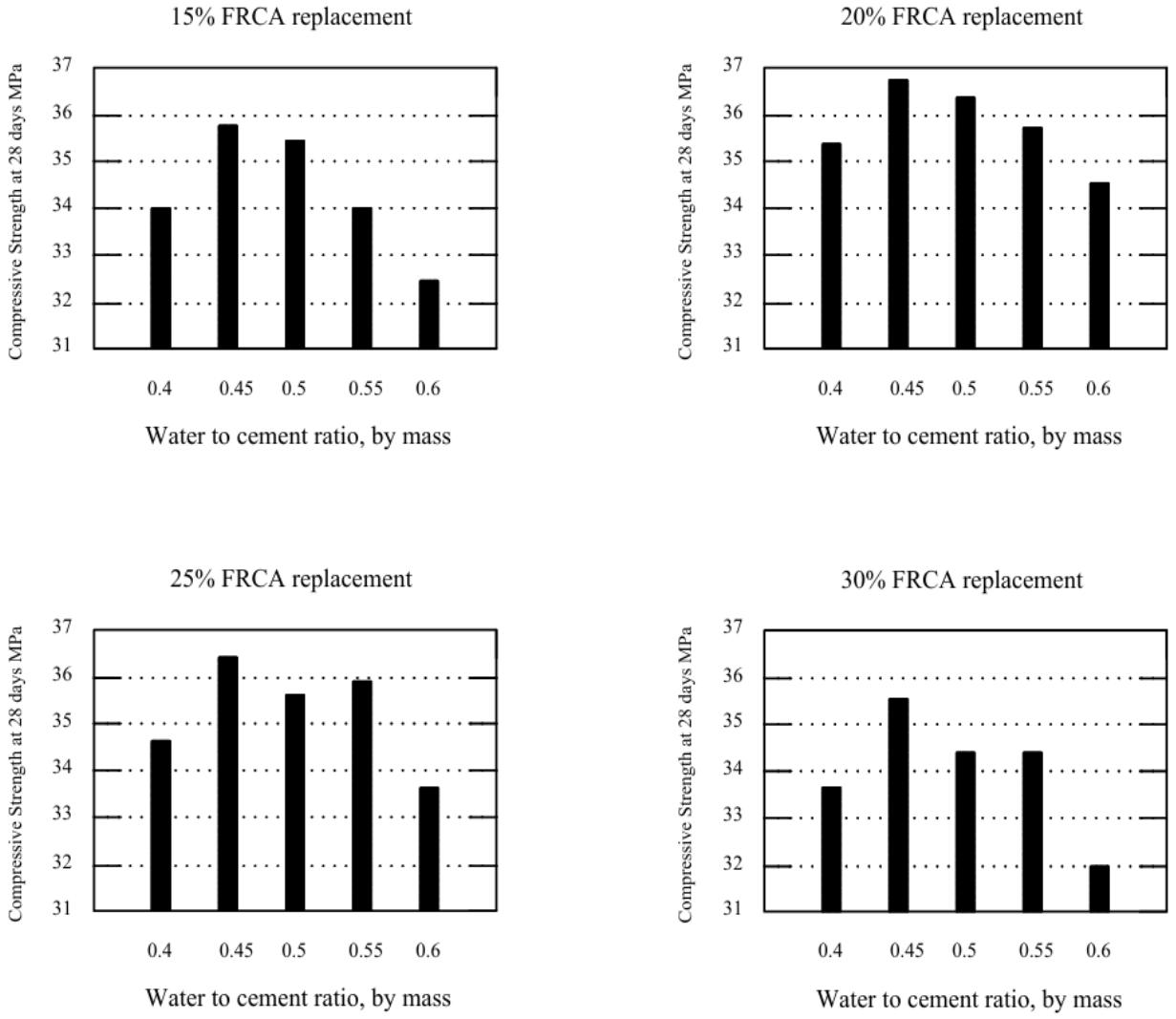

Figure 4.3: – Compressive strength for different FRCA replacement [84].

On the other hand, studies investigating the impact of water-to-cement (w/c) ratio on the mechanical properties of fiber-reinforced concrete (FRC) have yielded valuable insights, especially in environments with harsh conditions. Lowering the w/c ratio is a well-established

method to bolster the durability and strength of concrete, chiefly by diminishing porosity and pore sizes within the material [79]. For instanmce, this consolidation of the concrete matrix not only enhances compressive strength but also fortifies resistance against detrimental agents like chlorides, thereby diminishing the risk of corrosion to internal steel reinforcements. Moreover, the bond strength between the concrete matrix and fiber reinforcements, notably glass fiber reinforcement polymer (GFRP), experiences enhancement with reduced w/c ratios, thereby reinforcing the structural integrity of the composite material [80].

4.2- Ice Temperature Sensitivity

4.2.1- Introduction

In contrast to traditional concrete structures built with mortars, the idea of constructing with ice is a relatively new frontier in engineering. Thus, a thorough examination was essential to uncover the various factors affecting the mechanical properties of these icy structures.

In the context of ice structures, their integrity is susceptible to various factors such as fracture, creep, and melting. While fracture and creep can be predominantly addressed during the construction phase through reinforcement measures, the focus here is on temperature sensitivity of this substance.

Generally, melting initiates when the ice surface temperature reaches 0 °C. It is noteworthy that this doesn't necessarily align with the air temperature, as factors like evaporation and heat conduction may cool the surface considerably. For instance, in dry air with a 40% relative humidity, well-ventilated ice might only start melting at around +5 °C. Furthermore, if the bulk ice is much colder than 0 °C, the surface may remain un-melted even at higher air temperatures. sOn the other hand, solar exposure can influence melting dynamics, causing it to occure at temperatures slightly below 0 °C, especially if the ice surface is in direct sunlight. The impact of this varies based on impurities and the ice structure. A pure, bubble-free ice surface reflects less than 2% of incident radiation, whereas air bubbles increase reflection to 50%.

Also, foreign particles like dust, sand, and organic materials decrease reflection. Consequently, during sunny periods, preventing contaminants or applying reflective substances like white ice (e.g., snow) on the surface can effectively reduce melting of uncovered ice surfaces.

In colder temperatures significantly below zero degrees Celsius, ice undergoes changes that impact its strength and behavior. First, the lower temperatures cause water molecules in the ice to slow down, making the ice harder and more brittle. This increased hardness results from the molecules packing more closely together, creating a more rigid structure. Second, the molecular bonding between water molecules in the ice matrix becomes stronger in colder temperatures. This enhanced bonding contributes to the overall strength of the ice. However, it is necessary to note that while lower temperatures generally increase ice strength, extremely low temperatures can make ice more susceptible to brittle fracture. This means that sudden impacts or stress may lead to rapid crack propagation through the ice structure.

4.2.2- Experimental data

In this section of the study, we conducted experiments with a total of 12 specimens prepared at three different freezing temperatures: -18°C (which was discussed previously), -21°C, and -24°C. Each specimen's size and preparation process were discussed in detail earlier (Section 3.1.2).

To systematically investigate the impact of freezing temperature and fiber volume, the specimens were organized into four groups for each freezing temperature. The first group, termed Plain Ice (PI), serves as a control group, solely considering the effect of freezing temperature. The second group, denoted FRI-1, consists of specimens with 9.75 grams of fibers. This group allows us to

explore the influence of an additional fiber volume on the ice specimens. In the third group, named FRI-2, specimens contain 14 grams of bio fibers. This group aims to examine the effects of a different fiber volume compared to the second group and understand any variations in performance. The fourth and final group, FRI-3, comprises specimens with 19.5 grams of fibers. This group provides insights into the potential impact of higher fiber volumes on ice strength and behavior.

By systematically varying the freezing temperature and fiber volume in these groups, our study aims to comprehensively analyze and understand the combined effects of these factors on the properties of the ice specimens. This structured approach allows us to draw meaningful conclusions about the role of freezing temperature and fiber content in influencing the strength and characteristics of the ice samples.

Before the experiments were started, as shown in Table 3.2, important measurements were taken for all the samples. These measurements were conducted on samples exposed to freezing temperatures of -21°C and -24°C, focusing on the dimensions (size) and weight of each sample.

(a) (b)

Figure 4.4: – (a): Detaching the Ice Samples from the Polystyrene Mold. (b): De-molded ice specimens.

Table 4.2. Size and density measurements for specimens with freezing temperatures of -18°C, -21°C and -24°C.

Freezing Temperature		Fiber	Sample	B	H	L	Wt (before)	Density (before)	wt (after)	Density (after)
°C		(g/dm^3)		(mm)	(mm)	(mm)	(N)	(kg/m^3)	(N)	(kg/m^3)
-18	PI	0	1	41.02	39.97	159.53	2.28	870	2.28	870
			2	42.53	39.75	159.17	2.35	870	2.34	870
			3	43.18	40.17	159.12	2.45	890	2.44	890
	FRI-1	39	1	38.17	40.25	159.57	2.16	880	2.16	880
			2	38.57	40.65	159.67	2.25	900	2.25	900
			3	39.75	41.3	159.76	2.16	820	2.16	820
	FRI-2	56	1	39.11	41.43	160.14	2.33	900	2.33	900
			2	41.45	40.53	160.11	2.34	870	2.34	870
			3	43.05	40.81	160.19	2.34	830	2.34	830
	FRI-3	78	1	43.02	41.4	160.4	2.37	830	2.37	830
			2	43.01	40.78	160.34	2.4	850	2.38	850
			3	41.85	40.85	159.43	2.34	860	2.34	860
-21	PI	0	1	42.68	41.2	158.78	2.41	863.18	2.40	859.59
			2	45	40.75	158.49	2.57	884.28	2.56	880.84
			3	43.78	40.81	158.75	2.53	892.00	2.52	888.47
	FRI-1	39	1	41.2	42.12	158.42	2.46	894.83	2.46	894.83
			2	40.66	42.03	158.75	2.48	914.14	2.46	906.76
			3	40.68	42.8	158.73	2.54	919.07	2.54	919.07
	FRI-2	56	1	45.19	40.29	158.64	2.46	851.69	2.46	851.69
			2	44.55	40.2	158.63	2.41	848.32	2.41	848.32
			3	42.88	39.85	159.21	2.30	845.42	2.30	845.42
	FRI-3	78	1	41.1	44.3	159.03	2.49	859.95	2.49	859.95
			2	45.78	40.19	158.73	2.55	873.15	2.54	869.72
			3	40.63	43.75	159.05	2.55	901.95	2.54	898.41
-24	PI	0	1	41.73	40.82	159.12	2..37	874.38	2.32	855.94
			2	41.22	41.5	159.40	2.38	872.84	2.37	869.17
			3	43.2	41.8	159.19	2.42	841.86	2.42	841.86
	FRI-1	39	1	40.68	40.9	160.50	2.16	808.86	2.37	887.50
			2	42.85	40.32	159.23	2.25	817.87	2.30	836.05
			3	43.18	40.98	159.42	2.16	765.70	2.37	840.14
	FRI-2	56	1	42.14	41.86	158.42	2.46	880.30	2.45	876.72
			2	42.06	42.5	159.37	2.46	863.52	2.45	860.01
			3	43.4	42.1	159.18	2.46	845.81	2.44	838.94
	FRI-3	78	1	42.29	41.3	159.28	2.37	851.92	2.38	855.52
			2	45.11	41.24	158.96	2.4	811.58	2.42	818.34
			3	45.2	40.95	159.05	2.34	794.86	2.39	811.84

In the last column of Table. 4.2, it is demonstrated that the density remains relatively constant with the addition of fibers. Specifically, the average value of 870 kg/m3 closely aligns with measurements from previous experimental studies [54].

After the preparation of specimens and the initial measurements, our testing process closely mirrored the procedures performed previously. In the initial step, each sample underwent a three-point bending test. Subsequently, the specimen was halved, and a compressive test was carried out consecutively. These two tests enabled us to assess both the flexural strength and compressive strength for each sample within each freezing temperature category.

While the results of the tests conducted at -18 degrees Celsius were previously presented, attention is now turned to representing the results of these tests on specimens with freezing temperature of -21°C and -24°C. Specifically, the focus here is on presenting the midspan deflection curves of the samples, as shown in Figures 4.6 and 4.7.

This detailed evaluation through bending and compressive tests provides valuable insights into the mechanical properties of the specimens at varying freezing temperatures and fiber content levels. Analyzing the midspan deflection curves allows us to further understand how these ice samples respond to different loads, contributing to a comprehensive assessment of their structural performance.

-18°C Freezing Temperature

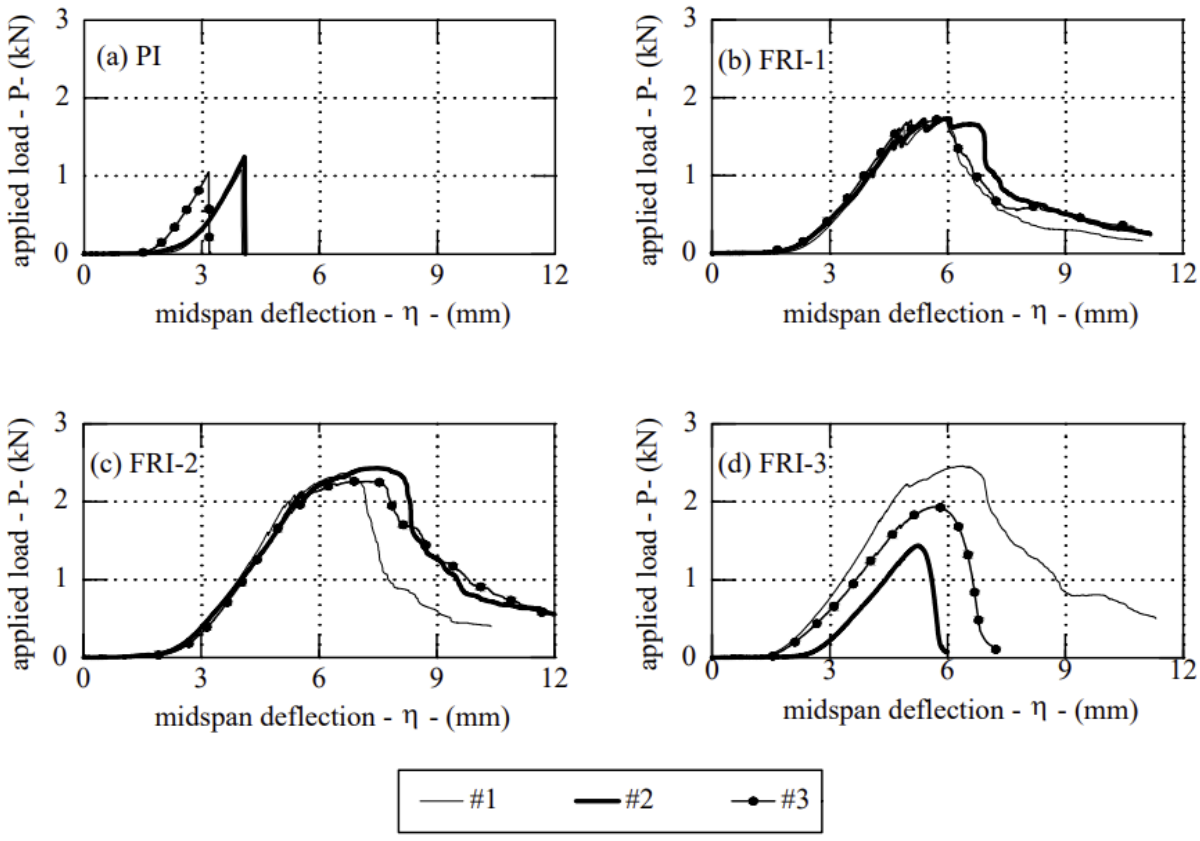

Figure 4.5: – Load-midspan deflection diagrams measured with three-point bending tests on specimens with freezing temnperature of -18°C.

-21°C Freezing Temperature

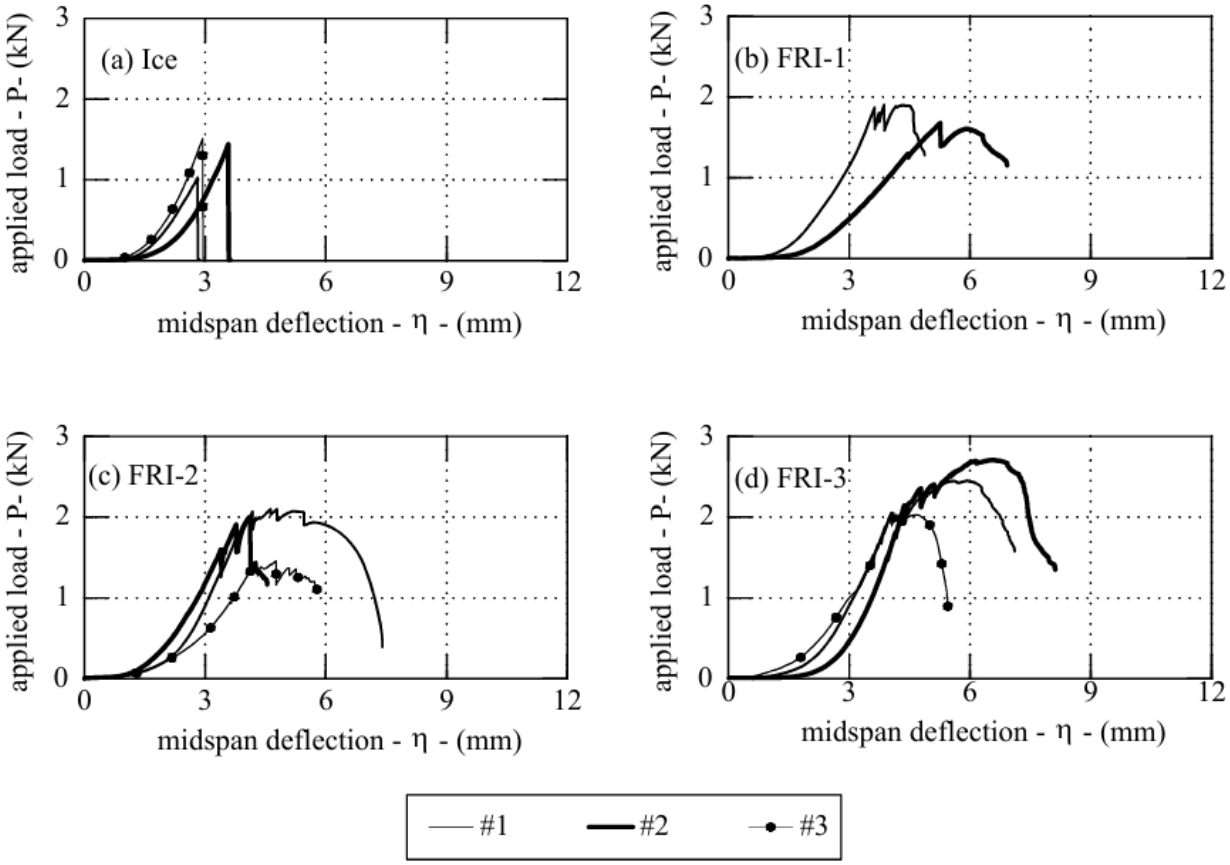

Figure 4.6: – Load-midspan deflection diagrams measured with three-point bending tests on specimens with freezing temnperature of -21°C.

-24°C Freezing Temperature

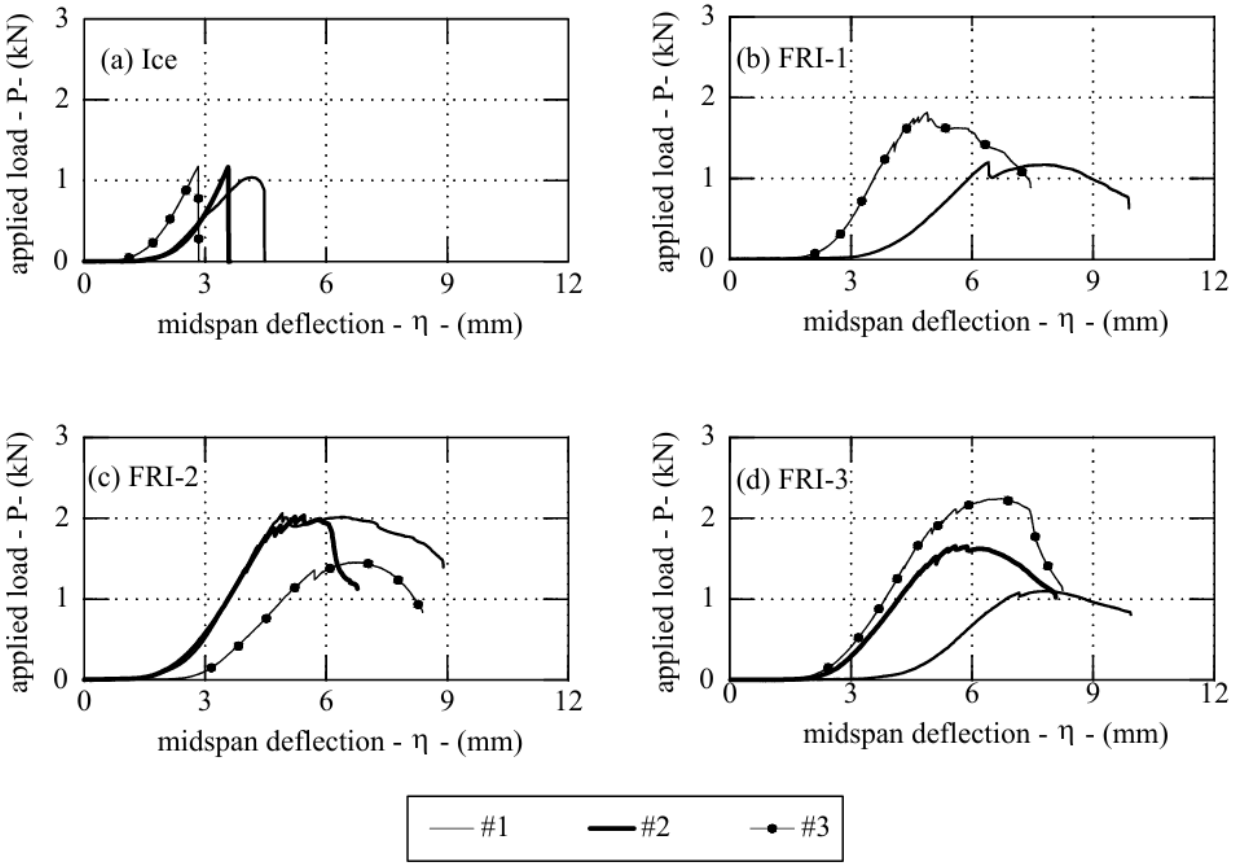

Figure 4.7: – Load-midspan deflection diagrams measured with three-point bending tests on specimens with freezing temnperature of -24°C.

As mentioned earlier, following the initiation of the first crack, multiple cracks develop, leading to the formation of a deflection hardening branch. Following this stage, a softening tail becomes evident, and loads decrease with the increase in deflection. Like the previous description, two key loads (P_{cr} at the initiation of the first crack and P_u at the maximum load) are of significance in this context. The respective values for these loads can be found in the next Table. The table also presents the distance Δ between P_u and P_{cr}, expressed in terms of the difference between displacements η. Furthermore, Table 4.3 includes the recorded maximum load P_c from the compression tests.

Table 4.3. Mechanical properties measured in the three-point bending test.

Temperature	Name	Fiber	Sample	P_u	P_{cr}	Δ	P_c	W
(°C)		(g/dm^3)		(N)	(N)	(mm)	(N)	(N*mm)
-18	PI	0	1	1089	1089	0	3654.14	0.0
			2	1236	1236	0	2595.43	0.0
			3	1044	1044	0	3017.55	0.0
	FRI-1	39	1	1719	1617	1.025	5305.73	1709.0
			2	1725	1488	1.242	5042.40	1996.7
			3	1724	1600	1.060	3972.87	1761.8
	FRI-2	56	1	2365	2006	1.429	4681.68	3124.3
			2	2423	2101	1.907	4295.47	4313.0
			3	2251	1950	1.487	4880.62	3123.9
	FRI-3	78	1	2454	2220	1.401	4397.93	3274.6
			2	1435	1272	0.847	3736.93	1145.5
			3	1926	1692	0.917	3593.79	1658.3
-21	PI	0	1	1023.83	1023.83	0.00	3597.65	0.00
			2	1431.03	1431.03	0.00	3597.65	0.00
			3	1503.83	1503.83	0.00	3597.65	0.00
	FRI-1	39	1	1896.20	1468.09	0.55	5802.00	918.86
			2	1673.12	1291.59	0.80	5314.00	1192.24
			3	-	-	-	8798.70	1055.55
	FRI-2	56	1	2090.86	1317.79	1.24	7516.50	2113.55
			2	2000.69	1603.92	0.71	8033.80	1272.70
			3	1456.05	953.90	1.12	8362.65	1355.11
	FRI-3	78	1	2440.35	1519.32	2.33	9827.00	4603.22
			2	2714.83	1514.99	1.65	10634.00	3485.86
			3	2053.63	1346.78	0.96	11441.00	1630.42
-24	PI	0	1	1030.28	1030.28	0.00	4929.09	0.00
			2	1157.50	1157.50	0.00	4541.77	0.00
			3	1161.85	1161.85	0.00	6016.25	0.00
	FRI-1	39	1	1160.25	1199.86	1.66	8450.48	1955.06
			2	770.06	741.19	0.73	2277.84	549.31
			3	1805.95	1432.39	0.81	6739.77	1319.53
	FRI-2	56	1	2045.60	1646.71	0.61	6829.80	1119.16
			2	2020.44	1361.85	1.44	5303.10	2435.78
			3	1443.96	1349.26	1.09	8763.73	1516.62
	FRI-3	78	1	1087.74	1066.81	0.60	7129.10	650.23
			2	1641.13	1320.94	0.89	5407.22	1325.37
			3	2247.08	1712.59	0.72	5689.95	1417.01

4.2.3- Experimental discussion

In the context of three-point bending tests, assuming linear elastic material behavior and uncracked cross-sections, the flexural stress f can be determined using Eq. 2.2. Similar to the preceding section, equation 2.2 employs the values of P (specifically P_{cr} and P_u) to ascertain the cracking strength $f_{f,cr}$ and ultimate strength $f_{f,u}$.The outcomes of these strengths are elaborated in Table 4.4. The values of W are presented in Table 4.3. Finally, the compressive strength can be evaluated by dividing P_c in Table. 4.2 by the loading area 40 × 40 mm². The results are also reported in Table. 4.3.

In the initial phase of the discussion on experimental results, the focus was on assessing the impact of fiber addition on mechanical strength. Specifically, two sets of samples were compared: plain ice (referred to as PI) and samples enriched with 9.75g of fibers (designated as FRI-1), across three distinct freezing temperatures. The goal was to examine how fiber incorporation influences the mechanical properties of the samples under varying freezing conditions. This comparison sheds light on the role of fibers in shaping the mechanical characteristics of the samples.

The attention was particularly drawn to comparing FRI-1 with plain ice (PI), given that previous studies by other researchers [76] have also focused on similar fiber amounts. By comparing our findings with those of prior studies [76], we sought to validate our research, ensuring its credibility. This validation approach extends to the subsequent chapter of this thesis.

The outcomes of the research are succinctly presented in the forthcoming figure, facilitating a comprehensive examination of the mechanical performance between plain ice (PI) and ice samples reinforced with 9.75g of fibers (FRI-1). This comparison is systematically conducted across different freezing temperatures, covering the four parameters introduced earlier.

In the next phase of analysis, attention is drawn to the samples experiencing freezing temperatures, specifically at -24°C. A recurring pattern is observed, mirroring previous findings for samples with a freezing temperature of -18°C. Notably, there is a peak in mechanical behavior at 14 g of fiber (referred to as FRI-2). Following this point, a decline in mechanical properties is observed.

As highlighted earlier, this observation underscores the presence of an optimal fiber content responsible for achieving peak mechanical behavior. In other words, there exists a specific number of fibers that plays a pivotal role in maximizing the mechanical performance of the material. This optimal fiber content serves as a key factor in determining and enhancing the overall mechanical behavior of the material under consideration.

This pattern aligns with earlier understanding, attributing such behavior to the bonding dynamics between the matrix (in this case, water) and the reinforcing element (fibers). The decrease in mechanical properties after the peak suggests a potential saturation or limit to the reinforcing effects of the fibers within the matrix.

Table 4.4. strength values measured in flexural and compressive analysis.

Temperature		Fiber	Sample	$f_{f,cr}$	$f_{f,u}$	fc
(°C)		(g/dm^3)		(MPa)	(MPa)	(MPa)
-18	PI	0	1	2.49	2.49	2.28
			2	2.76	2.76	1.62
			3	2.25	2.25	1.89
	FRI-1	39	1	3.84	4.09	3.32
			2	3.29	3.82	3.15
			3	3.57	3.85	2.48
	FRI-2	56	1	4.48	5.28	2.93
			2	4.63	5.33	2.68
			3	4.08	4.71	3.05
	FRI-3	78	1	4.51	4.99	2.75
			2	2.52	2.85	2.34
			3	3.63	4.13	2.25
-21	PI	0	1	2.12	2.12	2.25
			2	2.87	2.87	2.25
			3	3.09	3.09	2.25
	FRI-1	39	1	3.01	3.89	3.63
			2	2.70	3.49	3.32
			3	2.86	3.69	5.50
	FRI-2	56	1	2.69	4.28	4.70
			2	3.34	4.17	5.02
			3	2.10	3.21	5.23
	FRI-3	78	1	2.83	4.54	6.14
			2	3.07	5.51	6.65
			3	2.60	3.96	7.15
-24	PI	0	1	2.22	2.22	3.08
			2	2.45	2.45	2.84
			3	2.31	2.31	3.76
	FRI-1	39	1	2.64	2.56	5.28
			2	1.60	1.66	1.42
			3	2.96	3.74	4.21
	FRI-2	56	1	3.35	4.16	4.27
			2	2.69	3.99	3.31
			3	2.63	2.82	5.48
	FRI-3	78	1	2.22	2.26	4.46
			2	2.58	3.21	3.38
			3	3.39	4.45	3.56

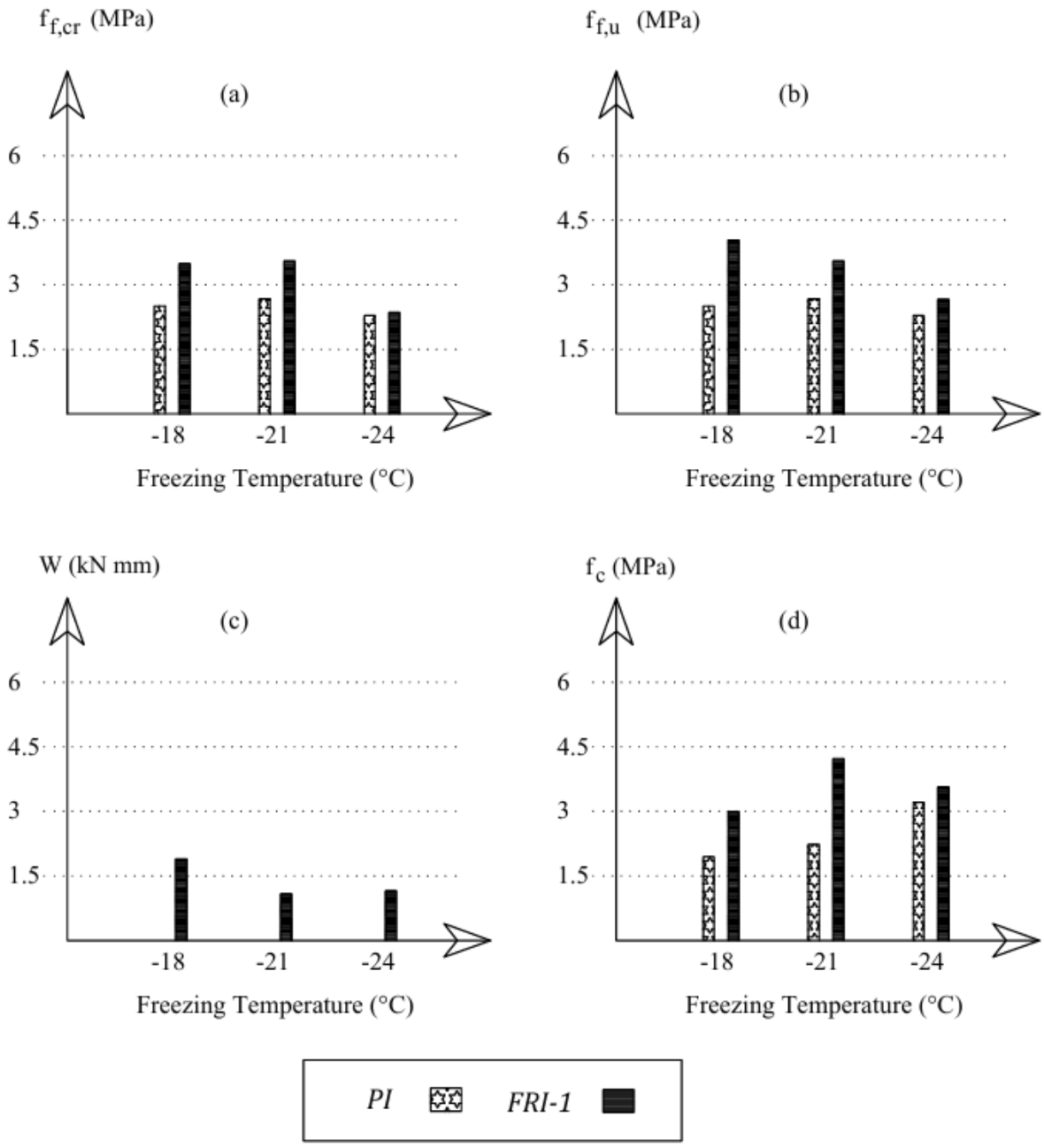

Figure 4.8: average flexural and compressive strength results of plain ice and FRI-1 for samples with different freezing temperature: (a) flexural strength at cracking (when P = P_{cr} in Eq. 2.2). (b) flexural strength at peak (when P = P_u in Eq. 2.2). (c) work (or the energy) released during the deflection-hardening (d) compressive strength of ice.

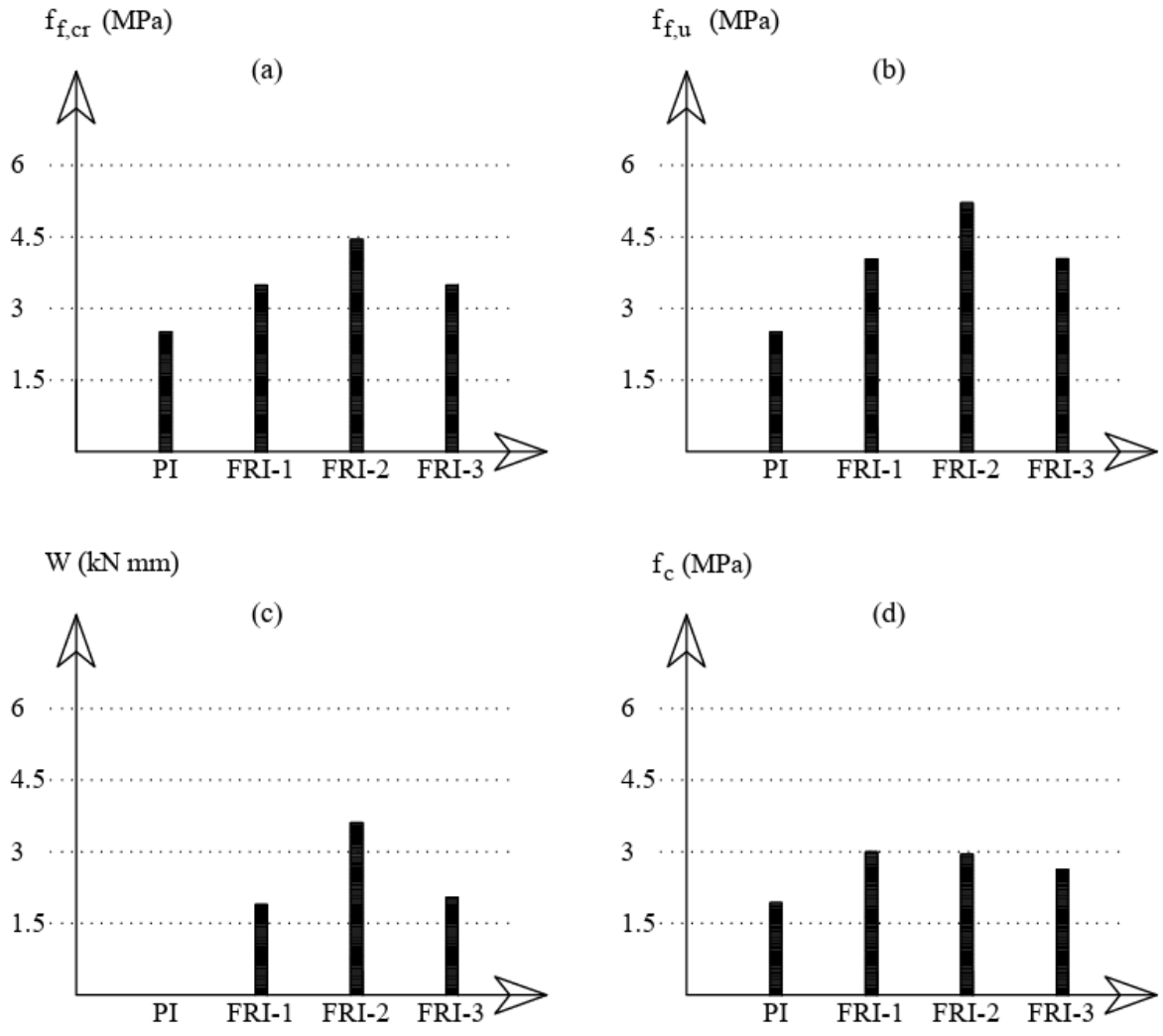

Figure 4.9: Average values of strength measured in flexural and compressive tests for specimens with -18°C freezing temperature: (a) flexural strength at cracking (when P = P_{cr} in Eq. 2.2). (b) flexural strength at peak (when P = P_u in Eq. 2.2). (c) work (or the energy) released during the deflection-hardening (d) compressive strength of ice.

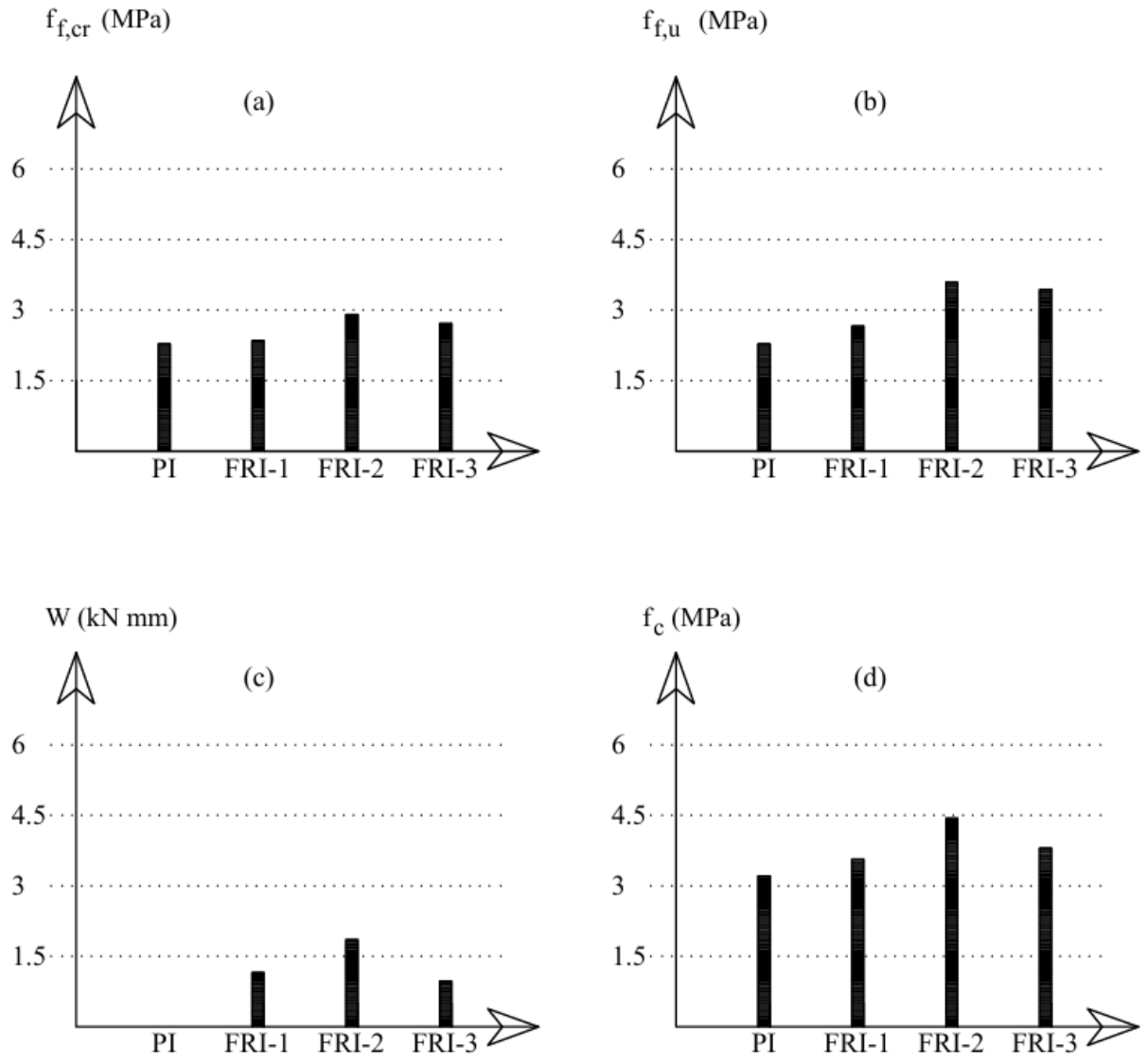

Figure 4.10: Average values of strength measured in flexural and compressive tests for specimens with -24°C freezing temperature: (a) flexural strength at cracking (when P = P_{cr} in Eq. 2.2). (b) flexural strength at peak (when P = P_u in Eq. 2.2). (c) work (or the energy) released during the deflection-hardening. (d) compressive strength of ice.

As also noted in the preceding chapter, the test results can also be depicted in relation to the quantity of fibers (QF), for these freezing temperatures. However, as illustrated in Fig. 4.11 and Fig. 4.12, the increase in QF does not uniformly enhance all mechanical properties. Indeed, the strengths and energy values do not exhibit a consistent trend with QF.

As depicted in the diagrams of Fig. 4.11, where the values of $f_{f,cr}$, $f_{f,u}$,W, and f_c are reported as a function of QF, The regression analysis, based on the least squares approximation of the

experimental data, leads to the derivation of a quadratic function similar to Eq. 3.1. The coefficients A, B, and C depend on the type of mechanical performance, as reported in Table 4.5.

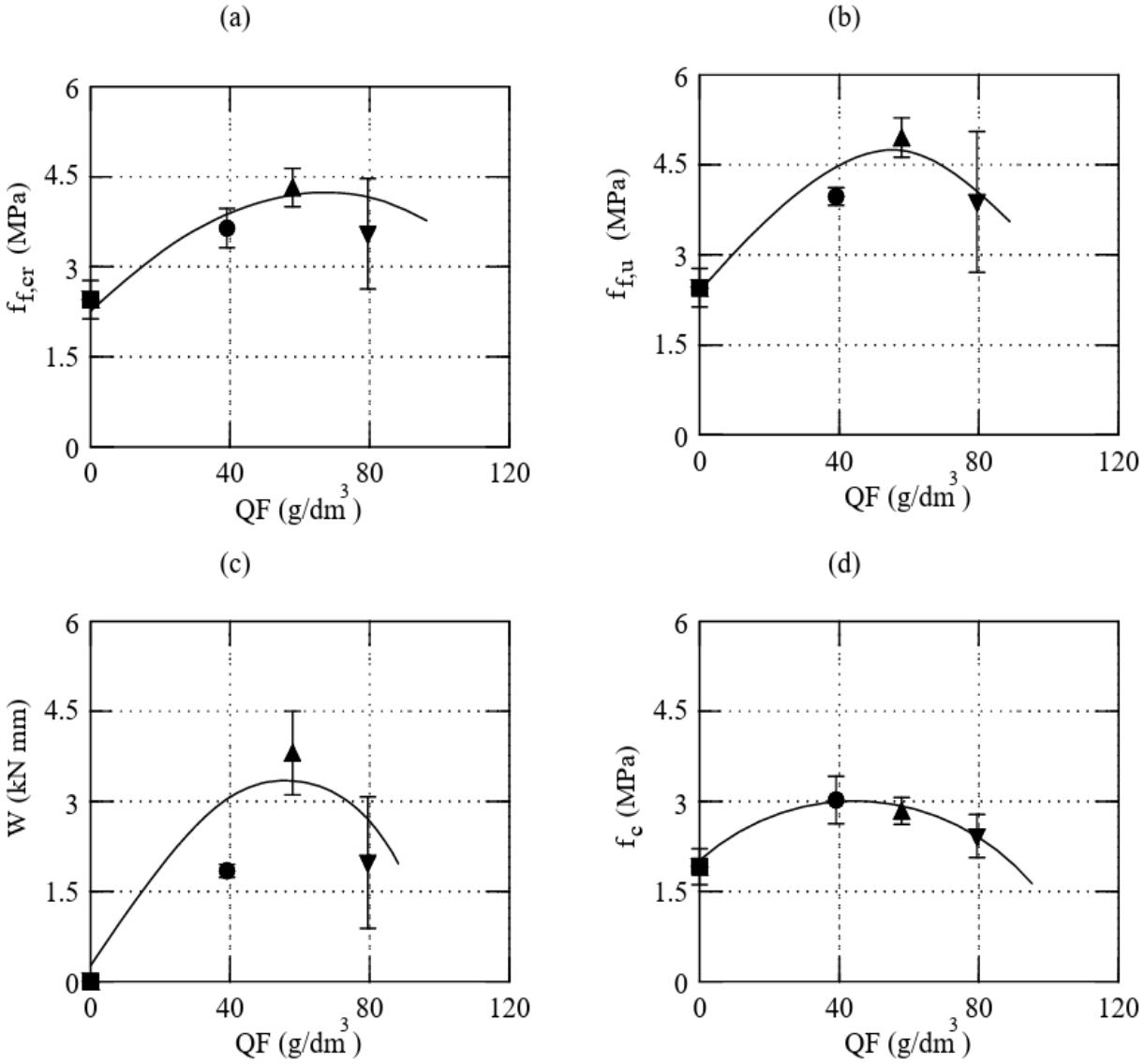

Figure 4.11: Quadratic regression of $f_{f,cr}$, $f_{f,u}$, W, and f_c, with respect to the quantity of fibers QF for samples with freezing temperature of -18°C.

In the preceding chapter, regression analysis was conducted on specimens subjected to a freezing temperature of -18 degrees Celsius. The results, along with a corresponding figure, indicate that the regression line closely resembles the one derived from the analysis of samples exposed to a freezing temperature of -24 degrees Celsius.

In the Fig. 4.12, the regression line derived from samples with a freezing temperature of -18°C is represented by a dashed line, while the solid line represents the regression of the results from samples with a freezing temperature of -24 degrees celicious.

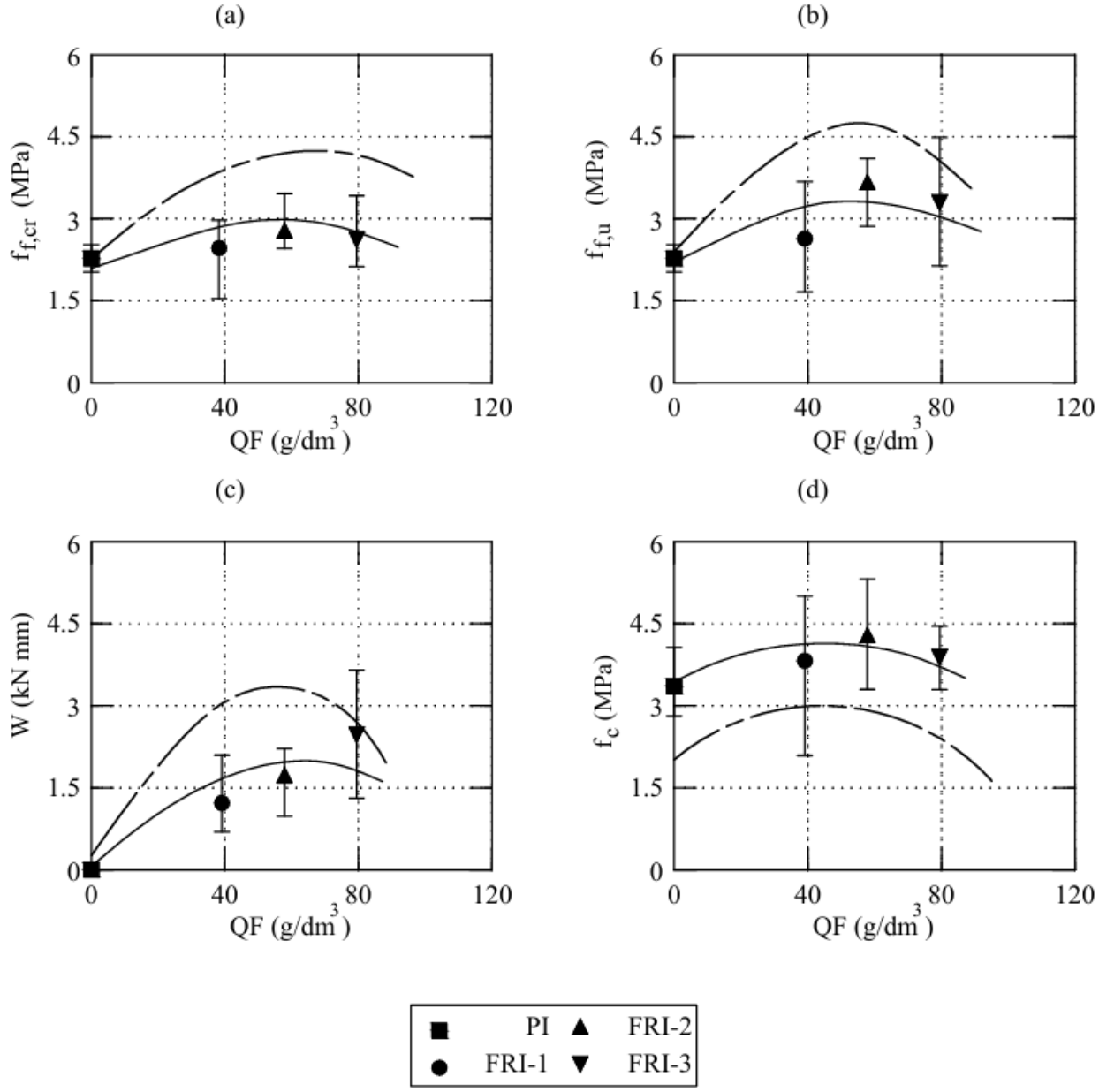

Figure 4.12: Quadratic regression of $f_{f,cr}$, $f_{f,u}$, W, and f_c, with respect to the quantity of fibers QF for samples with freezing temperature of -24°C.

Table 4.5. values of the parameters A and B and C in Eq. 3.1 for specimens with two freezing temperatures.

Temperature		A	B	C
-18 (°C)	$f_{f,cr}$	-0.0005 MPa / (g/dm^3)^2	0.058 MPa / (g/dm^3)	2.4525 MPa
	$f_{f,u}$	-0.0007 MPa / (g/dm^3)^2	0.0774 MPa / (g/dm^3)	2.4319 MPa
	W	-0.0009 kN mm / (g/dm^3)^2	0.1012 kN mm / (g/dm^3)	- 0.098 kN mm
	f_c	-0.0005 MPa/ (g/dm^3)^2	0.0467 MPa / (g/dm^3)	1.917 MPa
-24 (°C)	$f_{f,cr}$	-0.0002 MPa / (g/dm^3)^2	0.0076 MPa / (g/dm^3)	2.2997 MPa
	$f_{f,u}$	-0.0001 MPa / (g/dm^3)^2	0.0222 MPa / (g/dm^3)	2.2731 MPa
	W	-0.0002 kN mm / (g/dm^3)^2	0.0407 kN mm / (g/dm^3)	- 0.0025 kN mm
	f_c	-0.0002 MPa/ (g/dm^3)^2	0.0285 MPa / (g/dm^3)	3.1838 MPa

Based on the experimental data and Eq. (3.1), an optimal fiber content is identified for freezing temperatures of both -18°C and -24°C. In each scenario, FRI-2 demonstrates the highest mechanical performance with a bio-fiber content of QF=56 g/dm3. However, further increasing QF, as observed in FRI-3, leads to a decrease in all mechanical properties.

This phenomenon can be explained by the interaction between the matrix (water) and the reinforcing elements (bio-fibers). Exceeding a certain fiber quantity reduces the matrix area surrounding the fibers, weakening the bond between the matrix and reinforcing elements. Consequently, this results in premature failure of FRI under compression and bending stresses.

As previously mentioned, these findings are in line with those of various researchers in fiber-reinforced concrete (FRC), where each fiber content exhibits a threshold (maximum). Typically, a quadratic function, such as Eq. (3.1), can be employed to forecast the mechanical properties of FRC based on fiber content [71].

Another noteworthy observation in the analysis of samples subjected to a freezing temperature of -24 degrees Celsius is the reversal in the relationship between compressive strength and flexural strength when compared to samples at -18 degrees Celsius. In contrast to the latter, the samples at -24°C exhibit compressive strength surpassing flexural strength. This intriguing shift in strength characteristics is visually represented in the subsequent histogram, providing a clear illustration of the distinctive mechanical responses based on the freezing conditions.

The representation strongly suggests that as the freezing temperature decreases, the ice samples exhibit a notable increase in compressive strength at the expense of flexural strength. This shift implies a transition towards a more brittle material.

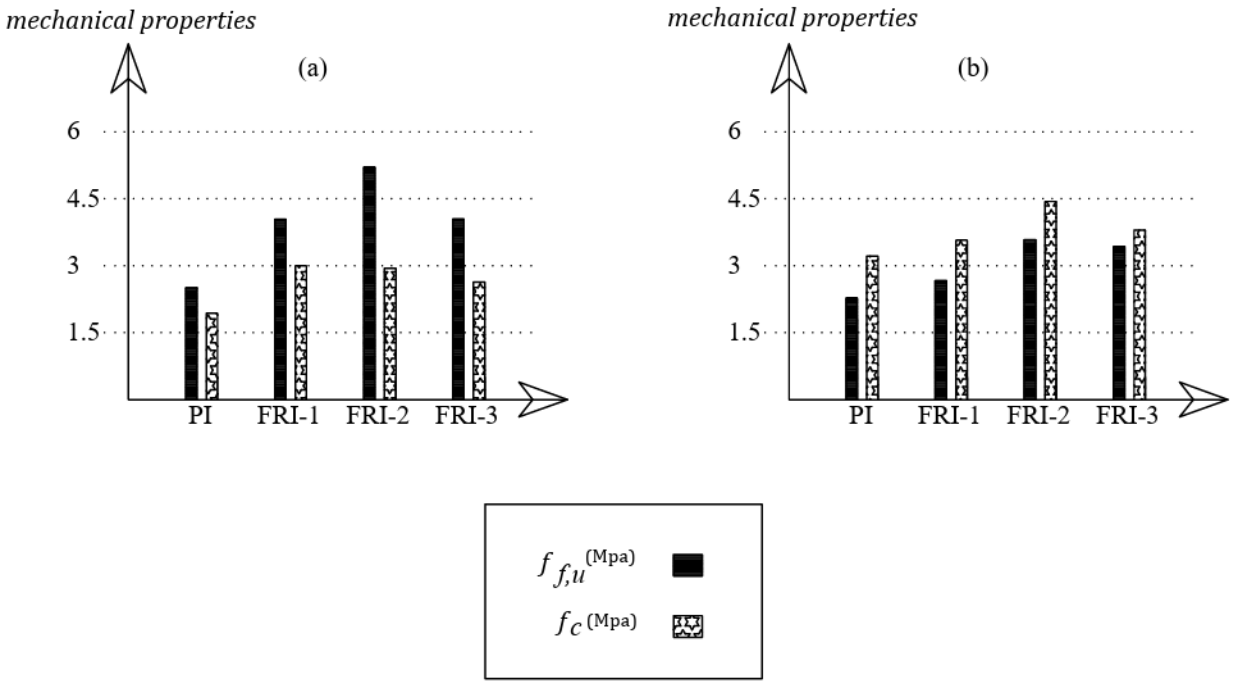

Figure 4.13: average flexural and compressive strength results for: (a) samples with freezing temperature of -18°C. (b) freezing temperature of -24°C.

4.3- Conclusion

In the first part of this chapter, the influence of the water-to-cement (w/c) ratio on the mechanical properties of cement-based materials was examined comprehensively. Several key conclusions emerge from the analysis of test results and experimental data:

1. Lower w/c ratios generally enhance compressive and tensile strength and durability by promoting denser packing of cement paste and improving the hydration process. However, these benefits must be balanced with considerations of workability and potential for increased shrinkage and creep.
2. The potential benefits of incorporating recycled concrete aggregates (FRCA) and fiber reinforcements were discussed, with findings indicating that, when managed effectively, these materials can further improve concrete performance. Specifically, the optimal replacement of FRCA enhances compressive strength, while reduced w/c ratios bolster the bond strength between the concrete matrix and fiber reinforcements.
3. Overall, understanding and managing the w/c ratio is essential for optimizing the performance of concrete structures, ensuring long-term structural integrity and durability.

The second part of this chapter focused on the temperature's impact on ice mechanical properties, leading to several conclusions:

4. Significant temperature sensitivity was observed in ice structures, with lower freezing temperatures (-24°C compared to -18°C) increasing ice hardness and brittleness. While this enhanced strength, it also heightened susceptibility to sudden fractures under stress. Careful management of freezing temperatures is crucial for optimizing the performance and durability of ice structures.
5. The addition of fibers significantly enhanced the mechanical properties of ice, especially at an optimal volume. Ice samples containing 14 grams of bio fibers (FRI-2) consistently exhibited superior flexural and compressive strength across varying freezing temperatures. However, exceeding this optimal fiber content resulted in diminishing returns, underscoring the importance of precise control over fiber volume in reinforcing ice structures.
6. The study identified 14 grams of fibers (FRI-2) as the critical threshold for maximizing ice strength and durability. Beyond this point, additional fibers did not contribute further to mechanical property improvements. This optimal fiber content serves as a fundamental guideline for designing resilient fiber-reinforced ice structures, providing valuable insights for future applications in ice construction and ensuring dependable performance under diverse environmental conditions.

Chapter 5:

Relationship Between Flexural Strength & Compressive Strength**

5.1- Introduction

5.1.1- State of the Art

Concrete, a widely used material for structural applications, is known for its high compressive strength but comparatively lower flexural strength. The ratio between flexural strength and compressive strength is an essential material property for concrete. Predicting flexural strength from compressive strength is of interest due to the complexity, cost, and time-consuming nature of flexural tests. Researchers and building guidelines often seek to establish relationships between these properties.

The flexural strength to compressive strength ratio is considered more or less constant for the same class of concrete. Higher compressive strength generally corresponds to higher flexural strength. This ratio has practical applications and is useful for predicting flexural strength without conducting specific flexural tests.

However, in the context of ice composite materials, there are aspects that still need improvement. The discussion mentions the need for understanding the ratio between flexural strength and compressive strength in ice composite materials. This ratio is crucial, and comprehensive information on this aspect is currently lacking in the literature.

In this section of the study, it is tried to establish a connection between the ratio of flexural strength to compressive strength (f_c) in plain ice specimens. To provide context, these results will be compared with the (f_f / f_c) ratio observed in cement-based materials. The methodology involves assessing the flexural and compressive strengths of both plain ice and mortars. These evaluations are conducted using test protocols outlined in UNI EN 196.

Following these tests, a novel relationship is proposed that captures the interplay between flexural and compressive strengths in both plain ice and mortar specimens. This approach allows us to draw comparisons between the (f_f / f_c) ratios of ice and cement-based materials, contributing to a deeper understanding of the mechanical properties of these materials and potentially unveiling insights that can inform future applications and designs.

At Politecnico di Torino (Italy), an experimental campaign has been conducted on cement-based mortars and plain ice. The following sections detail the specific experimental procedures employed for both materials, outlined separately for clarity.

**The section's content has been submitted as an article to the SEMC 2022 conference under the title 'Relationship between flexural strength and compressive strength in concrete and ice'.

5.1.2- Cement Based Mortar

For the investigation, each batch was meticulously prepared, and the composition of each batch was standardized. Specifically, each batch comprised three prisms, each measuring 40 × 40 × 160 mm^3. The materials used in the batches included cement (CEM II/B-LL 32.5 R), normalized sand (CEN Standard sand), which is characterized by siliceous rounded particles within a size distribution specified in Table 5.1 and tap water.

Table 5.1. Compositions of the UNI-sand according to UNI EN 196-1

square mesh size (mm)	2.00	1.60	1.00	0.50	0.16	0.08
Cumulative sieve residue (%)	0	7±5	33±5	67±5	87±5	99±5

The precise mixture proportions for these components are detailed in Table 5.2. This careful standardization of materials and their proportions ensures consistency across batches, allowing for reliable and meaningful comparisons in the subsequent experimental analyses. The use of standardized materials and proportions is a crucial aspect of the experimental design, providing a solid foundation for accurately assessing the mechanical properties of the cement-based mortars under investigation.

Table 5.2. Composition of the cement-based mortar.

Specimen	Cement (g)	Water (g)	Sand (g)
mortar	*450 ± 2*	*225 ± 1*	*1350 ± 5*

Following the casting process, the concrete prisms were de-molded a day later and subsequently stored under controlled conditions at 20°C (50% relative humidity). This standardized environment ensures consistent curing conditions for all specimens. The geometrical properties and weights of the prisms are detailed in Table 5.3. These properties, including dimensions and weight, provide crucial information for the subsequent analysis of the mechanical performance of the cement-based mortars. By maintaining a controlled and uniform curing environment, the study aims to minimize external factors that could influence the test results, thereby enhancing the reliability and validity of the experimental findings.

Table 5.3. Properties of the cement-based mortar.

Specimen	Length (mm)	Depth (mm)	Width (mm)	Weight (g)
C1	160	40.85	40.61	1670
C2	160	40.64	40.64	1670
C3	160	40.73	41.24	1670

Similar to the previous tests, the same three-point bending and compressive tests were conducted in this section. Specifically, the flexural strength tests, as illustrated in Figure 5.1.a, were performed after a 28-day period. An external load (P) was applied using a Baldwin-Zwick loading machine with a capacity of 50 kN. The tests involved driving the displacement of the loading cell, with the stroke moving at a velocity of 0.05 mm per minute. Throughout the tests, both the applied load (P) and the midspan deflection (η) of the beam were recorded until the specimen experienced complete failure.

Flexural tests were carried out by splitting the specimens into two halves, which were subsequently compressed. As depicted in Figure 5.1.b, the load (P) is applied to a loading area of 40 × 40 mm² in each half, utilizing a device with platens having a thickness of 10 mm. The compressive force is gradually increases at a rate of 200 N per second until failure occurs.

(a) (b)

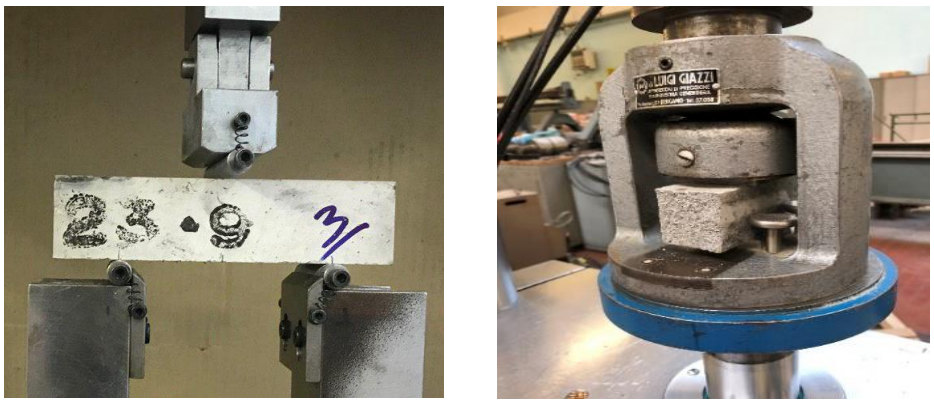

Figure 5.1: (a): Three-point bending tests for cementitious mortars, (b): Compressive test for cementitious mortars.

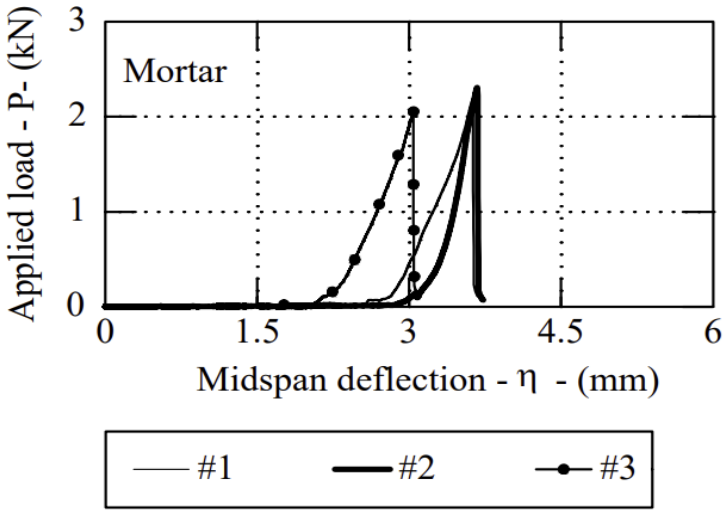

Figure 5.2: Load deflection diagram for cement-based mortar.

The diagram depicting the applied force (P) versus mid-span deflection (η) measured during the tests is presented in Figure 5.2. From these results, the flexural strength of the concrete mortars can be calculated using the following formula:

$$f_f = \frac{3PL}{2bd^2} \tag{5.1}$$

where:

- f_f is the flexural strength (MPa),
- P is the maximum value of the applied load,
- L is the distance between supports,
- b is the width of the specimen, and
- d is the depth of the specimen.

The values of f_f are detailed in Table 5.4. Following the three-point bending test, each specimen is divided into two parts, and compression tests are conducted on these parts. The values of compressive strength (f_c) measured on the mortar specimens are also reported in Table 5.4.

Table 5.4. Result of flexural and compressive tests performed on mortar specimens.

Specimen In Tension	Flexural Strength	Specimen In Compression	Compressive Strength
	(MPa)		(MPa)
Con-1	4.7	Con-1-A	31.93
		Con-1-B	30.46
Con-2	5.13	Con-2-A	30.66
		Con-2-B	29.8
Con-3	4.48	Con-3-A	30.23
		Con-3-B	28.1

5.2- Ice materials

5.2.1- Experimental Process

As with the mortar samples, ice prisms measuring 40 × 40 × 160 mm³ were created and examined. These were tested for tension and compression following the UNI EN 196-1 (2005) standard. To assess their strength in bending and compression, three-point bending tests (Figure 5.3.a and Figure 5.3.b) and compression tests (Figure 5.3.c) were conducted. To prevent the specimens from melting during these tests, rubber pieces were placed at the points where the machine and the ice specimens made contact.

(a) (b) (c)

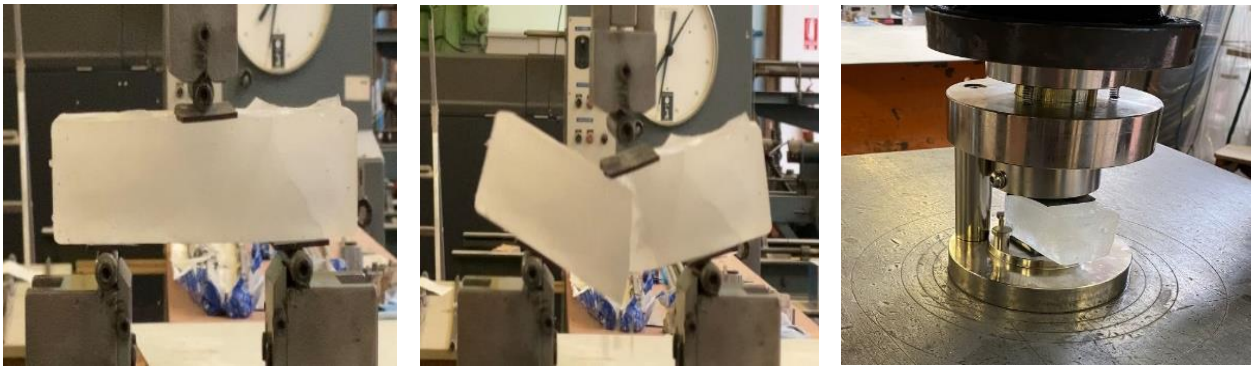

Figure 5.3: Tests on plane ice specimens: (a)-(b): Three-point-bending tests; and (c) Compression test.

A total of six ice specimens were examined, and their properties are detailed in Table 5.5. To create these specimens, tap water was poured into the molds and frozen at a temperature of -5 °C and -18 °C. Subsequently, after demolding, we tested the specimens at room temperature (20 °C).

Table 5.5. Ice specimen properties.

Specimen	Freezing Temperature	Length	Depth	Width	Weight Before Test	Weight After Test
	(°C)	(mm)	(mm)	(mm)	(g)	(g)
Ice-A	-5	158.83	40.41	40.43	233	232
Ice-B		158.39	39.51	40.41	243	241
Ice-C		160.03	40.12	39.43	235	232
Ice-A	-18	159.53	41.02	39.97	228	228
Ice-B		159.17	42.53	39.75	235	234
Ice-C		159.12	43.18	40.17	245	244

The bending test was performed by maintaining control over the midspan deflection at a speed of 3 mm/min. Throughout the test, there was no significant melting of the ice, and the weight of the specimens remained relatively constant (refer to Table 5.5). Subsequently, compressive tests were conducted by gradually increasing the applied load at a rate of 50 N per second. Fig. 5.4 displays the deflection-force diagrams of the ice prisms.

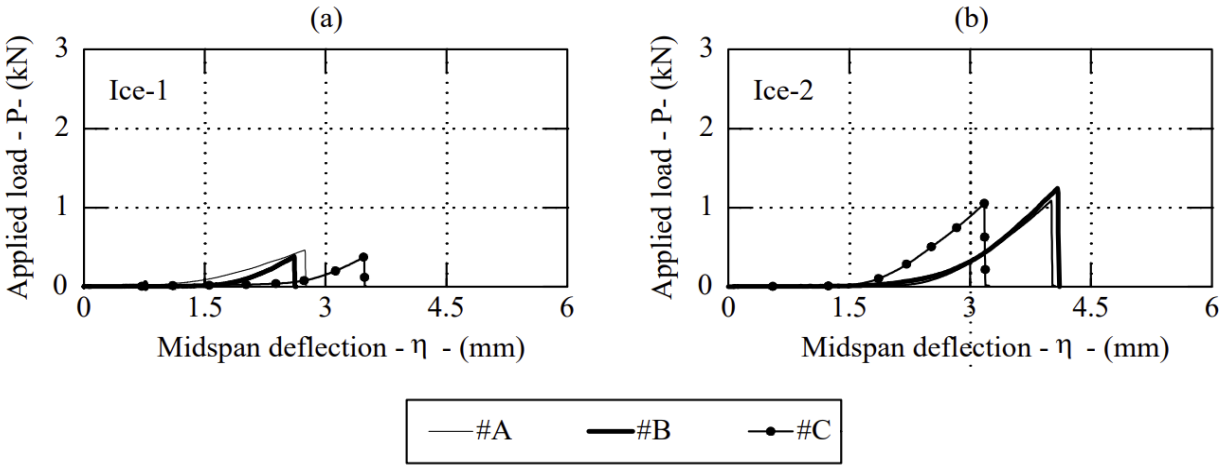

Figure 5.4: Load deflection diagram for Ice specimens.

Similarly, in this case, Eq. (5.1) was employed to calculate the flexural strength, which is presented in Table 5.6 along with the compressive strength. Upon comparison with the results for cement-based mortars (Table 5.4), it is apparent that both flexural and compressive strengths are relatively reduced, regardless of the freezing temperature. Ice exhibits a compressive strength that is only about 5% to 10% of what is seen in mortar samples. In terms of flexural strength, there is noted a significant increase as the freezing temperature drops. Specifically, at -18 °C, the average flexural strength is more than 2.5 times higher than that observed at -5 °C freezing temperature.

Table 5.6. Result of flexural and compressive tests on ice.

Specimen	Freezing Temperature	f_f	f_c
	(°C)	(MPa)	(MPa)
Ice-A	-5	1.03	-
Ice-B		0.89	1.65
Ice-C		0.87	1.75
Ice-A	-18	2.49	2.28
Ice-B		2.76	1.62
Ice-C		2.25	1.89

5.2.2- Experimental Analysis

Table 5.7 presents the compressive strength values of ice measured by Wu et al. (2020) [72]. According to their findings, the strength increases as the freezing point decreases. The compressive strength measured at -5°C, specifically 1.78 MPa, aligns quite closely with the average value obtained in our current tests, which is 1.7 MPa (refer to Table 5.6).

Table 5.7. Ice compressive strength evaluated by Wu et al (2020) at different temperatures.

Specimen	Temperature	Compressive Strength
	℃	*MPa*
1	-5	1.78
2	-10	2.59
3	-15	3.08

Even though the tests were conducted at ambient temperature, the melting of ice was not observed during the bending tests, nor were significant deviations in the compressive strength results noted when compared to measurements by other authors. The use of UNI EN 196 (2005) for measuring ice strength proves effective, as it provides a standardized approach for evaluating the mechanical properties of both cement-based mortars and ice.

Lowering the freezing temperature had a more noticeable impact on flexural strength than on compressive one. In fact, at a freezing temperature of -18 °C, the flexural strength surpassed the compressive strength. When the freezing temperature decreases from -5 °C to -18 °C, the compressive strength increases by approximately 15%, whereas the flexural strength escalates by almost 2.7 times.

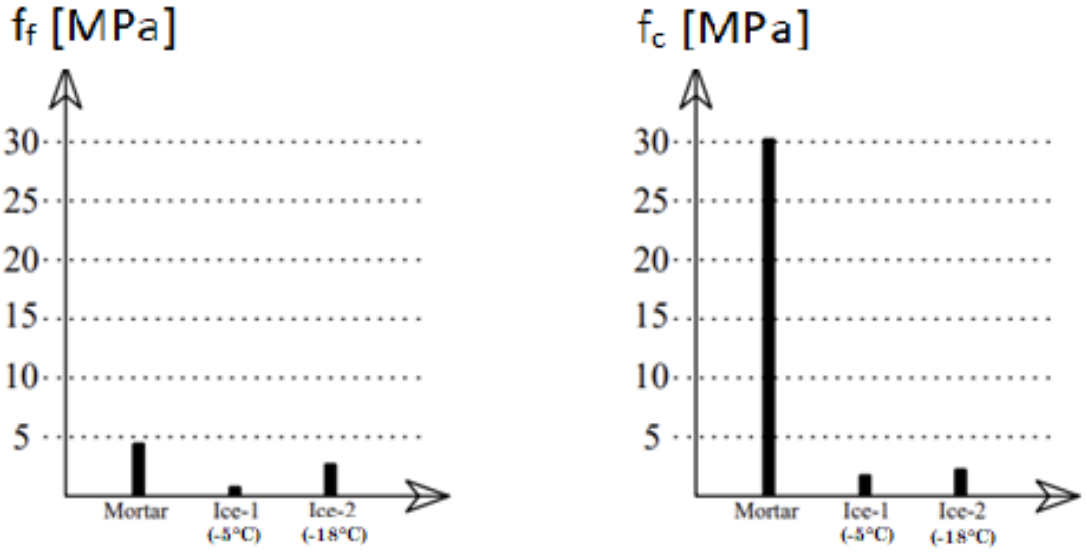

Figure 5.5: The average values of flexural and compressive strength of ice and mortar.

Given that assessing compressive strength is usually more straightforward, the flexural strength to compressive strength ratio varies between mortar and ice, as indicated in Table 5.8. To derive flexural strength from compressive strength in ice materials, the method proposed by Eurocode 2 (UNI EN 1992-1-1, 2004) can be applied. This approach allows for a more convenient estimation of flexural strength without the need for separate flexural tests.

Table 5.8. The ratio flexural/compressive strength in mortar and ice.

Material	f_f	f_c	Ratio	α
	(MPa)	(MPa)		
Mortar	4.77	30.2	0.16	0.32
Ice (-5℃)	0.93	1.7	0.54	0.42
Ice (-18℃)	2.50	1.93	1.29	1.04

In the context of mortar, the average tensile strength ($f_{ctm,fl}$) relies on both the mean uniaxial tensile strength (f_{ctm}) and the depth of the cross-section (h). Specifically, the flexural strength is precisely defined as follows:

$$f_{ctm,fl} = \max\{(1.6 - \frac{h}{1000}) \times f_{ctm} \; ; \; f_{ctm}\} \tag{5.2}$$

The value of h in this context is set at 40 mm. When the classification of the cement-based material is below 50/60, the calculation of f_{ctm} involves the following formula:

$$f_{ctm} = \alpha \times f_{ck}^{(2/3)} \tag{5.3}$$

In the present cement-based mortar, where the average compressive strength is 30.2 MPa and the flexural strength is 4.77 MPa, the calculated coefficient α using the mentioned formula is approximately 0.32. This value closely aligns with the Eurocode 2 recommendation for concrete (α = 0.3).

When applying the same formulas to ice with a freezing temperature of -5 °C, the higher flexural to compressive ratio necessitates a higher value of α. Specifically, to achieve a flexural strength of 0.93 MPa while having a compressive strength of 1.7 MPa, α must be 0.42. This value exceeds that of the cement-based mortar. This simply means that ice is relatively stronger in bending compared to its strength in compression than mortar is.

As the freezing temperature drops to -18 °C, the flexural to compressive value approximates 1.3. To attain a flexural strength of 2.5 MPa and a compressive strength of 1.93 MPa, α needs to be approximately 1.04.

5.3- FRC and FRI

5.3.1- Experimental Analysis

In analyzing all the FRC and FRI samples examined in this study, a distinct correlation emerged between flexural and compressive strength. This correlation provides valuable information for assessing either flexural or compressive strength when only one of these parameters is known. Given that the compression test is generally simpler and more prevalent, establishing a relationship between it and flexural strength offers practical advantages.

In the second chapter of this doctoral dissertation, concerning the FRC samples, it is important to highlight that building codes typically correlate the values of flexural strength at cracking ($f_{f,cr}$) and ultimate flexural strength ($f_{f,u}$) with the compressive strength (f_c) of concrete. However, in Fiber-Reinforced Concrete (FRC), flexural strength is notably influenced by the fiber volume fraction (V_f).

Table 5.9. The ratio flexural/compressive strength in mortar samples.

series	specimens	$f_{f,cr}$	$f_{f,u}$	f_c	W
		(MPa)	(MPa)	(MPa)	(N.mm)
Ref		7.19	10.22	49.9	1653
1	1-A	3.69	6.48	36.95	5250
	1-B	5.01	9.69	42.46	5531
	1-C	4.14	9.91	39.91	7374
2	2-A	2.33	10.05	39.25	7588
	2-B	3.72	17.79	46.16	17021

The outcomes of the flexural and compressive tests are displayed in the Table. 5.9. For both Series 1 and Series 2 of the cement-based composites, there exists a linear relationship between compressive strength (f_c) and flexural strength at cracking ($f_{f,cr}$), as depicted in Figure 5.6.a. Similarly, a linear relationship is observed between f_c and ultimate flexural strength ($f_{f,u}$), as demonstrated in Figure 5.6.b.

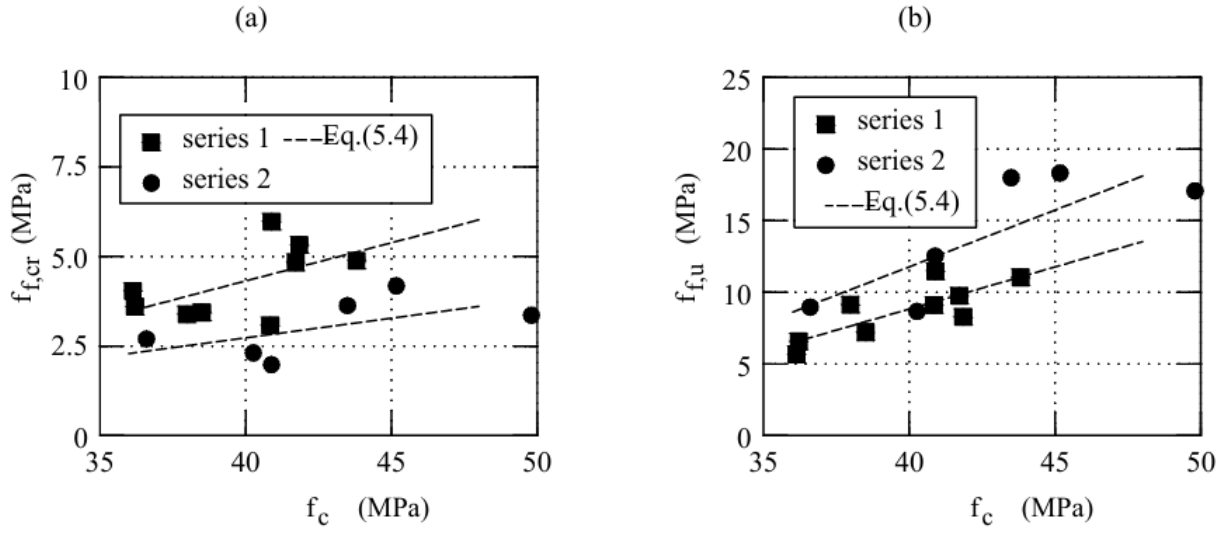

Figure 5.6: Possible relationships among the strengths: (a) f_c vs. $f_{f,cr}$; (b) f_c vs. $f_{f,u}$.

Accordingly, the following relationship can be written:

$$f = \alpha + \beta \cdot f_c \tag{5.4}$$

The values of α and β, depending on the types of f (i.e., $f_{f,cr}$ or $f_{f,u}$) are reported in Table 5.10.

Table 5.10. The parameters α and β to be used in Eq. 5.4 for cement based mortars.

series		α	β
1	$f_{f,cr}$	-4.21	0.213
	$f_{f,u}$	-14.7	0.589
2	$f_{f,cr}$	-1.65	0.109
	$f_{f,u}$	-19.9	0.791

Similar tests were conducted to assess the compressive and flexural strength of fiber-reinforced ice at three distinct freezing temperatures. Detailed explanations of these tests are provided in chapters three and four of this thesis. The results of these tests are also presented in the following table for reference.

Table 5.11. strength values measured in flexural and compressive analysis.

Temperature		Fiber	Sample	$f_{f,cr}$	$f_{f,u}$	fc
(°C)		(g/dm^3)		(MPa)	(MPa)	(MPa)
-18	PI	0	1	2.49	2.49	2.28
			2	2.76	2.76	1.62
			3	2.25	2.25	1.89
	FRI-1	39	1	3.84	4.09	3.32
			2	3.29	3.82	3.15
			3	3.57	3.85	2.48
	FRI-2	56	1	4.48	5.28	2.93
			2	4.63	5.33	2.68
			3	4.08	4.71	3.05
	FRI-3	78	1	4.51	4.99	2.75
			2	2.52	2.85	2.34
			3	3.63	4.13	2.25

Like the previous section, two significant values of flexural strength, namely at cracking ($f_{f,cr}$) and ultimate strength ($f_{f,u}$), are considered. Figure 5.7.a displays the dependence of $f_{f,cr}$ and f_c, while Figure 5.7.b illustrates the relationship between $f_{f,u}$ and f_c.

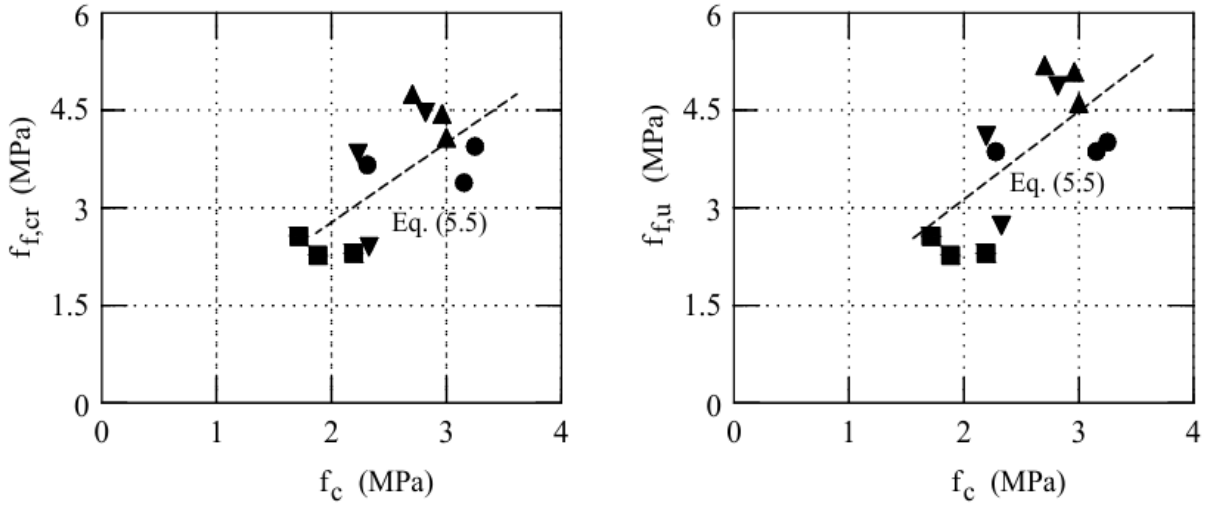

Figure 5.7: Linear regression between $f_{f,cr}$, $f_{f,u}$ and f_c

The values of both strengths demonstrate a tendency to linearly increase with the increment of compressive strength, a common occurrence in brittle materials such as concrete [48]. Consequently, the observed relationship between flexural and compressive strength can be used in the design of Fiber-Reinforced Ice (FRI) structures. Indeed, a linear relationship, derived through the least square approximation of experimental data, can be utilized to predict flexural strengths when compressive strength is known. Eq. 5.5 was derived assuming it passes through the point (0, 0), meaning it has a zero intercept. This results in a linear equation with only one coefficient.

$$f_f = (\lambda \,.\, \mathrm{f}_c) \tag{5.5}$$

where the coefficient λ depends on the type of flexural strength (see Table 5.12). The table also includes the R^2 value, which serves as an indicator of the reliability of these interpolations. Since these values are close to 1, indicating that a large proportion of the variability in the dependent variable is explained, they demonstrate the high reliability of these correlations. Eq. 5.5 can be effectively used to design FRI structures in bending, when only compressive strength is known.

Table 5.12. values of the parameters λ and R^2 in Eq. 5.5 for ice materials.

Strength	λ	R^2
$f_{f,cr}$	1.3602	0.9693
$f_{f,u}$	1.5137	0.9636

5.4- Conclusion

The experimental analyses conducted on cement-based mortars and ice yield the following conclusions:

1- Utilizing the experimental procedures outlined in UNI EN 196-1 (2005), both mortars and ice can effectively undergo measurement for flexural and compressive strength.

2- Cement-based materials exhibit significantly higher flexural and compressive strengths compared to ice.

3- Adapting the traditional approach recommended by Eurocode 2 (UNI EN 1992-1-1, 2004) for concrete allows for straightforward extension to ice when determining flexural strength from compressive strength.

In the subsequent phases of this study, constructing and analyzing a full-scale ice structure will enhance our understanding of how fiber addition and temperature variations impact the structure.

Conclusion

Here are the key conclusions drawn from the experimental investigation on Fiber-Reinforced Concrete (FRC):

1. New cement-based composites, incorporating a significant volume of recycled steel fibers, can be tailored through a two-stage procedure.
2. Optimal selection of the volume fraction of recycled steel fibers leads to improved mechanical properties in the two-stage cement-based composites, surpassing those of concrete made solely with virgin components.
3. While substituting virgin aggregate with recycled materials may lead to a reduction in flexural strength, this can be effectively compensated for by increasing the content of recycled steel fibers.
4. Eco-mechanical analyses indicate that using large volumes of recycled steel fibers enhances mechanical performance without exacerbating the environmental impact.

Additionally, the conclusions derived from the analysis in section focusing on the case study of HPFRC, highlight the following key points:

1. Optimal selection of the volume fraction of Recycled Steel Fibers (RSF) enables the attainment of mechanical properties comparable to those of the most common reinforced concrete formulations.
2. The established correlation between tensile strength ($f_{f,u}$) and fiber volume fraction (V_f) offers a practical approach for determining the appropriate amount of fibers, facilitating informed decision-making in concrete mixtures.

Regarding the Fiber-Reinforced Ice (FRI) aspect of this study:

1. Plain ice experiences a sharp drop in bearing capacity after reaching peak strength, indicative of a brittle failure.
2. FRI demonstrates a more gradual crack expansion and reduction in bearing capacity under load, representing a ductile failure.
3. FRI highlights improved mechanical properties compared to plain ice, with nearly double the ultimate flexural strength and a strain-hardening phenomenon after cracking.
4. The mechanical properties of FRI are sensitive to fiber content, with an optimal fiber content identified for maximum performance, such as FRI-2 with a fiber content of 56 g/liter.

Also, the experimental analyses conducted on both cement-based mortars and ice yield the following conclusions:

1. The flexural and compressive strengths of both mortars and ice can be effectively measured using the recommended experimental procedures.
2. Cement-based materials exhibit significantly higher flexural and compressive strengths compared to ice, indicating a notable difference in mechanical properties.
3. The traditional approach for obtaining flexural strength from compressive strength in concrete can be extended to ice, providing a consistent methodology for assessing ice's flexural strength.

In the concluding segment of this doctoral dissertation, several recommendations are provided for future research endeavors in this field of study:

1. Full-Scale Testing for Cementitious and Ice Materials: Developing comprehensive full-scale tests is essential to evaluate the performance and load-bearing capacity of real-size structures constructed with both cementitious and ice materials, in comparison to conventional materials.
2. Automated Processing for Cementitious Materials: There is a need to devise an automated process for cleaning, sorting, and cutting recycled fibers to required lengths in cementitious materials. This initiative aims to enhance the recycling process and improve fiber quality.
3. Eco-Mechanical Assessment Beyond Specimens: While the current research has focused on evaluating eco-mechanical properties of SFRC specimens under specific loads, further investigation is warranted. Future studies should extend to assessing the eco-mechanical performance of more intricate structures like RC frames and bridges, recognizing that material behavior may vary significantly in such contexts.
4. Temperature Sensitivity in Ice Structures: A more complete examination of temperature sensitivity in ice structures is recommended. Various tests should be devised to deepen understanding of this aspect, enhancing our comprehension of the behavior of ice materials under different thermal conditions.
5. Development of Analytical Models: Utilizing numerical models, particularly finite element analysis, can offer valuable insights into both cementitious and ice materials. An analytical model integrating such numerical approaches can contribute significantly to the understanding of these subjects.

These suggestions aim to guide future research efforts toward advancing knowledge and innovation in the field, addressing critical gaps and fostering deeper insights into the behavior and potential applications of cementitious and ice materials.

References

1- Sakai, K., and Noguchi, T., The Sustainable Use of Concrete, Taylor & Francis, London, UK, 2013. https://doi.org/10.1201/b12355

2- United Nations, "Resolution Adopted by the General Assembly on 25 September 2015—Transforming Our World: The 2030 Agenda for Sustain able Development (A/RES/70/1)," 2015, https://sustainabledevelopment./

3- A. Gupta, S. Chaudhary, "Effect of waste plastic as partial replacement of aggregate in concrete mixes," Waste Management, 2018, vol. 79, pp. 371-376.

4- R. Siddique, J. Khatib, I. Kaur, "Use of recycled plastic in concrete: A review," Waste Management, 2008, vol. 28, no. 10, pp. 1835-1852.

5- Y. Shao, T. Lefort, S. Moras, D. Rodriguez, "Studies on concrete containing ground waste glass," Cement and Concrete Research, 2000, vol. 30, no. 1, pp. 91-100.

6- M. Thomas, "Optimizing the use of fly ash in concrete," Portland Cement Association, 2007, vol. 5420, pp. 1-24.

7- G. Centonze, M. Leone, M.A. Aiello, Steel fibers from waste tires as reinforcement in concrete: a mechanical characterization, Constr. Build. Mater. 36. 2012. 46–57.

8- Bendixen, M.; Best, J.; and Lønsmann Iversen, L., "Time Is Running Out for Sand," Nature, V. 571, July 2019, pp. 30-31.

9- Xu, J.; Yao, Z.; Yang, G.; and Han, Q., "Research on Crumb Rubber Concrete: From a Multi-Scale Review," Construction and Building Materials, V. 232, No. 10, 2020, p. 117282. doi: https://10.1016/j. conbuildmat.2019.117282

10- Alsaif, A.; Koutas, L.; Bernal, S. A.; Guadagnini, M.; and Pilak outas, K., "Mechanical Performance of Steel Fibre Reinforced Rubber ised Concrete for Flexible Concrete Pavements," Construction and Building Materials, V. 172, May 2018, pp. 533-543. doi: https://10.1016/j. conbuildmat.2018.04.010

11- Fantilli, A. P.; Mihashi, H.; and Vallini, P., "Multiple Cracking and Strain Hardening in Fiber-Reinforced Concrete under Uniaxial Tension," Cement and Concrete Research, V. 39, No. 12, 2009, pp. 1217-1229. doi: https://10.1016/j.cemconres.2009.08.020

12- Habert G., and Roussel N. Study of two concrete mix-design strategies to reach carbon mitigation objectives. Cement & Concrete Composites, Vol. 31,2009, pp. 397–402.
13- Monteiro, P. J. M.; Miller, S. A.; and Horvath, A., "Towards Sustain able Concrete," Nature Materials, V. 16, June 2017, pp. 698-699. doi: https://10.1038/nmat4930
14- Naaman, A. E., and Reinhardt, W., "Proposed Classification of HPFRC Composites Based on Their Tensile Response," Materials and Structures, V. 39, June 2006, pp. 547-555.
15- Fantilli, A. P.; Mihashi, H.; and Vallini, P., "Multiple Cracking and Strain Hardening in Fiber-Reinforced Concrete under Uniaxial Tension," Cement and Concrete Research, V. 39, No. 12, 2009, pp. 1217-1229. doi: https://10.1016/j.cemconres.2009.08.020
16- Mobasher, B. M&S highlight: Naaman & Reinhardt, Proposed classification of HPFRC composites based on their tensile response. Published in Materials Structure 3 February 2022. Materials Science, Engineering. https://doi.org/10.1617/s11527-021-01860-1
17- Brühwiler, E. "Structural UHPFRC": Recent Applications in Rehabilitation and Strengthening of Bridges in Switzerland June 2023. https://doi.org/10.21838/uhpc.16651
18- Denarié, E Brühwiler, E «Cast-on site UHPFRC for improvement of existing structures - Achievements over the last 10 years in practice and research,» in HPFRCC7: 7th workshop on High Performance Fiber Reinforced Cement Composites, 2015 Stuttgart, Germany. Corpus ID. 111010904
19- Martínez, J. Characterisation of the tensile behaviour of UHPFRC by means of four-point bending tests. Published 1 April 2017. Engineering, Materials Science https://DOI:10.4995/thesis/10251/79740
20- A. Martínez-Ibernón, M. Roig-Flores, Influence of Cracking on Oxygen Transport in UHPFRC Using Stainless Steel Sensors. Published in Applied science 28 December 2019. DOI: https://10.3390/app10010239
21- Seung-Won Choi, Jongkwon Choi, Seong-Cheol Lee. Probabilistic Analysis for Strain-Hardening Behavior of High-Performance Fiber-Reinforced Concrete. Published in Materials 27 July 2019. Engineering, Materials Science. DOI: https://10.3390/ma12152399
22- Duyen Trinh-Duc, Piotrowski, A. Estimation of Post-Cracking Dissipation Capabilities of Fiber Reinforced Concretes in Three Point Bending Test Monitored with Application of

Digital Image Correla-tion System. Published in Materials 1 September 2021. DOI: https://10.3390/ma14175088

23- C. Zanuy, Pedro Javier Irache, Alejandro García-Sainz. Composite Behavior of RC-HPFRC Tension Members under Service Loads. Published in Materials 24 December 2020. Engineering, Materials Science. DOI: https://10.3390/ma14010047

24- Rinaldi, Z. Grimaldi, A. Influence of high performance fiber rein-forced concrete on the ductility of beam el-ements. Published 2005. Engineering, Materials Science

25- JSCE (Japan Society of Civil Engineers), recommendation for design and construction of high-performance fiber reinforced cement composites with multiple fine cracks (HPFRCC) march 2008, https://www.jsce.or.jp/committee/concrete/e/hpfrcc_jsce.pdf

26- Bahij, S.; Omary, S.; Feugeas, F.; and Faqiri, A., "Fresh and Hardened Properties of Concrete Containing Different Forms of Plastic Waste—A Review," Waste Management (New York, N.Y.), V. 113, July 2020, pp. 157-175. doi: https://10.1016/j.wasman.2020.05.048

27- Ítalo Linhares Salomão, Pinheiro, P. Exploring Analytical Hierarchy Process for Multicriteria Assessment of Reinforced Concrete Slabs. Published in Applied Sciences 24 August 2023 Engineering DOI: https://10.3390/app13179604

28- Fantilli, A. P.; Mancinelli, O.; and Chiaia, B., "The Carbon Footprint of Normal and High-Strength Concrete Used in Low-Rise and High-Rise Buildings," Case Studies in Construction Materials, V. 11, Dec. 2019, p. e00296. doi: https://10.1016/j.cscm.2019.e00296

29- Xing, W. Tam, V. Life Cycle Assessment of Sustainable Concrete with Recycled Aggregate and Supplementary Cementitious Materials. Published in Social Science Research. 1 June 2023. Engineering, Environmental Science, Materials Science. DOI: https://10.2139/ssrn.4208048

30- Fantilli, A. P., and Chiaia, B., "Eco-Mechanical Performances of Cement-Based Materials: An Application to Self-Consolidating Concrete," Construction and Building Materials, V. 40, Mar. 2013, pp. 189-196. doi: https://10.1016/j.conbuildmat.2012.09.075

31- Damineli B.F, Kemeid F.M, Aguiar, Vanderley M. J. Measuring the eco-efficiency of cement use.2010. https://doi.org/10.1016/j.cemconcomp.2010.07.009

32- Flower D.J. Sanjayan J.G. Green house gas emissions due to concrete manufacture. 2007. http://dx.doi.org/10.1065/lca2007.05.327

33- Swiss Centre for Life Cycle Inventories, "The Ecoinvent Database, Version 3.7, 2020," http://www.ecoinvent.ch.

34- FIB model code for concrete structures. 2020. http://www.fib-international.org/

35- Mondal. B, Mukherjee. S, Sarkar. S. Advances in Materials Science and Engineering: A Review Published in 2018, Advances in Materials Science and Engineering. https://www.hindawi.com/journals/amse/2018/7497392/

36- Zhang Y. Perspective of China's participation in polar development and governance. J Qingdao Univ Sci Technol. 2016. (Soc Sci Ed) 32:75–78.

37- Marthinsen A. Ice used as a permanent construction material. In Proceedings of 5th International Conference on Offshore Mechanics and Arctic Engineering (OMAE), Tokyo, 1986. Japan, ASME, Vol. IV, pp. 120–32.

38- Glockner P.G. Reinforced ice and ice domes: opportunities for the North. Int. J.Space Struct. 1988, pp. 84–102. https://doi.org/10.1177/026635118800300203

39- E. Bashaw, J. Drage, Applied Ice Engineering for Exploring Arc-tic Natural Resources. Published 27 June 2013. Environmental Science, Engineering DOI: https://10.1061/9780784412978.032

40- Makkonen L. Ice and construction. 1994. Technical Research Centre of Finland, Espoo, Finland

41- Haynes F., Martinson C.R. Ice reinforced with geogrid. In Proceedings of 8th International Conference on Offshore Mechanics and Arctic Engineering (OMAE), 1989. The Hague, Netherlands, ASME, Vol. IV, pp. 179–85

42- Karelov. A, Shkhinek. K, Belyaev. N, Using of Ice for Constructing Islands in the Arctic Conditions. Published 29 January 2015. Environmental Science, Engineering. DOI: https://10.4028/www.scientific.net/AMM.725-726.245

43- Syromyatnikova. A, Fedorova .L.K, Prospects for the application of ice compo-site materials for the construction of ice crossings Published in Arctic 1 June 2022 Environmental Science, Engineering, Materials Science. DOI: https://10.25283/2223-4594-2022-2-281-287

44- Vaughan, D. G., Comiso, J. C., Allison, I., Carrasco, J., Kaser, G., Kwok, R., ... & Zhang, T. (2013). Observations: Cryosphere. In: Climate Change 2013: The Physical Science Basis. Contribution of Working Group I to the Fifth Assessment Report of the Intergovernmental Panel on Climate Change

45- Yue W., Xiaonan L., Xiuming L., Pron A. The property of fiber reinforced ice under uniaxial compression.2020. Materials and Structures, 53 (29) https://doi.org/10.1617/s11527-020-01463-2

46- Petrovic J Review mechanical properties of ice and snow. 2003. J Mater Sci 38:1–6

47- Petrenko V, Whitworth R. Physics of ice. 2010. Oxford University Press, London

48- Fantilli A.P., Frigo B., Dehkordi F.M. (2022). Relationship between flexural strength and compressive strength in concrete and ice. Current Perspectives and New Directions in Mechanics, Modelling and Design of Structural Systems, 1st Ed., CRC Press, 6 pp, ISBN9781003348443.

49- Murdza, A., Polojarvi, A., Schulson, E.M., & Renshaw, C.E. (2021). The flexural strength of bonded ice. The Cryosphere, 15, 2957–2967. https://doi.org/10.5194/tc-15-2957-2021

50- Renshaw, C.E., & Schulson, E.M. (2017). Strength-limiting mechanisms in high-confinement, brittle-like failure: Adiabatic transformational faulting. Journal of Geophysical Research: Solid Earth, 122, 1088-1106. https://doi.org/10.1002/2016JB013407

51- Nixon, W.A. and Smith, R.A. (1987) The fracture toughness of some wood-ice composites. Cold Regions Science and Technology, 14, 139– 45.

52- Nixon W.A., Smith R.A. The fracture toughness of some wood-ice composites. Cold Regions Science and Technology, 1987. 14, 139– 45. https://doi.org/10.1016/0165-232X(87)90029-2

53- [50 N.K. On development of fiber-ice-composites. Cold Reg Sci Technol. 1993. 21:195–199. https://doi.org/10.1016/0165-232X(93)90007-U

54- Vasiliev N.K., Pronk A.D.C., Shatalina I.N. A review on the development of reinforced ice for use as a building material in cold regions. 2015. Cold Reg Sci Technol 115:56–63. https://doi.org/10.1016/j.coldregions.2015.03.006

55- Iliescu, D., Murdza, A., Schulson, E.M., & Renshaw, C.E. (2017). Strengthening ice through cyclic loading. *Journal of Glaciology*, 1-7. https://doi.org/10.1017/jog.2017.32

56- Gold, L.W. The Habbakuk Project—Building ship from ice, in Proceedings of International Conference on Port and Ocean Engineering under Arctic Conditions (POAC), 1989. Luleå, Sweden, Vol. 1, pp. 1211–28.

57- Frederking, R. and Svec, O. (1985) Stress-relieving techniques for cantilever beam tests in an ice cover. Cold Regions Science and Technology, 11, 247–53.

58- Weber, L.J., Nixon, W.A., 1996a. Fracture toughness of freshwater ice, Part I. Experimental technique and results. ASME J. Offshore Mech. Arct. Eng. 118.

59- Weber, L.J., Nixon, W.A., 1996b. Fracture toughness of freshwater ice, Part II. Analysis and micrography. ASME J. Offshore Mech. Arct. Eng. 118.

60- Weber, L.J., Nixon, W,A., 1996c. Hysteretic behavior in ice under fatigue loading. In: Proc. 15th Int, Conf. Offshore Mechanics and Arctic Engineering, Florence, Italy, Vol. 4, pp. 75-81.

61- Najjar, M. F., "Innovating Two-Stage Concrete with Improved Rheo logical, Mechanical and Durability Properties," PhD dissertation, Univer sity of Western Ontario, London, ON, Canada, 2016, https://core.ac.uk/download/pdf/61692853.pdf

62- European Committee for Standardization, "Methods of Testing Cement—Part 1: Determination of Strength (UNI EN 196-1)," CEN, Brus sels, Belgium, 2005.

63- Fantilli, A. P.; Chiaia, B.; and Gorino, A., "Unified Approach for Minimum Reinforcement of Concrete Beams," ACI Structural Journal, V. 113, No. 5, Sept.-Oct. 2016, pp. 1107-1116. doi: https://10.14359/51688927

64- Fantilli, A. P., and Chiaia, B., "Eco-Mechanical Performances of Cement-Based Materials: An Application to Self-Consolidating Concrete," Construction and Building Materials, V. 40, Mar. 2013, pp. 189-196. doi: https://10.1016/j.conbuildmat.2012.09.075

65- Swiss Centre for Life Cycle Inventories, "The Ecoinvent Database, Version 3.7, 2020," http://www.ecoinvent.ch

66- ANAGENNISI, "Innovative Reuse of All Tire Components in Concrete (Final Report)." https://cordis.europa.eu/docs/results/603/603722/final1-final-report-v1-7.pdf

67- Farjon A. (2005). Pines: Drawings and descriptions of the genus Pinus. Brill, Architecture, 2nd Ed., 235 pp, ISBN-13: 978-9004139169

68- Fantilli A.P., Dehkordi F.M. (2022) Two – Stage Cementitious Composites Containing Recycled Steel Fibers. ACI Materials Journal, V. 119, No. 2. http://dx.doi.org/10.14359/51734300

69- Vasiliev N.K., Pronk A.D.C., Shatalina I.N., Janssen F.H.M.E., Houben R.W.G. (2015) 273 A review on the development of reinforced ice for use as a building material in cold 274 regions. Cold Reg. Sci. Technol. 115, https://doi.org/10.1016/j.coldregions.2015.03.006

70- Fantilli A.P., Dehkordi F.M. (2021) Tailoring HPFRC with materials from end of life tires - HPFRC ottenuti con materiali provenienti dagli pneumatici a fine vita. In: Costruire in calcestruzzo: realizzazioni, ricerca, attualità e prospettive. Proceedings of *Italian Concrete Days 2020*, *pp. 743-752.*

71- Zhao C., Wang Z., Zhu Z., Guo Q., Wu X., Zhao R. (2023) Research on different types of fiber reinforced concrete in recent years: An overview. Construction and Building Materials 365 (2023) 130075. https://doi.org/10.1016/j.conbuildmat.2022.130075

72- Wu, Y. Lou, X. Liu, X. Pronk, A. 2020. The property of fiber reinforced ice under uniaxial Compression, Materials and Structures

73- Najjar M.F., Soliman A.M., and Nehdi M.L. (2014) Critical overview of two-stage concrete: Properties and applications. Construction and Building Materials, Vol. 62, pp. 47–58.

74- Bažant Z.P, Wittmann F.H, 1982. Creep and Shrinkage in Concrete Structures, J. Wiley and Sons,

75- Bartlett F.M, MacGregor J.G, Effect of moisture condition on concrete core strengths, ACI Mater. J. 91 (3) (1994) 227–236.

76- J. Bisschop, L. Pel, J.G.M. van Mier, Effect of aggregate size and paste volume on drying shrinkage microcracking in cement-based composites, in: F.-J. Ulm, Z.P. Bazant, F.H. Wittmann (Eds.), Creep, Shrinkage and Durability Mechanics of Concrete and other Quasi-Brittle Materials, Elsevier, 2001, pp. 75–80.

77- Brooks J.J, Neville A.M, 1997. A comparison of creep, elasticity, and strength of concrete in tension and compression, Mag. Concr. Res. 29 (100) 131–141.

78- Baroghel-Bouny V, Godin J, Experimental study on drying shrinkage of ordinary and high-performance cementitious materials, in: V. BaroghelBouny, P.-C. Aïtcin (Eds.), Shrinkage of Concrete, RILEM Publication PRO 17, Paris, France, 2000, pp. 215–232.

79- Burlion N, Bourgeois F, J.-F. Shao, 2005. Effect of desiccation on mechanical behaviour of concrete, Cem. Concr. Comp. 27. 367–379.

80- Wittmann F.H, Surface tension, 1968. shrinkage and strength of hardened cement paste, Mater. Struct. 1 (6). 547–552.

81- Yurtdas I, Peng H, Burlion N, Skoczylas F, 2005, Influences of water by cement ratio on mechanical properties of mortars submitted to drying. https://doi.org/10.1016/j.cemconres.2005.12.015

82- Okajima T, Ishikawa T, Ichise K, 1980. Moisture effect on the mechanical properties of cement mortar, Trans. Jpn. Concr. Inst. 2. 125–132.

83- Singhn S.B, Munjal P, Thammishetti N, 2015. Journal of Building Engineering, Role of water/cement ratio on strength development of cement mortar, https://doi.org/10.1016/j.jobe.2015.09.003

84- Alawode O, O.I. Idowu O.I, 2011. Effects of Water-Cement Ratios on the Compressive Strength and Workability of Concrete and Lateritic Concrete Mixes. https://www.akamai.university/files/theme/AkamaiJournal/PJST12_2_99.pdf

85- Lisa E. Burris a, Kimberly E. Kurtis, 2022, Water-to-cement ratio of calcium sulfoalu-minate belite cements: Hydration, setting time, and strength development https://doi.org/10.1016/j.cement.2022.100032

86- Peng Wang , Lin-yu-wen Ke b, Hao-liang Wu a b, Christopher K.Y. Leung, 2022, Effects of water-to-cement ratio on the performance of concrete and embedded GFRP reinforcement. https://doi.org/10.1016/j.conbuildmat.2022.128833